공학박사 학위논문

CFD를 이용한 174K ME-GI LNG선의 카고컴프레서룸 내부의 가스 감지기 최적위치 선정에 관한 연구

A study on the optimal location of gas detector using CFD in the cargo compressor room of the 174K ME-GI LNG vessel

지도교수 강 호 근

2018 년 8월

한국해양대학교 대학원

기관시스템공학과

이 상 원

논 문 제 목

년 월 일

이 상 원

공학박사 학위논문

CFD를 이용한 174K ME-GI LNG선의 카고컴프레서룸 내부의 가스 감지기 최적위치 선정에 관한 연구

A study on the optimal location of gas detector using CFD in the cargo compressor room of the 174K ME-GI LNG vessel

지도교수 강 호 근

2018년 08월

한국해양대학교 대학원

기관시스템공학과

이 상 원

본 논문을 이상원의 공학박사 학위논문으로 인준함

위원장 : 임태우 인

위 원 : 김동준 인

위 원 : 김도엽 인

위 원 : 이영범 인

위 원 : 강호근 인

2018 년 06 월 22 일

한국해양대학교 대학원

List of Tables

List of Figures

CFD를 이용한 174K ME-GI LNG 선의 카고컴프레서룸 내부의 가스 감지기 최적위치 선정에 관한 연구

Lee, Sang Won

Department of Marine System Engineering

Graduate School of Korea Maritime and Ocean University

Abstract

최근에 LNG선에 증발가스(Boil Off Gas)를 연료로 사용하기 위하여, 고압의 압축기나 고압펌프와 LNG 기화기를 장착한 LNG 선이 많이 건조 되고 있다. 이는 LNG 연료가 다른 연료에 비해서 친환경적이고 국제해사기구의 엄격한 환경 요구기준을 만족시키는 대안의 연료로 간주 되기 때문이다. 그러나 안전과 관련하여 가스의 누출, 폭발, 화재 등과 같이 조사 하여야 할 많은 사항이 있다. IGC code 가 적용된 LNG 선은 오랫동안 운행하여 왔으며, 거기에는 많은 적합한 안전 규약이 있다. 그러나, LNG 연료 추진선박의 경우는 안전규약이 충분치가 않다. 왜냐하면 IGF code 가 적용된 LNG 연료추진선박은 충분히 참고할 만한 실적이 없었기 때문이다. IGF code 의 대부분의 안전규약은 IGC code 의 요구에 따라 적용 되어 왔기 때문에 LNG 연료추진선의위험요인을 막기 위해서 부적합한 규약이 많이 있다. IGC code 와 IGF code 에 의해서 적용되는 카고컴프레서룸 내부의 가스 감지시스템의 경우는 단지 가스 감지기의

개수만이 정의되어 있고, 가스 감지기의 위치에 대한 규정은 없어 선주의 요구나 조선소와 선급의 동의에 따라 설치된다. 카고컴프레서룸의 최소한의 가스 감지기의 수는 세 개 이지만 감지기의 위치에 대한 규정은 없다. 그러므로 선주는 IGF 나 IGC code 의 가스감지 시스템 규약에 대해 의존도가 높지는 않다. 본 연구는 고압의 LNG 연료 처리 장비를 갖추고 있는 LNG 선의 카고컴프레서룸 내부의 가스누출 및 확산에 관한 논문이며, IGC 와 IGF code 에 상술된 가스 감지기의 수와 위치의 안전규정에 대하여 합리적인 방법을 제시하고자 한다. ME-GI(Man Electronic-Gas Injection) 엔진을 장착한 174K LNG 선박의 카고컴프레서룸 내부의 LNG 가스의 누출 및 확산을 시뮬레이션 하기 위하여, 기계실 내부의 구조, 장비의 배치, 배관의 3차원 배치를 실재와 동일하게 설계 하였다. 본 연구는 고압가스 분출과 저압가스 분출시뮬레이션으로 구성된다. 고압가스 분출의 경우는 고압펌프와 LNG 기화기의 이송파이프에서 파공홀(Pinhole)의 크기를 4.5, 5.0, 5.6 mm 로 분류하여 분출질량유량 별로 시뮬레이션을 수행하였다. 저압가스 분출의 경우는 VR(Vapor Return)컴프레서의 이송파이프에서 파공홀의 크기를 100 과 140 mm로 분류하여 분출질량유량 별로 가스시뮬레이션을 수행 하였다. 174K LNG 선박의 가스시뮬레이션의 결과 고압가스 분출의 경우는 최대 분출량이 적용된 5.6 mm 파공홀의 경우 환기능력에 대한 것이 입증 되었고, VR 컴프레서의 이송파이프의 저압가스 분출의 경우도 파공홀의 크기를 100 과 140 mm 로 나누어 분출 유량이 1.8 과 3.5 kg/s 에 따른 환기능력에 대해 입증하였다. 그러나 CFD시뮬레이션을 통해 카고컴프레서룸 내부의 가스 감지기를 다른 최적 지점으로 이동하여 추가해야 하는 것이 확인되었다. 본 연구의 CFD 결과는 위험기반의 설계, 분석에 유용하고, 최적의 가스감지센서의 위치에도 유용하다고 하겠다.

KEY WORDS: LNG 액화천연가스;IGC code 산적액화가스운반선의 건조와 설비에 대한 국제규칙; Gas Detector 가스 감지기; CFD 전산유체역학; Gas leak 가스누출

A study on the optimal location of gas detector using CFD in the cargo compressor room of the 174K ME-GI LNG vessel

Lee, Sang Won

Department of Marine System Engineering

Graduate School of Korea Maritime and Ocean University

Abstract

Recently many high pressure gas fueled LNG vessels which are combined with high pressure fuel gas compressor or high pressure pump/vaporizer have been building because LNG fuel is regarded as environment friendly and it satisfies the IMO requirements. However there are many reasons to examine its safety requirements such as gas leakage, explosion, and fire. Since LNG carriers applied with IGC code have sailed for long time so there are many adequate safety regulations available. However safety regulation for LNG-fueled vessels are still insufficient, because LNG -fueled vessels applied with the IGF code do not have enough reference. Most safety regulations applied for the IGF code are in accordance with the safety requirements of IGC code to cover the insufficient of safety regulations in the IGF code to prevent the risk in LNG-fueled vessels. In particular, for gas detection system applied in the machinery room by IGF/IGC code just defines the number of gas detectors. There are no rules for their locations, so the gas detectors are installed in accordance to the agreement among the ship-owners, shipyard and the classification societies. The minimum number of detectors in the machinery room (cargo compressor room) by IGF/IGC code is three but there are no rules for the detecting points. Therefore, ship-owners do not heavily rely on the detecting system defined by IGF/IGC code. Therefore this study considers gas dispersion in the cargo compressor room of LNG carrier equipped with high pressure cargo handling equipment, bringing up reasonable method of safety regulation, the number of gas detector and its location, specified in the IGF/IGC code.

To perform LNG gas dispersion simulation in cargo compressor room, the geometry of the cargo compressor room, and the arrangement of equipment and piping are designed with the same 3-dimensional size as 1 to 1 scale. Scenarios for a gas leak were examined for high pressure and low pressure leak simulation. For high pressure gas leak, the size of the pinhole was divided into 4.5, 5.0, and 5.6 mm from the discharge pipes of the high-pressure pump and LNG vaporizers to simulate by mass flow rate of the eruption. For low pressure gas leak, the size of the pinhole from the discharge pipe of VR (Vapor Return) compressor was divided into 100 and 140 mm in size to carry out a gas simulation by the mass flow rate.

The results show that the cargo compressor room of 174K ME-GI LNG vessels has no serious risk problems regarding the flammable gas concentration since it is verified that ventilation assessment was safe for a 5.6 mm pinhole for high pressure leak as gas rupture condition and the low pressure gas explosion in the discharge pipe of VR compressor was also divided into 100 and 140 mm in size to demonstrate ventilation capability according to 1.8 and 3.5 kg/s. However, based on the CFD simulation, it is verified that the actual gas detection sensors in cargo compressor room should be moved to other optimum points and their quantity should be increased. The CFD results of this study will be useful for risk based design and analysis and optimum gas detection points can be applied.

Key Words: LNG; IGC code; Gas Detector; CFD; Gas leak

1. Introduction

1.1 Outline

Owing to recent environmental issues, the IMO has adopted regulations to address the emission of air pollutants from ships and has adopted mandatory energy efficiency measures to reduce the emissions of greenhouse gases from international shipping under Annex VI of the IMO’s pollution prevention treaty (MARPOL). In addition, IMO regulates air pollutants from international shipping, particularly nitrogen oxide (NOx) and sulphur oxide (SOx) emitted from ships. The NOx emission limit values depend on the maximum operating speed (n, rpm) of the engines, as shown in Fig. 1-1. Tier I and II limit values are global, whereas tier III values are applied to NOx emission control areas.

Tier	Ship construction date on or after	Total weighted cycle emission limit (g/kWh) n = engine’s rated speed (rpm)		
		n < 130	130≤n < 2000	n ≥ 2000
I	1 January 2000	17.0	$45 \cdot n^{(-0.2)}$ e.g., 720 rpm – 12.1	9.8
II	1 January 2011	14.4	$44 \cdot n^{(-0.23)}$ e.g., 720 rpm – 9.7	7.7
III	1 January 2016	3.4	$9 \cdot n^{(-0.2)}$ e.g., 720 rpm – 2.4	2.0

Fig. 1-1 IMO MARPOL Annex VI requirement of NOx emission

The sulphur limit values and implementation dates are listed in Fig. 1. MARPOL Annex VI regulations include caps on the sulfur content of fuel oil as a measure to control SOx emissions. Rigorous fuel quality provisions are required in the Emission Control Area (ECA) as compared with the global area.

Outside an ECA established to limit SOx and particulate matter emissions	Inside an ECA established to limit SOx and particulate matter emissions
4.50% m/m prior to 1 January 2012	1.50% m/m prior to 1 July 2010
3.50% m/m on and after 1 January 2012	1.00% m/m on and after 1 July 2010
0.50% m/m on and after 1 January 2020*	0.10% m/m on and after 1 January 2015

Fig. 1-2 IMO MARPOL Annex VI requirement of SOx emission limits

Furthermore, the IMO adopted mandatory technical and operational energy efficiency measures, which are expected to greatly reduce the amount of CO_2

emissions from international shipping in 2011. These mandatory measures, namely the Energy Efficiency Design Index (EEDI) and Ship Energy Efficiency Management Plan (SEEMP), entered into force on January 1, 2013.

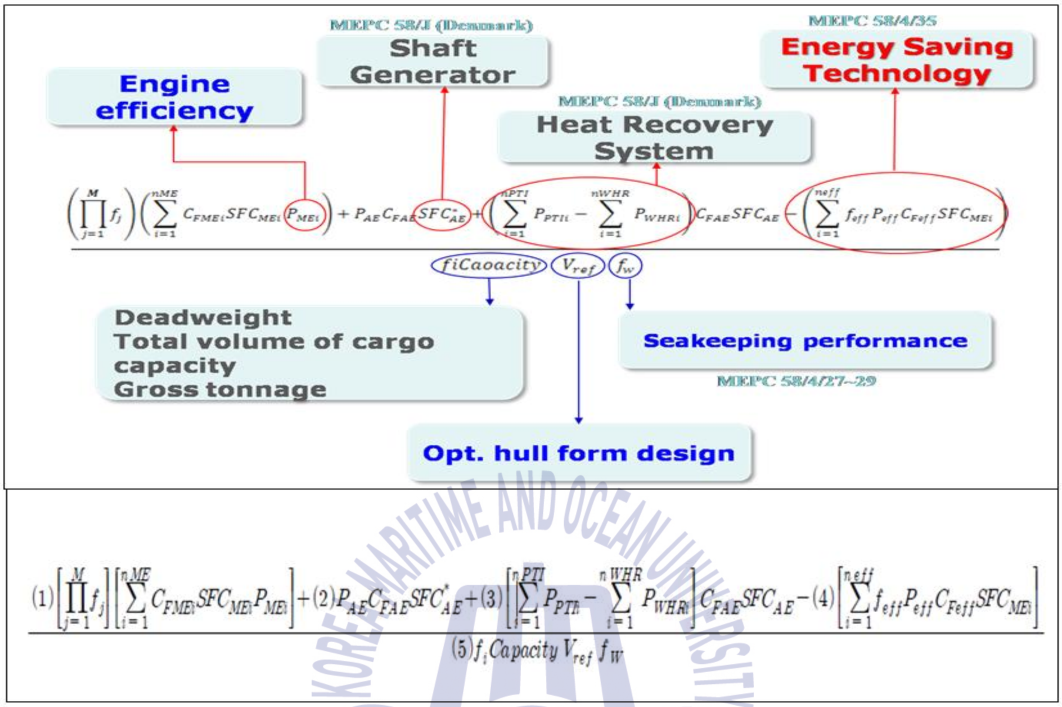

Fig. 1-3 EEDI base line and index

Fig 1-3 shows that EEDI base line and index, formula (1) and (2) are CO2 emission quantity from main engines and auxiliaries engines, (3) and (4) are considering the reduction of the Green-house-gas emission quantity and (5) is the ship's maximum work rate per hour. To comply with recent IMO's requirements, LNG fuel is in the limelight as an effective solution. So LNG fuel supply system is applying to many vessels in the world.

In case of LNG carriers, the global LNG market will transport LNG to gas plants worldwide. After gasification, the gas is distributed for energy purposes to supply the national distribution network or to be used as transport fuel. Most LNG carriers can provide propulsion by firing BOG on board ships at boilers in tanks. Other premises, on the other hand, operate as HFO. About 370 LNG tankers are currently in operation, of which 260 have steam turbines that can burn HFO or BOG gases. Another 60 LNG tankers are equipped with dual fuels, with the use of dual fuels on a steam trend.

In case of the LNG fueled ship, the number of worldwide operations of LNG carriers is still limited. According to the recent information from DNV-GL, 47 ships could run on LNG fuel by the end of 2014 and another 48 will be delivered by the end of 2018. This means that the fleet size will double between 2013 and 2008.

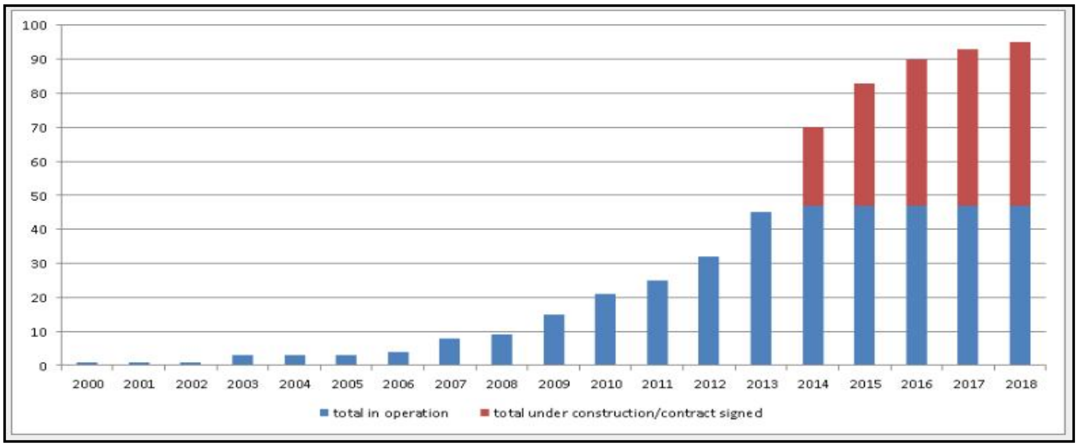

Fig. 1-4 LNG-fuelled fleet (Released from DNV-GL)

The next Fig. 1-5 provides a breakdown of the LNG-fuelled fleet per vessel type. Although the fleet is currently controlled by local ferries and platform supply vessels (PSV), the order sheet is increasingly differentiating and heading for larger ships such as container ships and general cargo ships. LNG will be particularly advantageous for ships operated by ECAs, especially vessels used for offshore transportation, such as ferries and external shipping, but it will also provide a supply container to transport containers from larger ports within ECA.

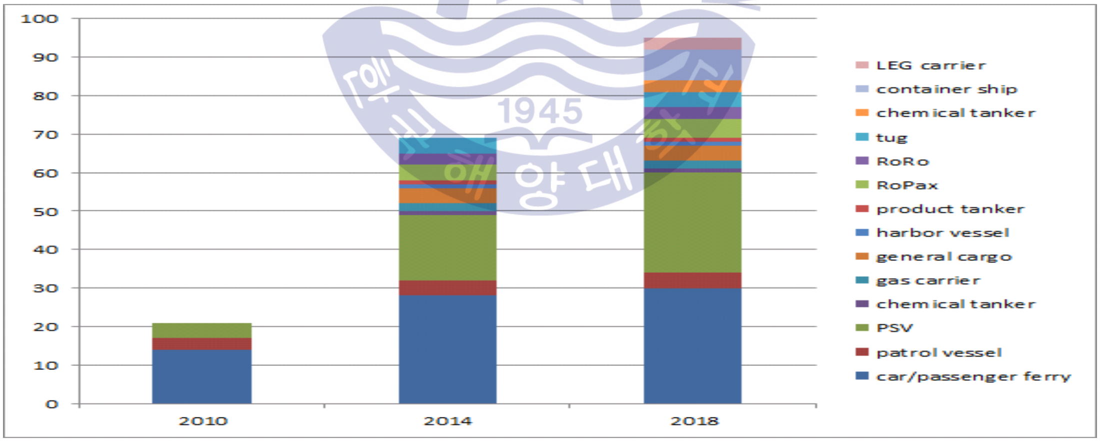

Fig. 1-5 Breakdown of LNG-fuelled fleet (www.lngbunkering.org/lng/vessels, 2017)

However, LNG is easily vaporized to 600 times volume. And it is changed to flammable gas as mixture with air. Flammability range is about 5 ~ 15 volume percent. Natural gas could be considered the most environmentally friendly fossil fuel, because it has the lowest CO_2 emissions per unit of energy and because it is suitable to be used in high efficiency combined cycle power stations. For an equivalent amount of heat, burning natural gas produces about 30 percent less carbon dioxide than burning petroleum and about 45 percent less than burning coal.

1.2 Background

1.2.1 Fuel supply systems of LNG ship

LNG ship's propulsion systems have been developed in so far. The main reason is to increase the energy efficiency and satisfy IMO's requirements ANNEX VI of the MARPOL Convention related with CO_2, SOx and NOx reduction. LNG propulsion system is closely related with the generation and consumption of the cargo boil off gas. The freight transport BOG is created and processed for the following reasons.

- Heat Transfer due to the difference of LNG cargo with external temperature.
- The LNG is injected into the cargo tank during ballast to keep the cargo temperature constant.
- Result of energy released by slogging between walls and fluids in an LNG tank caused by turbulence during the operation of a vessel.

- If no re-liquidation procession is made, the BOG is used as fuel in the propulsion system and the excess BOG remaining after the fuel is burned in the Gas Combustion Unit (GCU).
- Where there is a re-liquefaction process, the BOG is transported back to the cargo tank in liquid state by the heat exchanger

Fig.1-6 shows that the classification of propulsion systems related with Boil-off gas. The steam turbine (ST) propulsion has been the main system of the LNG vessel since 1960. The system applies to simultaneous combustion of a boiler. BOG generated during transport and heavy oil is fed to the propulsion turbine and electric turbo generator.

From the beginning of 2000, the LNG propulsion system has been at a turning point. ST is being replaced with an internal combustion engine for better efficiency because not only BOG but also heavy fuel oil can be burned in fuel. These engines are available in different types of fuel and are referred to as the Dual Fuel (DF). Developed around 2003, the DF engine (4s) employed the Otto cycle concept using approximately 1-8 % of diesel as pilot fuel used for ignition in gas combustion chambers. However, as LNG availability is technically improved in the two stroke engines (2S), the LNG fuel injection system is facing a new takeoff (Fernández, 2016)

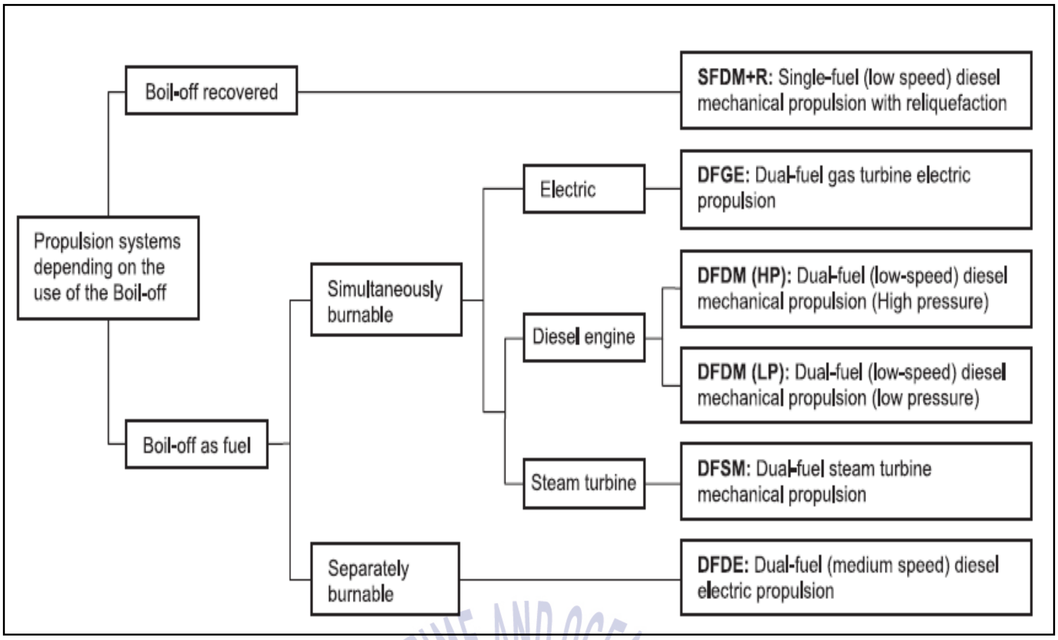

Fig. 1-6 Classification of propulsion systems related with Boil-off gas (Fernandez,2016)

This study will describe the recent leading propulsion system such as DFDE, X-DF and ME-GI.

1.2.1.1 DFDE (Dual Fuel Diesel Electric)

DFDE propulsion system consist of two(2) low duty compressors, one(1) forcing vaporizer, one(1) fuel gas pump for four(4) stroke DF generator engines(4 sets) as shown on the Fig. 1-7.

In the early stage of LNG transport, the propulsion system by steam turbines was applied because the natural BOG from the freight tanks could not be processed primarily. However, current four-stroke diesel engines are capable of burning up gas and have become a more efficient main driving system than steam turbines. Currently, for LNG carriers, four DF engines are installed in the engine room. LD compressor sends BOG from the cargo tank to the fuel gas of the DF engine, and if the fuel gas is insufficient, to feed the fuel vaporizers. When BOG is fuel in gas mode, the engine operates at a lean air/fuel rate on an Otto cycle basis by spraying a small amount of diesel oil into the combustion chamber as pilot fuel for ignition. However, when the BOG is inadequate, the engine is run by liquid fuels such as DO or HFO. In this situation BOG must be disposed of by combustion at GCU. Compared to the complex steam system of steam turbine propulsion diesel engines are more familiar to the crew and easy to use, but many cylinders can make maintenance costs and over-hole scheduling points vulnerable.

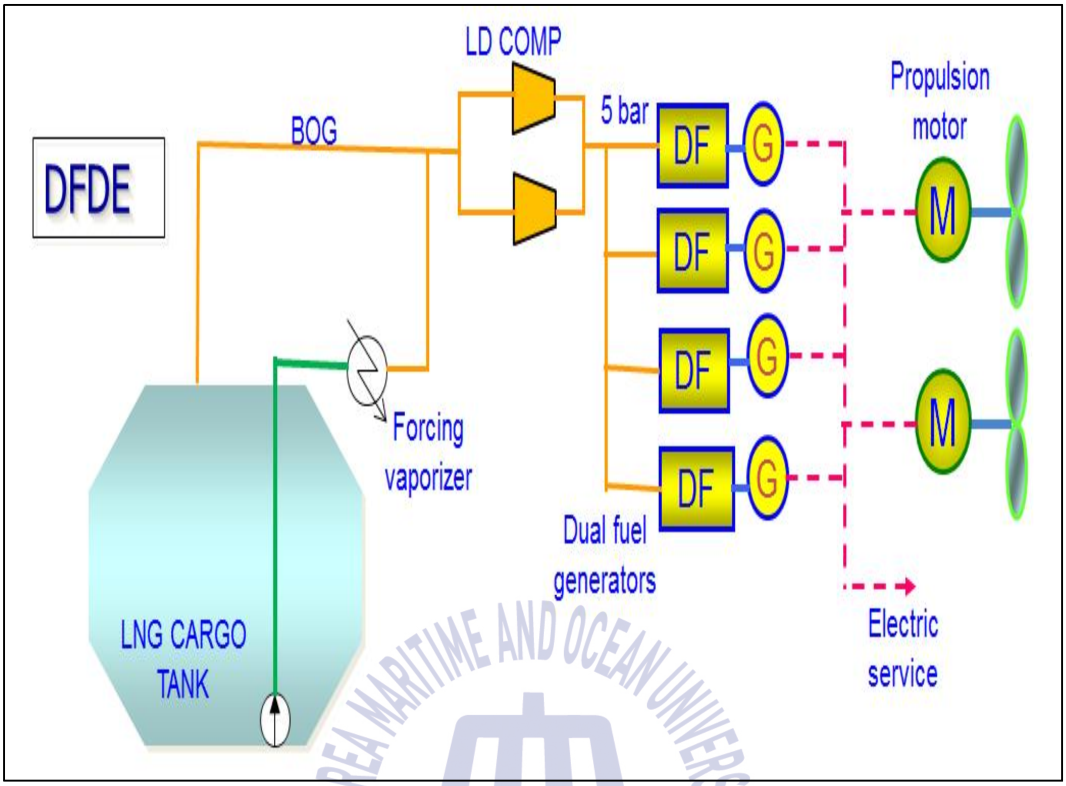

Fig. 1-7 Schematic diagram of DFDE

1.2.1.2 X-DF

X-DF propulsion system consist of two(2) low duty compressors, one(1) forcing vaporizer, one(1) fuel gas pump and control valve for the purpose of reducing the fuel gas pressure to the DF engines.

Fuel gas is supplied to the 2 main engines with 16 bar fuel gas service pressure and 4 stroke DF generator engines with 5 bar as shown on the Fig. 1-8. An important advantage of X-DF engine compared with others is low pressure gas handling is possible with a maximum 16 bar pressure and satisfy IMO's Tier III environment regulations without additional exhaust gas treatment. LNG and air are mixed in the cylinder prior to compression and no additional external engine compressors are needed and additional parasitic load is avoided. X-DF engine adopted Otto cycle offers the possibility to apply the most cost-effective low-pressure gas supply system. Moreover the consumption pilot fuel is approximately just 1 percent of the total energy at full load and therefore the lowest for any low speed 2-stroke engine technology (Brochure of Wartsila low-speed dual fuel solution, 2017).

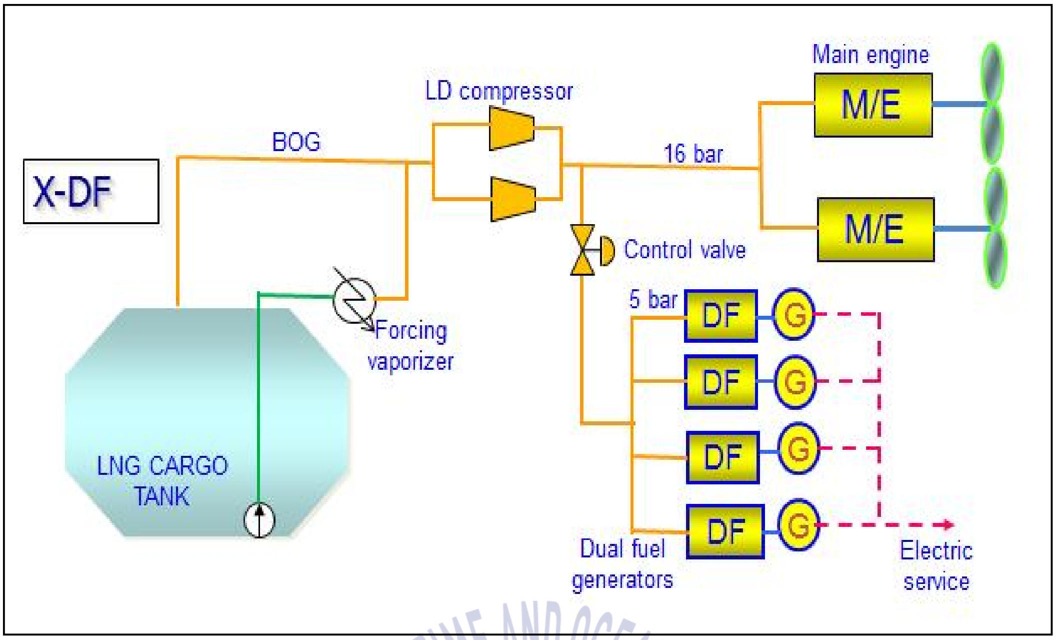

Fig. 1-8 Schematic diagram of X-DF

1.2.1.3 ME-GI

ME-GI propulsion system consist of one high pressure fuel gas compressors with 5 stages, one forcing vaporizer, one fuel gas pump and control valve for the purpose of reducing the fuel gas pressure to the 4 stroke DF generator engines. Two high pressure pumps and one high pressure vaporizer is applied from liquefied gas to make fuel gas in case of shortcoming of BOG. Fuel gas is supplied to the two main engines with 305 bar fuel gas service pressure and four stroke DF generator engines with 5 bar as shown on the Fig. 1-9.

"MAN" was the first to develop 2 stroke DF engines to be installed on LNG vessels. The main difference from 4 stroke DF engines is the injection of gas, since it is performed directly in the combustion chamber at high pressures 305 bar. To achieve this high pressure fuel gas compressor must be installed with the capacity to deal with the total demand of the engines individually (Sinha, 2011). An important advantage of ME-GI propulsion system comparing to others can make effective re-liquefaction system without additional electric power by HP compressor pressure only. Compressed BOG with 305 bar/45°C is feed to the main engines with fuel gas. Remaining warm fuel gas is heat exchanged with BOG(-110°C) from the cargo tanks. Finally 305 bar LNG in sub cooled state changes to liquefy with low pressure by Joule-Thomson effect and send to the cargo tank to recovery energy. However, additional exhaust gas treatment is needed to satisfy IMO's Tier Ⅲ environment regulations.

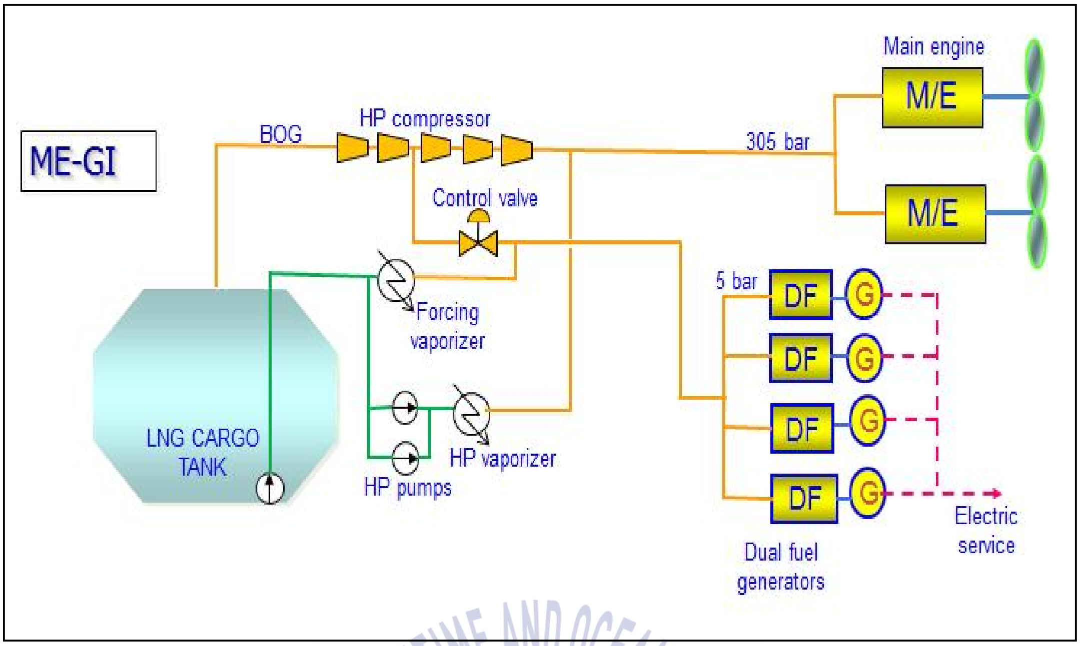

Fig. 1-9 Schematic diagram of ME-GI

1.2.2 Rule and regulation in cargo compressor room

Important requirements for New IGC code related with cargo compressor room are as follows.

"Chapter 12.1.1 Electric motor rooms, cargo compressor and pump-rooms, spaces containing cargo handling equipment and other enclosed spaces where cargo vapours may accumulate shall be fitted with fixed artificial systems capable of being controlled form outside such spaces. The ventilation shall be continuously to prevent the accumulation of toxic and/or flammable vapours, with a means of monitoring acceptable to the Administration be provided." (IGC code, 2014)

"Chapter 12.1.2 Artificial ventilation inlets and outlets shall be arranged to ensure sufficient air movement through the space to avoid accumulation of flammable, toxic or asphyxiant vapours, and to ensure a safe working environment". (IGC code, 2014)

"Chapter 12.1.3 Ventilation system shall have a capacity of not less than 30 changes of air per hour, based upon the total volume of the space". (IGC code, 2014)

"Chapter 13.6.12 Every installation, the number and the positions of detection heads shall be determined with due regard to the size and layout of the compartment. So we bring up the reasonable method of the safety regulation, the number of gas detector and its location, specified in the IGF/IGC code". (IGC code, 2014)

1.2.3 Problem statement

Below Fig. 1-10 is "Gas dangerous plan of 174K ME-GI LNG vessels". The location of Cargo compressor room is marked with arrow. It is regarded as dangerous gas zone 1. Hazardous area zones are defined in accordance with IEC(International Electrochemical Commission) 60092-502, Clause 4.2. Hazardous zones are distinguished as Zone 0, Zone1 and Zone2, the definition is the same as followings.

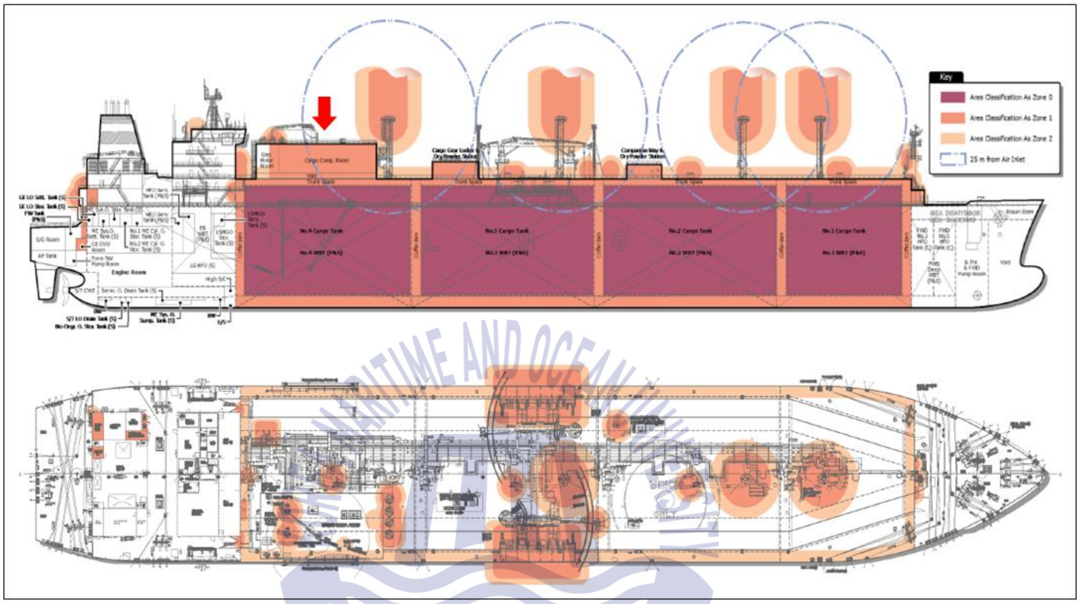

Fig. 1-10 Gas dangerous plan (Released from DSME)

Fig. 1-11 174K ME-GI LNG vessel (Released from DSME)

Zone 0 is in which an explosive gas atmosphere is present continuously or is present for long period. The interior of cargo tanks, any pipework of pressure-relief or other venting system for cargo tanks, pipes and equipment containing the cargo or developing flammable gases or vapors.

Zone 1 is in which an explosive gas atmosphere is likely to occur in normal operation. Cargo compressor room, an open deck within 3 m of any cargo tank outlets, water ballast tanks, void spaces adjacent to cargo tanks, areas or semi-enclosed spaces on open deck within 6 m radius vertical cylinder of unlimited height and 6 m radius hemisphere below any cargo outlet, etc. are defined as Zone 1.

Zone 2 is unlikely to occur in normal operation of the explosive gas atmosphere, and rarely occurs when it occurs and can exist for short periods. Area of 1.5 m surrounding open or semi-enclosed spaces of Zone1 is defined as Zone 2.

In the past, the fuel supply system was composed of low pressure. However, recently ME-GI LNG vessels have been building in shipyard, they are equipped with high pressure fuel supply system. The risk of a leak has increasing due to the application of a high-pressure fuel supply system to re-liquid the BOG in order to save cargo and energy on the fuel efficiency aspect of the main engines. Fuel gas service pressure from "HP Fuel gas compressor" and "High pressure pump/vaporizer" of fuel gas is 305 bar. Recent nearly thirty of 174K ME-GI LNG vessels have been designing and constructing with typical cargo handling equipment and piping arrangement. However, there are lots of reasons to examine its safety requirements such as gas leakage, explosion, fire and etc.

None the less, gas leak and dispersion simulation had not been considering with whole equipment and piping arrangement in the compressor room. Gas detection points have been positioning with only simple air flow simulation and agreements of the ship-owner and shipyard because the location and number of the gas detection sensor is not specified in IGC/IGF code and actual gas simulations are time-consuming. But since the behavior of the gas is very different from that of the high and low pressure, it is not correct to predict with a simple air simulation, so it is positively necessary to install optimum number of gas detection sensors and location.

Since the piping and equipment layout depend on the characteristics of the fuel delivery system, it is necessary to analyze the behavior of the gas using CFD codes, locate the gas detection sensors, and verify the performance of the ventilation system. "The Fluent software solves the Navier-Stokes equations for gas flow, coupled with the energy and diffusion equations, simulates the gas mixture by modeling each chemical species independently" (Gavelli et al., 2008). And "CFD has established itself as valuable tools for risk assessment and safety analysis in process industries and design of the concept ship" (Kang, 2013). "Increasing use of CFD is seen in evaluating the risk from dispersion applications in the coming years" (Kang, 2013). So commercial CFD code ANSYS FLUENT 14.0 has been used to carry out the gas simulation. CFD code had been used in various places in the field of shipbuilding engineering. But (Kim et al., 2011) research is the first and only one regarding the gas dispersion and explosion machinery room of gas fueled ship to analyze the leaked gas dispersion and quantify the potential overpressure for Very Large Crude oil Carrier(VLCC), CFD code (CFX & FLACS) are used.

This research analyzed the gas leak and dispersion not only high pressure leak and but also low pressure leak according to the scenarios that can occur. Ventilation capability and gas detection sensor locations were verified through comparison between actual gas detection sensor and virtual monitor points. Gas leak simulation by CFD in cargo compressor room of 174K ME-GI LNG vessels is the first time study considering actual room structure, equipment and piping arrangement. LNG vapor gas dispersion simulation is complex and too much time is needed to do calculation. But flammable gas cloud prediction is very important to the builders as well as the ship-owners for identifying safety issues. This CFD modeling is based on the various specific scenarios which actually may be occurred during the ship's operation. The quantitative analysis presented in this paper is designed to make it easy for users to understand.

1.2.4 Objective

This research focuses on the actual CFD model of LNG gas dispersion for the potential scenarios and review IGC code whether the requirements are appropriate to user.

The main objectives of the study are as followings.

- Modeling of cargo compressor room structure, equipment and piping
- Physical properties setting of actual condition.
- Examination of gas dispersion modeling with “Fluent” in the cargo compressor room according to scenario.
- Verification of the ventilator capabilities.
- Decision of optimum gas detection points compared to actual gas sensors.
- Study of New IGC(International Gas Carrier) code through the CFD analysis.

2 Relevant technologies of LNG ships

2.1 LNG characteristics

LNG is natural gas converted to liquid form for storage and transportation. LNG occupies about 1 of 600th of the volume of natural gas. Natural gas becomes a liquid state at -162° C in atmospheric pressure. LNG is a cryogenic liquid with extreme low temperature. Tissues of plant or animal upon contact with the cryogenic liquid may be brittle, lost strength. LNG is odorless, colorless, non-flammable, non-toxic and noncorrosive. Important characteristics of LNG include chemical composition, boiling point, density and specific gravity, flammability, ignition and flame temperatures (The international group of liquefied natural gas importers, 2017).

2.1.1 Chemical Composition

The chemical composition of natural gas is followed of the gas source and type of disposal. "It is a mixture of methane, ethane, propane and butane with small amounts of heavier hydrocarbons and some impurities, notably nitrogen and complex sulphur compounds and water, carbon dioxide and hydrogen sulphide which may exist in the feed gas but are removed before liquefaction". Methane is the major component as shown on the Table 2-1.

Table 2-1 Typical chemical composition of LNG (GIIGNL, 2017)

Chemical	Chemical formula	Low(%)	High(%)
Methane	CH_4	87	99
Ethane	C_2H_6	<1	10
Propane	C_3H_8	>1	5
Butane	C_4H_{10}	>1	>1
Nitrogen	N_2	0.1	1
Other hydro carbons	Various	Trace	Trace

2.1.2 Boiling Point

The boiling point of LNG is different its basic composition, but -162°C is typical temperature at atmospheric pressure. When cold LNG comes in contact with water, air and the environment, It begins to boil at the junction, since the ambient temperature is higher than the LNG boiling point. Fig. 2-1 shows LNG boiling at the surrounding temperature and Table 2-2 shows some properties of Cryogens at their normal boiling. "The liquefaction process cools natural gas to change it to a liquid which reduces the volume occupied by the gas by approximately 600 times". LNG is converted into natural gas by the LNG regasification process for supplying to industrial and residential consumers (GIIGNL, 2017).

Table 2-2 Some properties of Cryogens at their normal boiling point(www.thermopedia.com, 2017)

	He_4	n-H_2	D_2	Ne	N_2	CO	F_2	Ar	O_2	CH_4	Kr	Xe	C_2H_4
Normal boiling point(K)	4.22	20.4	23.7	27.1	77.3	81.7	85	87.3	90.2	111.6	120	165	169.4
Liquid density(kg/m3)	125	71	163	1205	809	792	1602	1393	1141	423	2400	3040	568
Liquid density/vapor density	7.4	53	71	126	175	181	267	241	255	236	270	297	272
Enthalpy of vaporisation(KJ/kg)	20.42	446	301	86	199	216	175	161	213	512	108	96	482
Enthalpy of vaporisation(KJ/kg-mole)	80.6	899	1211	2333	5565	6040	6659	6441	6798	8206	9042	12,604	13,534
Volume of liquid vaporized by energy input of 1W-hr(cm3)	1410	114	74	35	22	21	14	16	15	17	14	13	13
Dynamic viscosity of liquid(μNsec/m2)	3.3	13.3	28.3	124	152	-	240	260	195	119	404	506	170
Surface Tension(mN/m)	0.1	1.9	~3	4.8	8.9	9.6	14.8	12.5	13.2	13.2	5.5	18.3	16.5
Thermal conductivity of liquid(mWm-1K-1)	18.7	100	~100	113	135	-	-	128	152	187	94	74	192
Volume of gas at 15 ° C released from 1 volume of liquid	739	830	830	1412	681	806	905	824	842	613	689	520	475
* Pressure of 1.01325 bar Source : Cryogenic Engineering, ed. B.A. Hands, Academic Press(1986)													

Fig. 2-1 LNG boiling at the surrounding temperature (GIIGNL, 2017)

2.1.3 Density and Specific Gravity

The density of LNG is between 430 kg/m3 and 470 kg/m3, less than half the density of water. Specific gravity or relative density of LNG gas is significantly less than the air, will be easily dispersed in open or well ventilated areas.

Under ambient conditions, LNG will become a vapor, as LNG is vaporizing, the cold vapors will condense the moisture in the air, often causes the formation of a white cloud vapor until the gas is warms, diluted, and distributed as shown in the Fig. 2-2.

Fig. 2-2 LNG vapor cloud (GIIGNL, 2017)

In case of a relative humidity of higher than 55%, the flammable cloud is totally included in the visible vapor cloud. And since the relative humidity is less than 55%, flammable clouds may be outside partially or completely visible clouds. This means that the steam can be fired even when the ignition source is away from the visible vapor cloud. The magnitude of the vapor cloud depends on the wind speed, direction and other weather conditions, and can be easily predicted by appropriate calculations. Cold vapors will rise because they are enough warmed by ambient air. At the boiling point temperature with -162°C and atmospheric pressure, LNG vapors have a relative density of about 1.8. It means that when initially released, the LNG vapors will remain near the ground due to heavier than air. "However as methane vapors begin to rapidly warm and reach temperatures around -110°C, the relative density of the natural gas will become less than 1 and the vapors become buoyant". At ambient temperatures, specific gravity of natural gas is about 0.6. It means that natural gas vapors are much lighter than air and will rise quickly. Cold LNG vapors with below -110°C will be negatively buoyant and more likely to build up in low areas until the vapors warm. As a result, LNG emissions from closed spaces or low places can replace air and cause breathing difficulties in this area (GIIGNL, 2017).

2.1.4 Flammability

Flammability is the ability of a material to burn or ignite and cause fire or combustion. Three things are needed to support a fire such as a source of fuel, air and a source of ignition as shown on Fig.2-3.

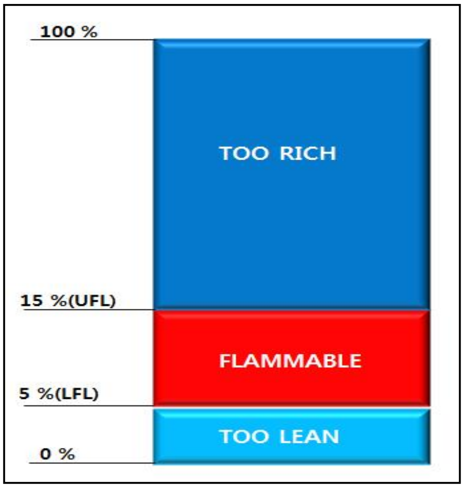

Fig. 2-3 Fire Triangle **Fig. 2-4** Flammability range of methane

Flammable range refers to the concentration range of gas or vapor which is burnt when a source of ignition enters. The limits are commonly called the "Lower Flammable Limit" (LFL) and the "Upper Flammable Limit"(UFL) as shown on Fig. 2-4.

The LFL and UFL is 5 % and 15 % methane by volume in air. Outside this range, the mixture of methane and air is non-flammable. Table 2-3 shows flammability limits for methane compared with other fuels. Many of the materials around us are highly flammable and it is important to recognize the limit of each material's flammability to ensure safe handling and use. Materials with a wide range of flammables have longer time to be in the range that can cause fire hazards, making them dangerous for emergency responders. For example, hydrogen and acetylene have a very wide range and can burn acetylene by each time the vapor is in the air more than 2 % to 80%.

Table 2-3 Flammability limits of hydrocarbon fuels (Source: NPFA Fire Protection Handbook)

Fuel	Lower Flammable Limit (%)	Upper Flammable Limit (%)
METHANE	5	15
BUTANE	1.86	7.6
KEROSENE	0.7	5
PROPANE	2.1	10.1
HYDROGEN	4	75
ACETYLENE	2.5	> 82.0

The proportion of methane in closed storage tanks or vessels is essentially 100 % in case of mostly liquid and some vapor state. It is rapidly mixed with less than 5 % of LNG vapor leaking from tanks in well-ventilated areas, resulting in less than 5 % of methane being mixed. The rapid mix ensures that the required concentration is obtained so that the fuel can be triggered only in small areas near the leak (GIIGNL, 2017).

2.1.5 Ignition and Flame Temperatures

The ignition temperature, also referred to as the automatic ignition temperature, is the lowest temperature at which gases or vapors for example natural gas in the air spontaneous combustion without the presence of sparks or flames. This temperature is dependent on the air-fuel mixture and pressure. For an air-fuel mixture with 10 % methane, the automatic ignition temperature is approximately 540° C. If the temperature is higher than the automatic ignition temperature, the ignition is performed for a shorter exposure time. Table 2-4 shows the standard state automatic ignition temperatures for some fuels, showing that diesel oil and gasoline are automatically burned at temperatures lower than LNG. The exact automatic ignition temperature of the natural gas changes depending on the element. Automatic ignition temperatures are reduced in case methane in natural gas begins to evaporate or is removed from the mixture. In addition to the ignition exposed to heat, the vapor in LNG can be fired immediately with flames, flames or static electricity when it is within fire's reach (GIIGNL, 2017).

Table 2-4 Auto-ignition temperature of some fuels at standard conditions (Source: BV 2009)

	NATURAL GAS	DIESEL OIL	GASOLINE
AUTO IGNITION TEMPERATURE	599 ° C	260 ~371° C	226~471 ° C

2.2 Hazards of LNG

The following potential hazards of LNG could be arise from LNG spill and discuss in the following pages(Cormier, 2008).

-Cryogenic hazards

-Over-pressurization

- Flash fire

- Pool fire

-Jet fire

-Rapid phase transition

-Vapor cloud explosion

-Rollover

2.2.1 Cryogenic hazards

LNG is stored and carried at cryogenic condition about−163°C. Cryogenic hazards are such as extreme thermal effects related with freezing of living tissue due to direct contact with very cold liquid. The embrittlement and subsequent failure due to cryogenic fluids affect carbon steel loses ductility and strength at cryogenic condition. Careful material selection is strongly requested in the LNG industry (Cormier, 2008).

2.2.2 Over-pressurization

The over-pressurization of LNG gas is the one of the recognized hazards in facilities. Insulation of this container or closing the pipe at both ends while the vessel or pipe contains a large quantity of liquid will cause the liquid to heat up, expand and evaporate. The vaporized gas will increase the pressure in the tank, pipe and incur the failure of the pipe and vessels. So safety protective equipment such as relief valves should be equipped in the LNG industry (West & Mannan, 2001 cited in Cormier, 2008).

2.2.3 Flash fire

A flash fire is a sudden and intense fire occurred by ignition of a mixture of air. As LNG evaporates due to boiling liquid, it will begin to mix with the surrounding air. The generated vapor travels in the wind and produces heavier cold vapor compared to air. As the cold vapor clouds continue to move in the wind, they are mixed with the additional air and diluted more. And some vapor portion will be between 4.4% and 16.5% with the flammable limits. If this portion of the flammable vapor comes in contact with an ignition source such as flames, sparks and electricity, the vapor may be ignited. The flame can then be propagated back to the vapor source, especially when the flammable areas of the cloud are persistent. Simple combustion of such uncontaminated vapor can ignite substances in the flame path and cause secondary fires, which can cause serious burns in people trapped in clouds. Damage to the equipment will generally be limited since then time of exposure to the fire will be relatively short (Zinn, 2005 cited in Cormier, 2008).

Fig. 2-5 Flash fire

2.2.4 Pool fire

If the LNG is accumulated as liquid state and encountered with ignition source, a pool fire can take place. Ignition can be happened at the pool location or the pool can be ignited by a vapor cloud fire. If the LNG spill expands from the source and continue to evaporation, pool fire will be lasted. Compare to a vapor cloud fire, the effects are more local but take longer (Qiao, et al., 2005, Zinn, 2005 cited in Cormier, 2008).

Fig. 2-6 Pool fire

2.2.5 Jet fire

If the flammable liquid is released from the pressurized tanks accidentally, the leak may be in the form of a spray of liquid droplets and vapor. If ignited, the resulting fire is called jet fire. Such a fire may also occur in pressurized vapor leakage. Jet fires represent the same type of hazards as pool fires. That is, direct fire contact and radiant heat from a jet fire is larger than full fire of similar size (Cormier, 2008).

Fig. 2-7 Jet fire

2.2.6 Rapid phase transition(RPT)

The phenomenon of rapid vapor transition has been observed when LNG is released under water. LNG vaporizes violently upon coming in contact with water. Although there is no combustion, loud "bangs" is occurred. This is known as a cold explosion or physical explosion, referred to as rapid phase transition (Cormier, 2008).

Fig. 2-8 Rapid Phase transition

2.2.7 Vapor cloud explosion

The explosion resulting from the ignition of a cloud of flammable vapor, gas, or mist in which flame speeds accelerates to sufficiently high velocities to produce significant overpressure.

When flammable vapor clouds caused by LNG leakage from wind driven accident reach the restricted area, overpressure or gas explosion may occur. Damage from such an explosion is limited to the area itself closed. Most buildings will have little resistance to reach their internal pressure limits, and they will actually explode (Kuhwoi, et al., West & Mannan, 2001 cited in Cormier, 2008).

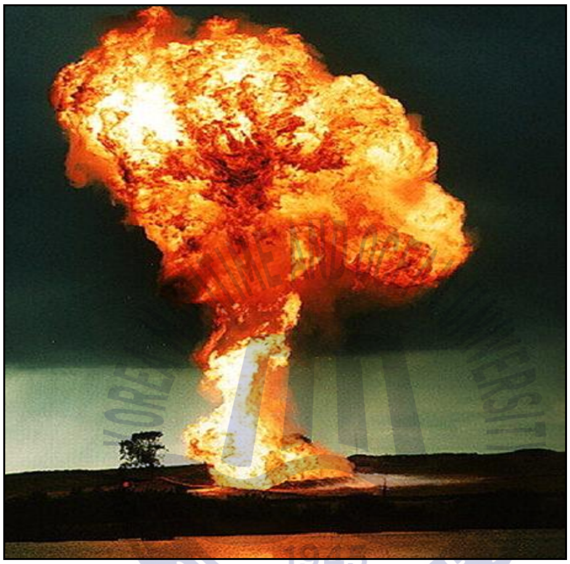

Fig. 2-9 Vapor cloud explosion

2.2.8 Rollover

"The addition of LNG with different densities to partially filled LNG tanks or the preferable evaporation of nitrogen has been known to lead to the formation of stratified layers. The difference is due to different LNG source or the weathering of LNG in the tank. "Owing to heat and mass transfer, the densities of the two layers approach each other. Consequently, mix of these two layers can cause a very rapid increase in boil off rates and tank pressure. So rollover may result in excessive loss of valuable fuels, or cause an extreme accident (Cormier, 2008).

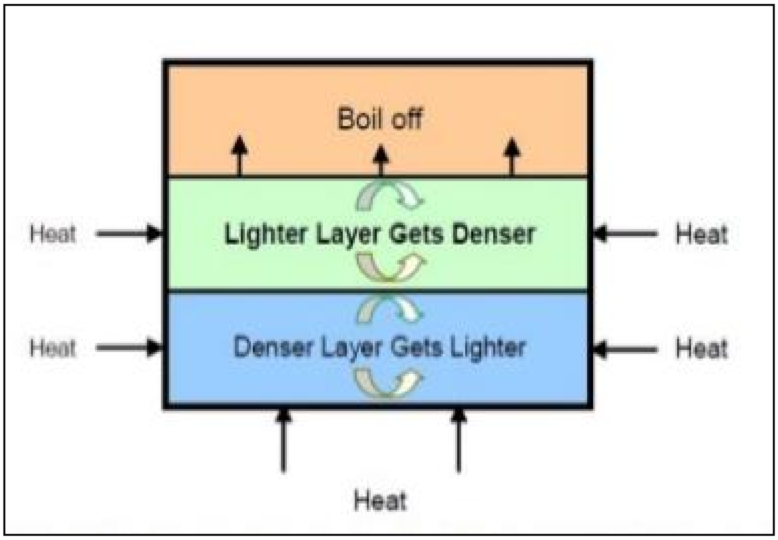

Fig. 2-10 Rollover

2.3 Gas detection system principles

A gas detection system with different technologies and principles can be used to detect the presence of various combustible and toxic gases. Point detection and open path detection are introduced. Gas detector consists of a sensor, a transmitter and a control module mainly.

"The function of the sensor is to convert the presence of a combustible or toxic gas into an electrically measureable signal. Then the signal is amplified by the transmitter and sent to the control module. The transmitter together with the sensor is called the detector head, control he module may be located at the same place with the detector head or other places. Some of the functions of the control module are alarm set point adjustments along with readouts, indication of status and give recorder outputs." The point detection and the open path detection principle have different fields of application (Båfjord, 2011).

2.3.1 Point detection

The point gas detector measures the concentration of target gases at the detector point. The flammable gas concentration is measured in % LFL and the concentration of toxic gases is measured in ppm or ppb (Honeywell, 2007 cited in Båfjord, 2011). A point gas detector will be used a limited area around its location. So as to measure the concentration, it needs to be in "physical contact" with the target gas. The point detection principle is applied to catalytic, infrared, electrochemical and semiconductor. "Since a point gas detector is only able to measure the gas concentration in a given point the gathering of information regarding gas dispersion in a module requires several point gas detectors distributed throughout the module. Point gas detectors are useful for coverage of limited areas" (Båfjord, 2011).

2.3.2 Open path detection

"An open path gas detector measures the amount of the target gas along a beam path. "An open path detector will be used for combustible gas detection and the infrared detection technology. The amount of combustible gas along the beam path is measured in LEL(Lower Explosive Limit) meter. LEL-m is the gas concentration times the length of the beam path. A small dense gas cloud with 100% LEL of one meter is the same output as a large dispersed gas cloud which has 5% LEL of 20 meters as shown on the Fig. 2-11.As a result of these two different gas clouds can give the same output values. An open path gas detector only measures the amount of gas along the beam path and do not measure the gas concentration at the specific point. Open path gas detectors have a long monitoring range. So they can be used for enveloping areas and critical equipment. Gas detection system requires that the different gas detection principles are applied in accordance with their characteristics (Båfjord, 2011).

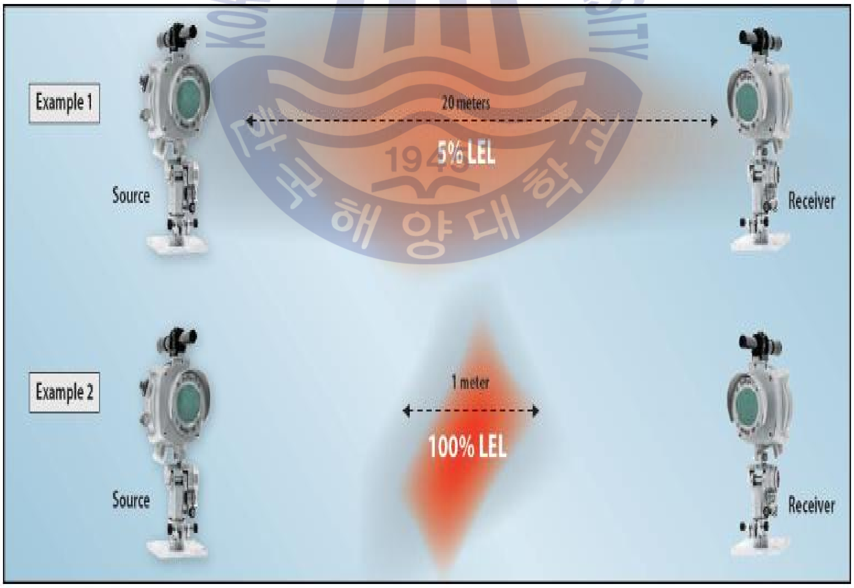

Fig. 2-11 Open path detection (Released from Omni instruments)

2.4 Kind of Gas detectors

Gas detection system applies for detection of combustible and toxic gases. Kind of gas detection system is the same as followings.

2.4.1 Catalytic

Catalytic detectors use the basic oxidation principle to detect a combustible gas. When the gas oxidizes, heat generates and the gas sensor converts this heat in to corresponding electric signals. A standard Wheat stone arrangement is used for this. The output from the gas sensor is equal to the concentration of gas in the area. The heater inside the sensor has two heating elements.

One is the active pellistor and the other is the inactive pellistor. Pellistor is solid device used to detect flammable gases with a large difference in thermal conductivitybetweenthe air. The active pellistor is placed in the catalyst. When the combustible gas reacts exothermically with the oxygen, temperature rises due to catalytic action.

The rise in temperature changes the resistance of the active pellistor. The catalytic reaction takes place on the surface of the catalyst. The inactive pellistor is non responsive to gas and gives the base line signal to compensate atmospheric temperature changes. This prevents false triggering of the alarm system (www.dmohankumar.wordpress.com, 2017).

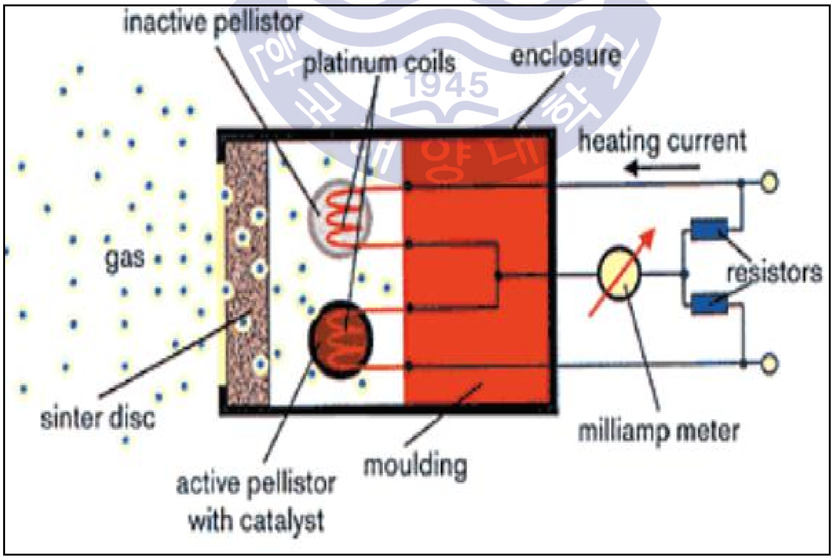

Fig. 2-12 Catalytic detection (www.archive.sensorsmag.com, 2017)

2.4.2 Infrared

Hydrocarbons have a certain property which allow for infrared measurement of their concentration. Most of the flammable gases and vapors are almost always detected by the infrared absorption of their properties. A double compensated infrared sensor and transmitter consists of an IR source, sapphire window, reflector, gas detector and reference detector. The radiation source of an infrared sensor is a flashing filament lamp, operated with low voltage, having a high percentage of Infrared radiation. Passing through an IR transparent window, this radiation is split into two parts by means of a beam splitter. One part is for the measuring detector, the other part is for the reference detector. A detector consists of a pyro-electric crystal converting the received radiation energy into a measurable voltage (Dragerpolytron, 2017).

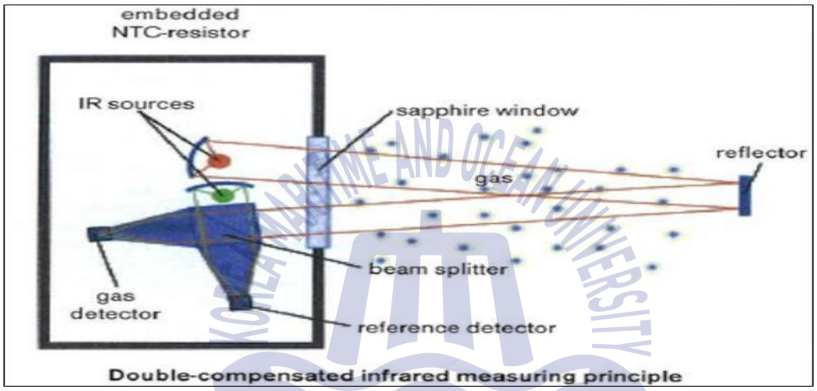

Fig. 2-13 Infrared detection (Dragerpolytron, 2017)

2.4.3 Electrochemical

Electrochemical detectors are used mainly to detect oxygen and toxic gases. "Each sensor is designed to be specific to the gas it is intended to detect. And electrochemical sensors are essentially fuel cells composed of noble metal electrodes in an electrolyte. The electrolyte is normally an aqueous solution of strong inorganic acids." When a gas is detected to the cell, a small current generates proportional to the concentration of the gas. An electrochemical sensor is composed of a diffusion barrier, a measuring-electrode, a counter-electrode and an electrolyte.

In case of free of chemically reactive gases, oxygen diffuses into the cell and adsorbs on both electrodes. The result is a stable potential between the two electrodes in which little, no current flows. In case chemically reactive gas passes through the diffusion barrier it is either oxidized or reduced depending upon the gas. The potential difference between the two electrodes causes a current to flow (www.cormsquare.com, 2017).

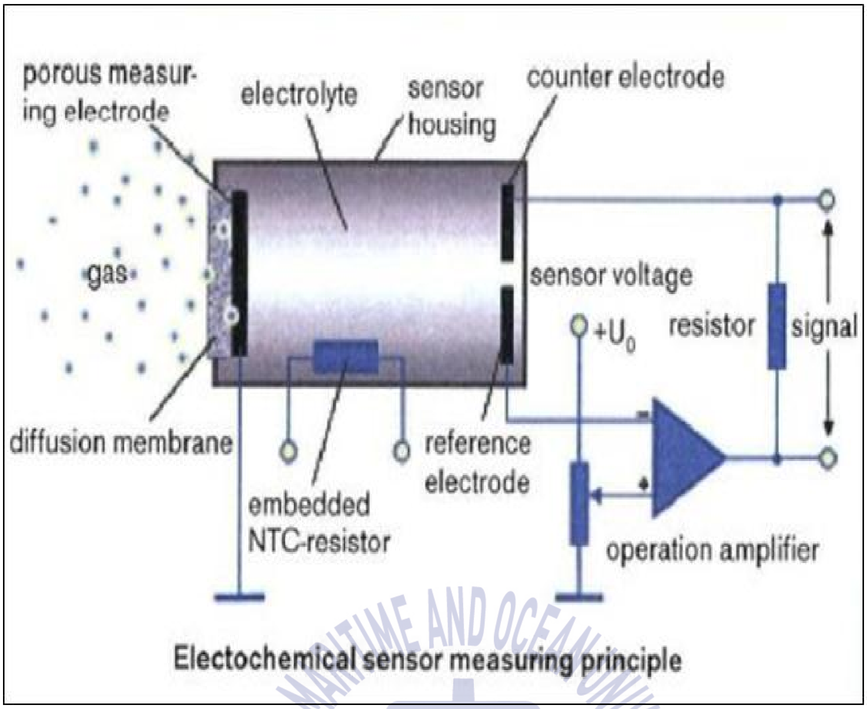

Fig. 2-14 Electro chemical detection (www.cormsquare.com, 2017)

2.4.4 Semiconductor

Operation principle is the same way as the catalytic sensors. They work because of the absorption of gas from the heated oxide surface. In reality, it is a thin layer of metal-oxide on a silicon slice by much the same process as is used in the manufacture of computer chips. After absorbing the sample gas from the oxide surface, catalytic oxidation enables the electrical resistance of the oxide to change, which can be associated with the concentration of the sample gas. The surface of the sensor is heated to a constant temperature of about 200-250 ° C to speed up its reaction and reduce the effects of ambient temperature changes. Semiconductor sensors can be simple, fairly robust and very sensitive.

They have been used with some success in the detection of H_2S gas and also widely used in the vendors of inexpensive gas detectors. But they have been found to be pretty unreliable for industrial applications, since they are not very specific to a particular gas and they can be affected by atmospheric temperature and humidity variations (Honeywell Analytics, 2017).

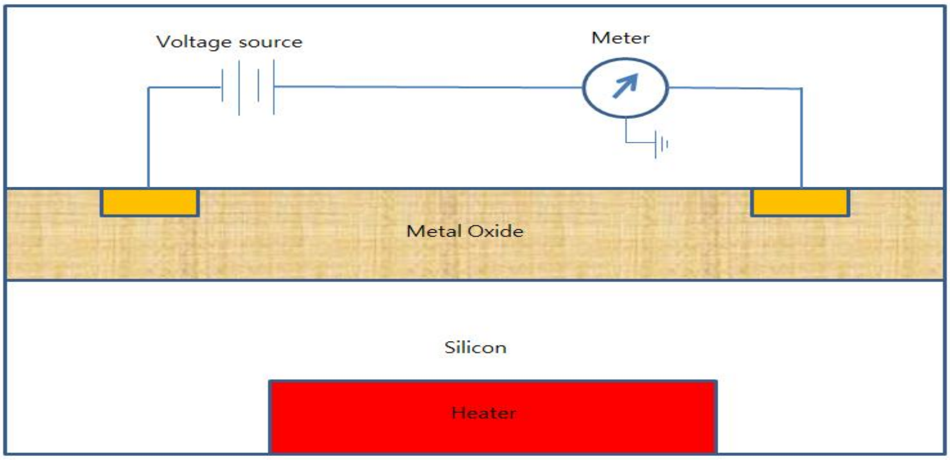

Fig. 2-15 Semiconductor detection (Honeywell Analytics, 2017)

2.5 Equipment in cargo compressor room

The LNG carrier had been designing and constructed carrying cryogenic liquefied natural gas -163 ° C, cargo handling equipment is located in cargo compressed room. The function of the main equipment in cargo compressor room is tabulated below as Table 2-5.

Table 2-5 Main Equipment of fuel gas supply system in cargo compressor room

No.	Name	Q’ty	Function
1	Hi pressure pump/vaporizer	1 set	To supply generating fuel gas to the main engines and generator engines
2	High pressure fuel gas compressor	1 set	To supply the natural boil off gas to the main engines and generator engines
3	Vapor return compressor	2 sets	To transfer the generated vapor to the shore during loading
4	LNG vaporizer	1 set	To supply cargo vapor to the cargo tanks
5	Vapor return heater	1 set	To heat the LNG vapor so as to warm up cargo tanks

6	Re-liquefaction equipment	1 set	To re-liquefy BOG to LNG
7	GCU gas blowers	2 sets	To increase the gas pressure from the cargo tanks and supply gas to GCU (Gas Combustion Unit)
8	Fuel gas heater	1 set	To heat fuel gas generated by High pressure pump and vaporizer
9	Vacuum pump	2 sets	To extract air from the insulation space of the cargo tanks for supplying inert gas
10	Cargo drain cooler	1 set	To cool down condensate lines from vaporizer and gas heater.
11	Gas valve train	2 sets	To supply the fuel gas to the main engines

2.5.1 Hi pressure pump/vaporizer

It is consist of two(2) main equipment, two(2) hi pressure pump and one(1) vaporizer. The high pressure pump will bring the LNG at the required pressure before vaporization and LNG is vaporized by the vaporizer. High pressure gas supplies to the main engines with 300 bar and low pressure gas which is reduced pressure by the control valve supplies to generator engines. The capacity and main particular of the LNG HP pumps shall be as follows.

Fig. 2-16 High pressure pump/vaporizer (Released from Cryostar)

No. of unit	Two(2)
Capacity	-
Head	6,400 mLC at SG of 0.5
Type	Reciprocating
Drive by	Electric motor with VFD(variable frequency Driver)

The LNG vaporizer shall be provided for generating of FG to supply LNG to ME-GI engines.

No. of unit	One(1)
Capacity	-
Service pressure	305 bar
Type	shell & tube type
Heating medium	Glycol water
Size	7,000WX3,670DX3,300H

2.5.2 High pressure fuel gas compressor

Fuel gas compressor shall be used to maintain the cargo tank pressure, transfer the natural boil off gas to the main engine and generator engines. Normally one(1) set is installed in cargo compressor room and service pressure is 305 bar. The capacity and main particular of the FG compressor shall be as follows.

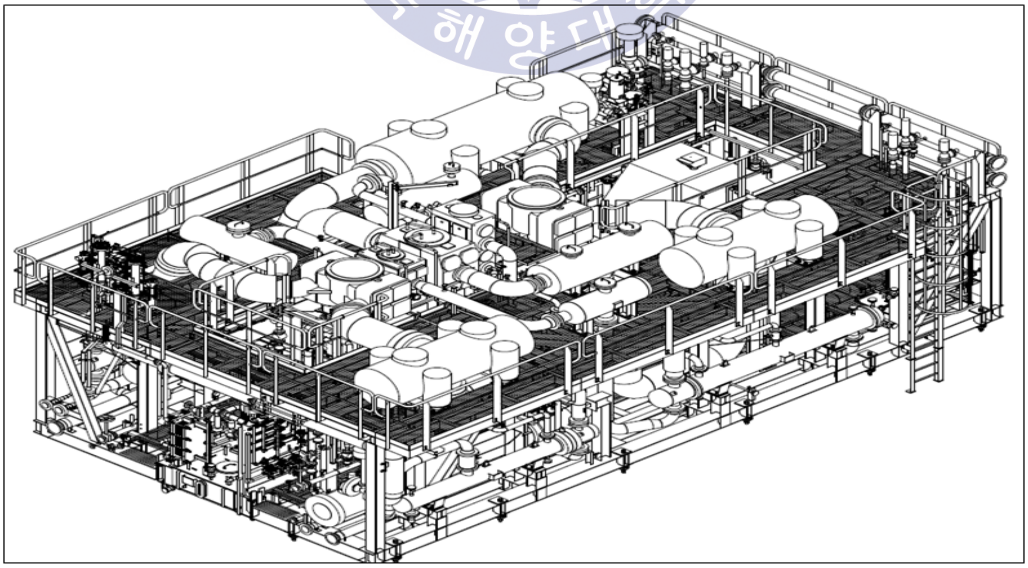

Fig. 2-17 High pressure fuel gas compressor (Released from BCA)

No. of unit	One(1)
Capacity	-
Service pressure	305 bar
Type	Reciprocating
Drive by	Electric motor
Size	1,3000WX8,150DX5,000H

2.5.3 Vapor return compressors

Vapor return compressor shall be used to transfer the generated vapor to the shore during loading and initial cooling down and recirculate the cargo vapor for cargo tank warming up. Normally two(2) sets are installed in cargo compressor room and service pressure is about 1 bar. The capacity and main particular of the vapor return compressor shall be as follows.

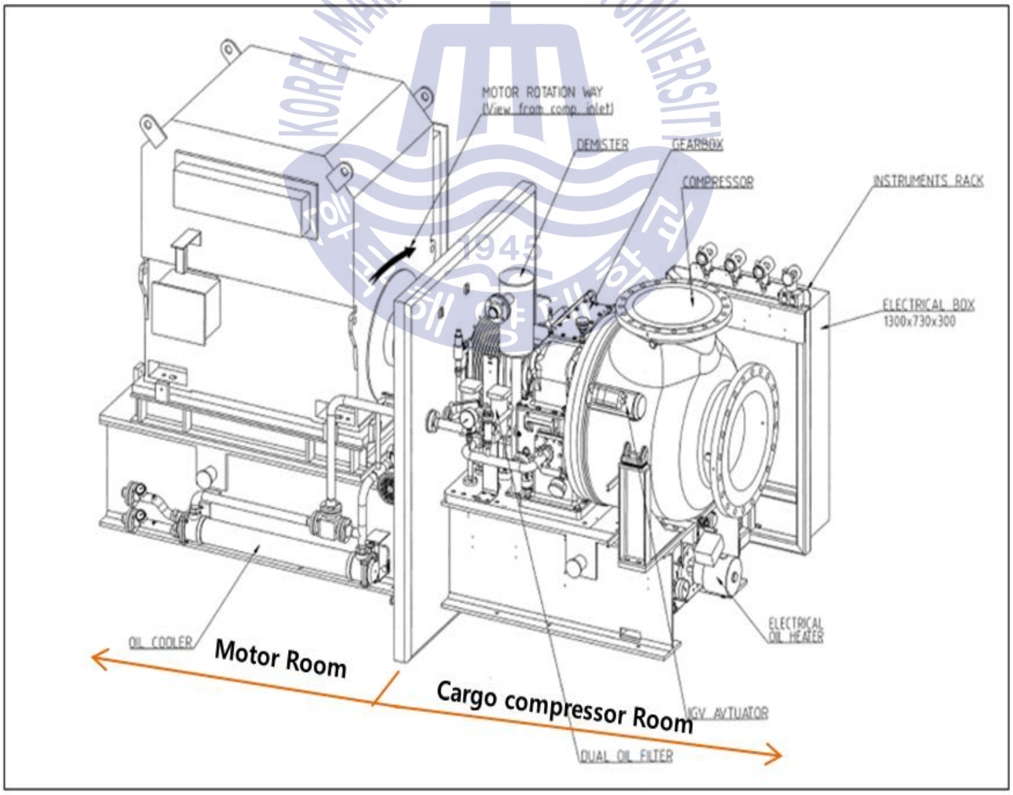

Fig. 2-18 Vapor return compressor (Released from Cryostar)

No. of unit	Two(2)
Capacity	-
Service pressure	1.0 bar
Type	Centrifugal
Drive by	Electric motor
Size	2,300WX2,370DX2,050H

2.5.4 LNG vaporizer

LNG vaporizer shall be used to supply cargo vapor to the cargo tanks when the cargo pumps are discharging at the design flow rate without the vapor supply from shore, purge inert gas from cargo tanks and supply inert gas to insulation space receiving liquid nitrogen.

Fig. 2-19 LNG vaporizer (Released from DSME)

No. of unit	One(1)
Capacity	-
Service pressure	9 bar
Type	Shell & tube type
Drive by	Steam heater
Size	4,033Wx630Dx1,750H

2.5.5 Vapor return heater

Vapor return heater shall be used to heat the BOG to the Gas combustion unit, heat the LNG vapor sent by both VR compressors so as to warm- up the cargo tanks and heat the inert gas during inerting operation.

Fig. 2-20 Vapor return heater (Released from DSME)

No. of unit	One(1)
Capacity	-
Service pressure	9 bar
Type	Shell & tube type
Drive by	Steam heater
Size	3,818Wx924Dx1,750H

2.5.6 Re-liquefaction equipment

Partial Re-liquefaction system shall be used for liquefaction of surplus natural boil off gas during laden voyage. It is composed of a heat exchanger, liquid-gas separator, and Joule-Thomson valves.

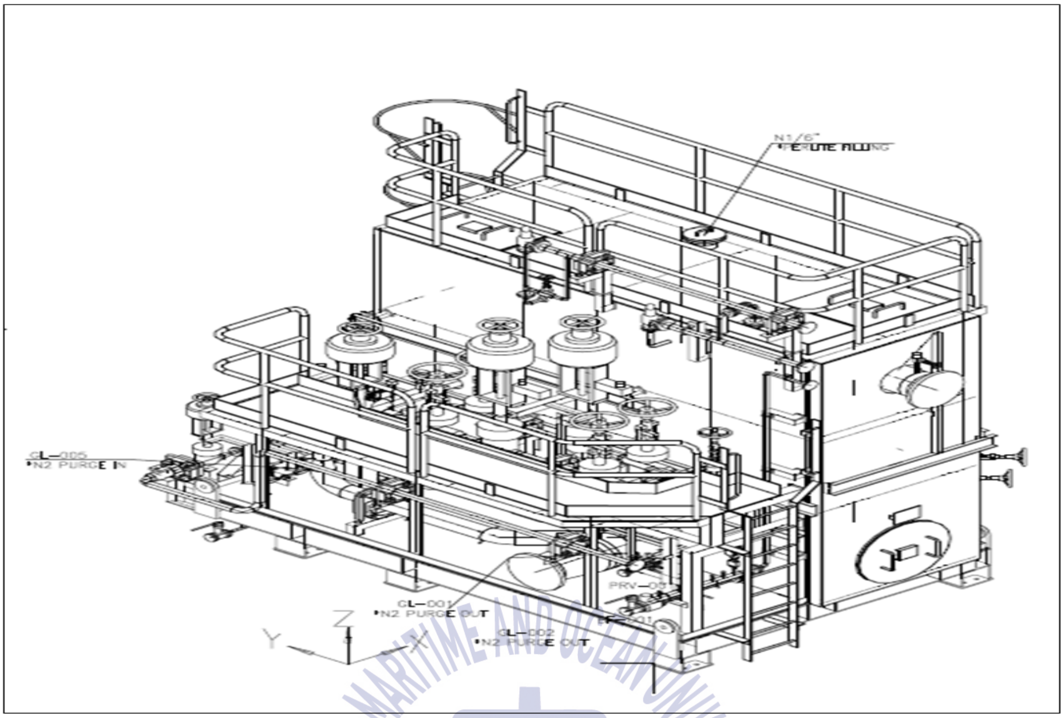

Fig. 2-21 Re-liquefaction equipment (Released from Sunbo)

No. of unit	One(1)
Capacity	-
Service pressure	305 bar
Type	Refrigerant cycle principle
Drive by	High pressure FG compressor
Size	4,900WX2,250DX4,000H

2.5.7 GCU gas blower

Two(2) sets gas blowers shall be used to boost the BOG when supplied directly from cargo tanks

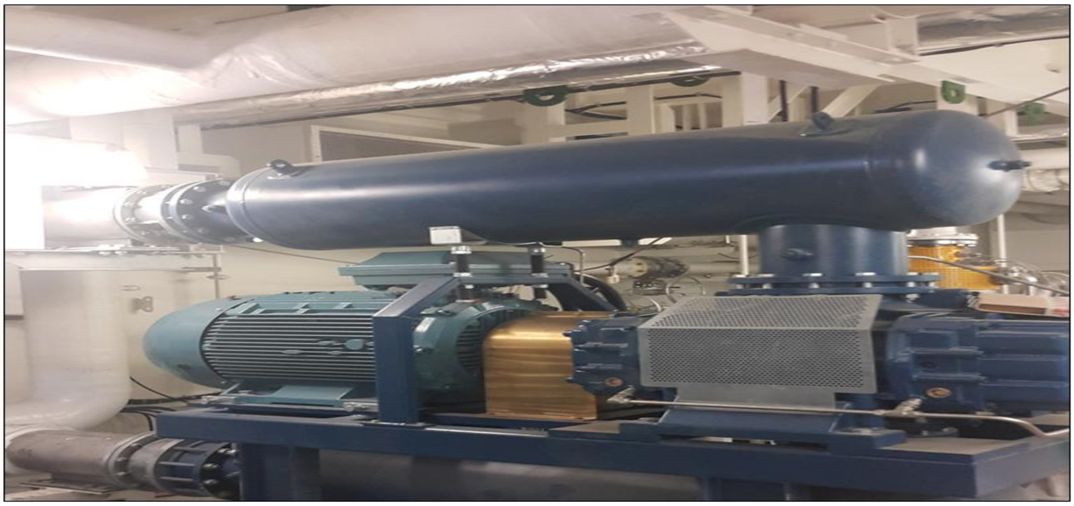

Fig. 2-22 Gas blower (Released from DSME)

No. of unit	Two(2)
Capacity	-
Service pressure	1 bar
Type	Positive displacement type
Drive by	Electric motor driven
Size	1,950WX800DX2,180H

2.5.8 Fuel gas heater

Fig. 2-23 Fuel gas heater (Released from DSME)

No. of unit	One(1)
Capacity	-
Service pressure	9 bar
Type	Shell & tube type
Drive by	Steam heater
Size	3,200Wx340Dx850H

2.5.9 Vacuum pumps

Two(2) sets vacuum pumps shall be provided to give the insulation space of the cargo tanks a vacuum for inerting.

Fig. 2-24 Vacuum pump (Released from Kowel)

No. of unit	Two(2)
Capacity	-
Service pressure	0.2 bar a.
Type	Screw type
Drive by	Electric motor
Size	2,635WX1,600DX1,378H

2.5.10 Cargo drain cooler

One(1) set cargo drain cooler shall be used to cool down condensate lines from vaporizer and gas heater.

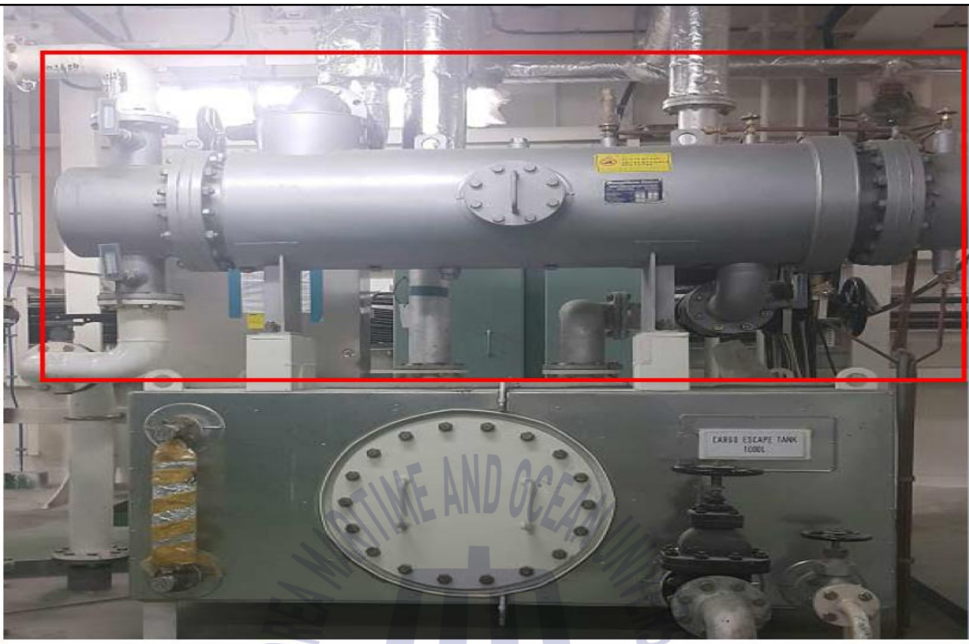

Fig. 2-25 Cargo drain cooler on the bilge tank (Released from DSME)

No. of unit	One(1)
Service pressure	7 bar
Type	Shell & tube type
Drive by	Steam heater
Size	2,100WX450DX800H

2.5.11 Gas Valve Train

It is designed for operation using Methane gas as engine fuel at a maximum working pressure of 400 bar. The Gas Valve Train is a single component designed for controlling and directing the flow of Methane gas delivered from the Fuel Gas Supply System to the engine or to the exhaust. The Gas Valve Train is a safety component whose main function it is to supply gas to the engine

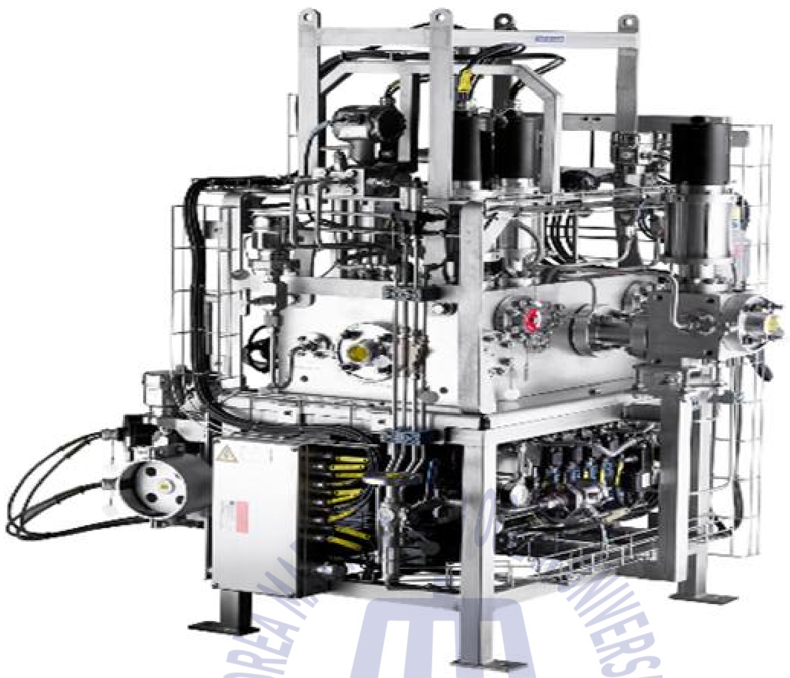

Fig. 2-26 Gas valve train (Released from Man Diesel & turbo)

No. of unit	Two(2)
Service pressure	305 bar
Size	1,300WX1,170DX1,400H

Fig. 2-27 shows that general arrangement of ME-GI & Re-liquefaction system in cargo compressor room. The main fuel gas consumers are two(2) sets of ME-GI main engine and four(4) sets of DFGE(Dual Fuel Generator Engine) which are located in engine room. Fuel gas with 305 bar can be supplied by high pressure fuel gas compressor or Hi pressure pump/vaporizer. Re-liquefaction equipment which is located in the cargo compressor room and the GCU(Gas Combustion Unit) which is located in the engine room can be used in case of excessive BOG treatment.

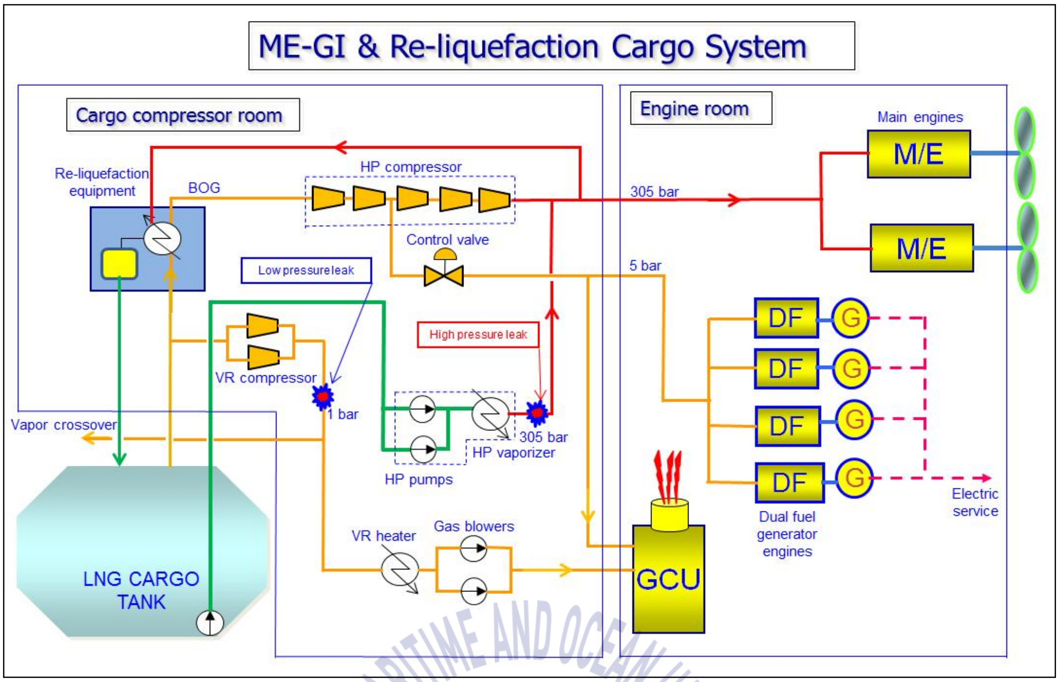

Fig. 2-27 General Arrangement of ME-GI & Re-liquefaction system (Concept design from DSME)

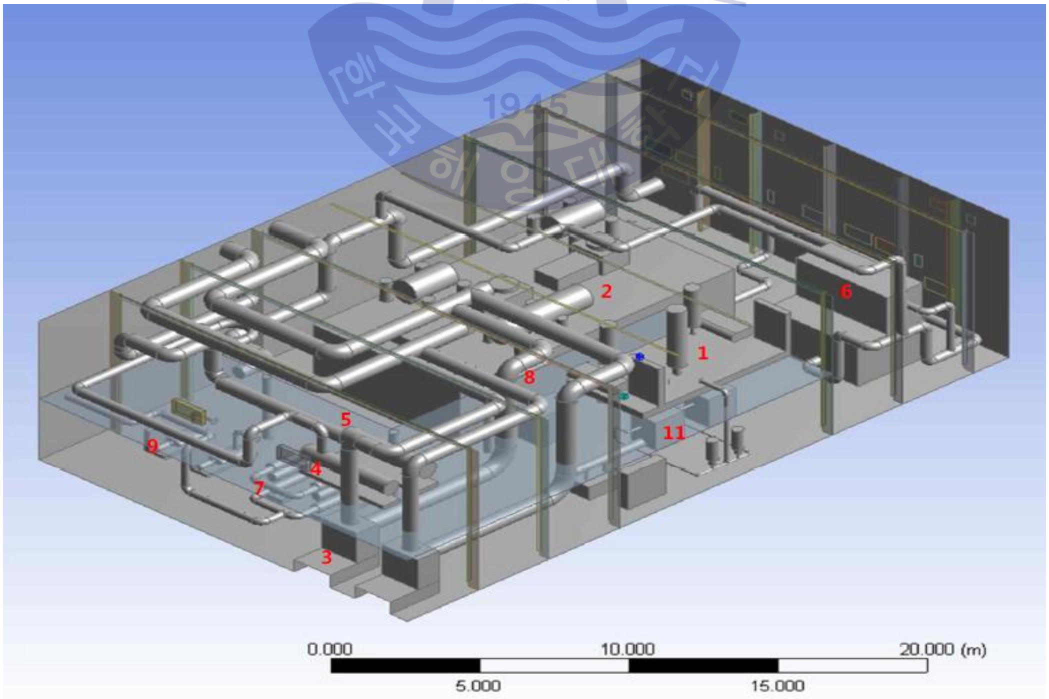

Fig. 2-28 Geometry in cargo compressor room iso1

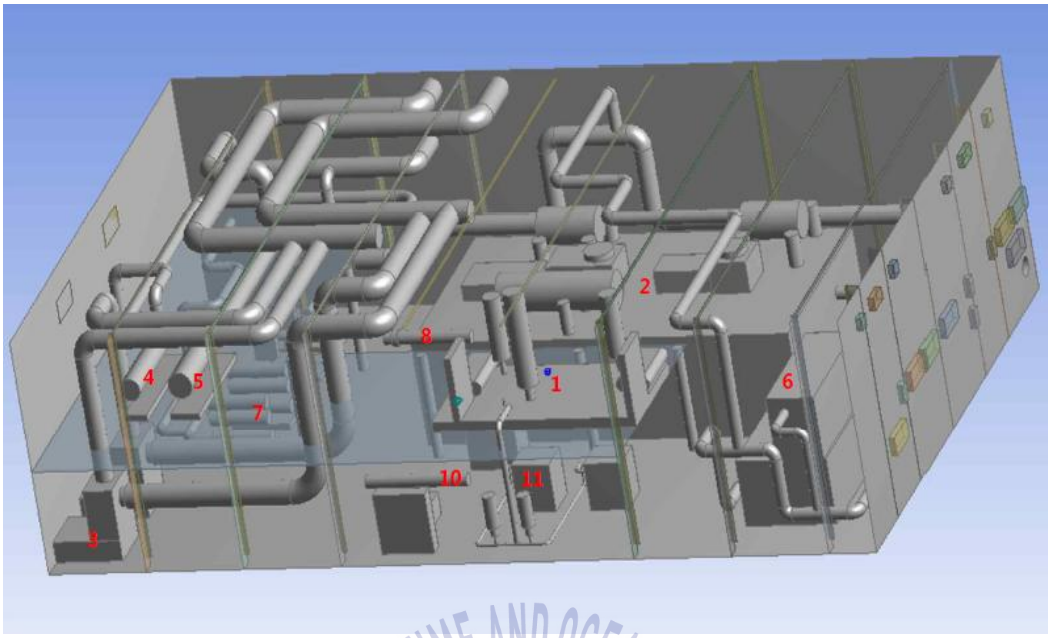

Fig. 2-29 Geometry in cargo compressor room iso2

3. Review of Precedent Literature

3.1 Gas dispersion, explosion and ventilation literatures

Min. D.C.(2012) studied CFD simulation to analyze the dispersion and explosion of combustible gas considering various variables including combustion type of leaked substances, geometry of facility, warm currents, barriers, the influence wind and other factors.

Kim. K.P.(2014) studied Natural Gas Dispersion and Explosion in Gas Fueled Ship. This study in particular shows near-field blast waves CFD method to understand the risk posed by the different gas leakages, and show some blast prediction validation examples.

Seok et al. (2013) studied basic study on fire and explosion prevention, numerical simulations on combustion was carried out through commercial grid generation.

Hooff and Blocken(2013) studied natural ventilation of indoor environments by the concentration decay method. CFD simulations can be used to assess indoor natural ventilation by solving the interaction between the urban wind flow and the indoor airflow. Air exchange rate (ACH) can be obtained from simulated volume flow through ventilation openings or from concentration breakdown methods commonly used in experimental studies. The flow of wind, indoor air flow and heat, and dispersion of water vapor and CO_2 are modeled based on a high-resolution grid based on a grid sensitivity analysis. The validated CFD models are used to analyze the significant horizontal and vertical CO_2 concentration gradient at the stadium.

Sun et al.(2015) studied dynamic simulation of hazard analysis of radiations from LNG pool fire. Dynamic simulation of flame generation was carried out assuming an LNG pool fire occurred in the fire area. Simulation results showed that LNG tanks in neighboring disk areas were able to withstand the radiation from heat flows, and areas related to human activities, such as security offices and public places, were safe enough to escape the risks. CFD methods are so effective that they take into account the LNG disaster analysis and provide realistic results for complex scenarios.

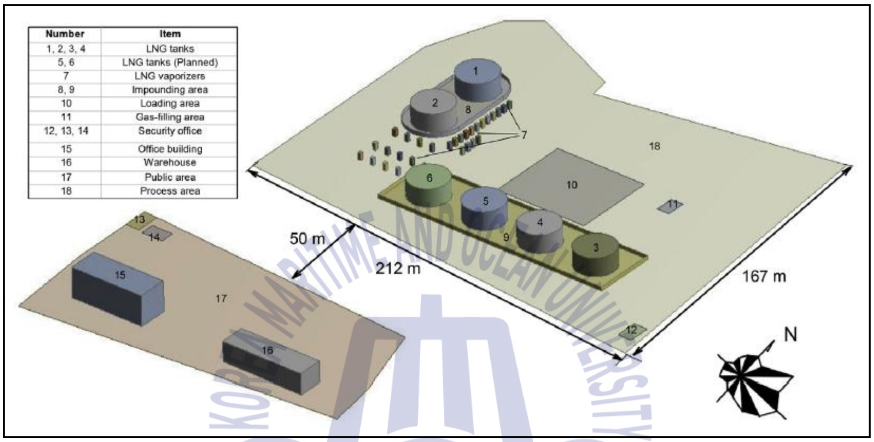

Fig. 3-1 Layout of the investigated LNG satellite terminal (Sun et al., 2015)

Gavelli et al. (2008) studied LNG spill test with Fluent which is widely used commercial code. This paper describes the important parameters that CFD models need to accurately predict the behavior of very low temperature runoff in an area that is exponentially more complex, and explains the gas concentration measured during the Falcon-1 test with fluency. Finally, this paper discusses the effects of the steam barrier on inclusion of a portion of the release, reducing the areas of risk that may be needed, and therefore reducing the vapor clouds that can be fired.

Benjamin et al. (2009) performed Medium-scale LNG tests at the Brayton Fire Training Field (BFTF). The CFD code showed good agreement with the data collected during the November 2007 test performed at BFTF. This paper showed the simulated setup and the comparison with the data collected for both scenarios. Release on water and concrete. Once the model was adjusted for experimental data, it was used to analyze its sensitivity to parameters that evaluate the effect on LFL distances and concentration levels. In addition, three turbulence models were compared. The source term was composed of turbulence intensity at the source, LNG pool geometry, mass evaporation rate, and LNG pool area. The vapor dispersion parameters were wind velocity, sensible heat flux, and obstacles effects. It was concluded that at low wind velocity, the source term parameters strongly influenced the LFL distance and the concentration level. On the other hand, at high wind velocity, the source term parameter had a slight effect on the LFL distance and the concentration levels.

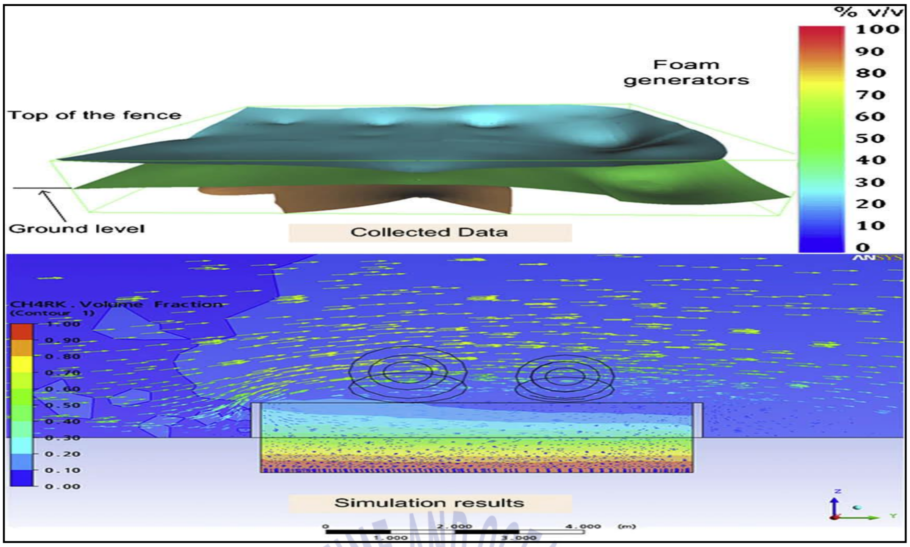

Fig. 3-2 Concentration profile for TEEX7 inside the fence and pit (Benjamin et al., 2009)

Heo(2013) studied structural response of offshore plants to Risk-Based Blast Load. The design overpressure load for the sample offshore plant is determined by the proposed stochastic approach to that of this study. Using the CFD analysis results using the flame acceleration simulator FLACS_ v.1, create an overpressure hazard curve.

Tauseef et al. (2011) studied CFD-based simulation of dense gas dispersion in presence of obstacles. In this paper, CFD was considered as a strong tool to realistically estimate the consequences of accidental losses in containment, since it allows consideration of the effects of complex terrains and obstacles present in fluid dispersion paths. The key to the diffusion simulation using CFD successfully is the accuracy of assessing the effects of turbulence due to the presence of an obstacle. The correct selection of the most appropriate turbulence model is therefore vital to the successful implementation of CFD in the dispersion modeling and simulation of toxic and/or flammable materials. In this paper, it was intended to use CFD to assess the distribution of heavy gases if there are obstacles.

Dan et al. (2010) studied explosion simulation for the filling station, in this research, the quantitative risk analysis for using alternative mixtures in existing recharging facilities has been studied by three type explosion model. TNT equivalent model, PHAST and CFD based FLACS to manage the risk effectively.

Koet al. (2015) studied three simulation approaches for turbulence applied for the computation of propane dispersion in a simplified real scale urban area with one building. Large Eddy Simulation (LES), Detached Eddy Simulation (DES), and Unsteady

Reynolds Averaged Navier-Stokes (RANS) are applied separately. LES and DES showed relatively similar results for the eddy structure and propane distribution, while the RANS prediction of the propane distribution was unrealistic. RANS was found to be inappropriate for computation of the gas dispersion process due to poor prediction performance for the unsteady turbulence.

Hanna et al. (2009) studied computational fluid dynamics model for the transport and dispersion of the dense chlorine cloud. Two accident location are studied, an actual railcar accident at an industrial site in Festus, MO, and a hypothetical railcar accident at a rail junction in the Chicago urban area. The results showed that large quantities of high-density gas releases from industrial sites or metropolitan areas could grow by more than 100 meters first when transported from the ground. Dark clouds can follow terrain drainage, such as a river. These barriers tend to slow down dark gas clouds near their source, which can reduce the cloud's density and increase its density. Depending on the strong winds, this obstacle could increase mixing and dilute as clouds grow.

Luketa-Hanlin(2007) studied LNG dispersion such as specification of the domain, grid, boundary and initial conditions. A description of the $k-\varepsilon$ model is presented, along with modifications required for atmospheric flows. Validation issues pertaining to the experimental data from the Burro, Coyote, and Falcon series of LNG dispersion experiments are also discussed. A description of the atmosphere is provided as well as discussion on the inclusion of the Coriolis force to model very large LNG spills.

Jang, et al.(2012) studied the "process of leaked gas, distribution patterns, and flames and overpressure generated from gas explosions in 2D and 3D virtual spaces" by reviewing more accurately analyzable computational fluid dynamics model by considering various variables including combustion types of leaked substances, geometry of facility, warm currents, barriers, the influence of wind, and others.

Kim, et al.(2015) studied "An explosion analysis for a gas supply machinery room of LNG-fueled container ship". The fuel gas concept is employed for the high pressure ME-GI engine where a leakage in the natural gas double supply pipe to the engines is the subject of the present analysis. The consequences of a leak are simulated with CFD tools to predict typical leak scenarios, gas cloud sizes and possible explosion pressures.

Baek, et al. (2016) studied a CFD simulation to compute the explosion risk of danger-frequent combustible gases - hydrogen, LNG, and LPG - within a limited space, and the outcomes were compared and analyzed to review the risk of explosion of each gas within a limited space.

Kang, et al. (2013) evaluated comparison of the risk according to the type of fuel by three-dimensional simulation tool(FLACS). The consequence analysis of fire explosion and jet-fire was carried out in the layout of typical high pressure gas filling stations using CNG, hydrogen and 30% HCNG.

Lee, et al. (2015) studied "The effect of facility confinement on explosion power for process plant facility". The level of confinement of a facility was simplified with "VBR(volume blockage ratio) and averaged size of obstacles". FLACS was used for simulating the CFD results showed that excessive pressure tended to increase as VBR increases and the number of obstacles increased. This study can be applicable to provide safety instructions for the containment of the facility in the event of flammable gases and steam leakage from process factories.

Chan (1992) studied "Numerical simulation of LNG vapor dispersion fenced storage area". The model was able to duplicate the key results of the experiment in two factors in most situations. For Falcon-l, the results were consistent with field observations with additional heat flux in the source region to model the over-temperature effect. In particular, steam clouds have been replicated for filling a enclosure with fences, whereas steam clouds contained in the fence have always been observed in pre-spill wind tunnel simulations. A simple approach to modeling turbulence and heat transfer in the source region is currently well performed, but more precise forecasting may require more detailed modeling of the source. Simulation results from the Falcon-4 experiment show that an LNG vapor fence can significantly reduce the blowing streets and dangerous areas of flammable steam clouds. However, since the steam fences may also prolong the cloud duration in the source areas, the likelihood of ignition and combustion in the steam fences and nearby areas may also increase.

Eidsvik (1980) studied "A model for Heavy Gas Dispersion in the atmosphere". A simple model for the dispersion of heavy and cold gas clouds is developed. The horizontal dimension of the cloud is assumed to increase due to the gravity drop in the cloud. Cold clouds heat up from the bottom and from air intrusion. It is assumed that the initial speed of restraint is proportionally linear to the forward speed and collapses into a rectangle. The upper surface entrainment is estimated as for atmospheric inversions and density interfaces in laboratory flows. Model predictions are shown to not vary decisively with changes in coefficients. Experimental data on the spread of heavy metals are correctly predicted. The risk of heavy gas clouds is expected to depend especially on environmental conditions, such as the roughness and average wind speed of the underlying surface.

Hannaa et al. (2004) studied "CFD model simulation of dispersion from chlorine railcar releases in industrial and urban areas" The following experiment was used to practice the assessment. "Kit Fox (52 trials with puff and plume releases of slightly dense CO_2 gas in arrays of billboard-shaped obstacles), MUST (37 trials with puff releases of neutrally buoyant tracer gas in an array of 120 shipping containers), Prairie Grass (43 trials with continuous plume releases of neutrally buoyant tracer gas over a flat agricultural field), and the EMU L-shaped building (a wind tunnel experiment involving a release from an open door in the courtyard area of an L-shaped building)” . All of these results are well compliant with the acceptance criteria for the distributed model. When evaluated with EMUL data, it is shown that 72 % of FLACS predictions are within two observation ranges and that the model can predict the dimensions of the recirculation factor behind a building. When evaluating other CFD models, it is recommended to use these broad data sets, including releasing the tracer from the object layout.

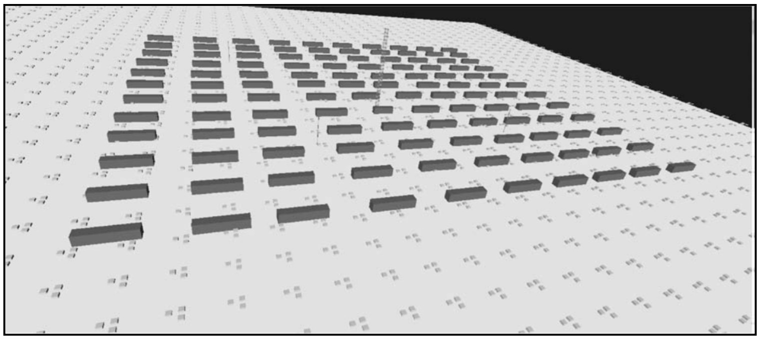

Fig. 3-3 Locations of 120 obstacles in MUST experiment (Hannaa et al., 2004)

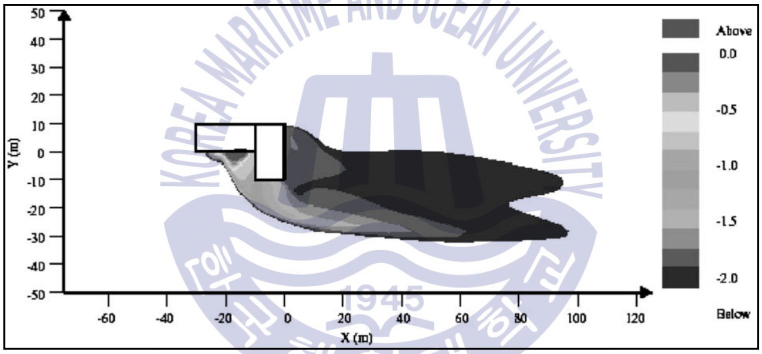

Fig. 3-4 Locations of 120 obstacles in MUST experiment (Hannaa et al., 2004)

Pontiggiaa et al. (2010) studied release of hazardous materials in urban areas major concern in industrial risk assessment. In urban areas, many buildings with complex geometries are associated with the move to 3D fields that strongly affect gas dispersion representing such a complex geometry realistically in a simple but detailed simulation model is complex and often can limit its utility. In this study, the method for building and switching to a 3D urban model led to a relatively fast and simple domain design technique by accessing spatial and geographical features. Since the magnitude of the results also depends on the absorbed doses depending on both concentrations and exposure time, a simple methodology for assessing doses could be developed to estimate the areas with a specific mortality probability, such as CFD code. The approach was developed and applied to case studies with different atmospheric layering conditions. The results were compared to those obtained using an integrated model. It was discovered that the integrated model can overvalue and underestimate the magnitude of the results associated with the release of hazardous substances in urban areas.

Koopmana and Ermak (2007) made lessons and learned from 1977 to 1989. "The Lawrence Livermore National Laboratory (LLNL) conducted a liquefied gaseous fuels spill effects program under the sponsorship of the US Department of Energy, Department of Transportation, Gas Research Institute and others. "The purpose of this program was to develop and validate tools that can be used to predict the effects of large liquid gas releases through field experiments and to predict the conditions that will not be tested. LNG spill experiments were conducted to study cloud formation, combustion, dispersion, and Rapid Phase Transition. Specific conclusions are the same as followings.

Fig. 3-5 Coyote Vapor burn and Coyote RPT (Koopmana & Ermak, 2007)

Vapor cloud of LNG is wider and lower than trace gas clouds, and tend to follow downward slope of the terrain due to weakened vertical turbulence and gravitational flows in the clouds. "Under low wind speed, stable atmospheric conditions, a bifurcated, two lobed structure develops". Navier-Stokes equations well explained the most complete description of LNG dispersion, but more highly parameterized. Lagrangian models were found to be well appropriated to emergency response applications. The heat flux measured by the LNG vapor cloud combustion exceeded the level required for the 3-degree burn and was large enough to ignite most of the combustible material. RPTs consist of two types, the source of generation and the concentrate. It has been observed that RPTs is doubling the combustion area and extending the combustion distance through the wind by 65 %.

Fig. 3-6 Falcon 1 spill showing LNG vapor overflowing the vapor fence (Koopmana & Ermak, 2007)

Middha et al. (2010) studied "CFD calculations of gas leak dispersion and subsequent gas explosions". Forschungszentrum Karlsruhe (FZK) conducted experiments with the release rates of vertical upward hydrogen on plates with two different geometric configurations at different rates. The dispersed clouds then ignited and recorded an explosive overpressure. Blind CFD simulations were performed prior to the experiments to predict the results. The simulated gas concentrations were found to be reasonably well associated with observations. It was then performed very well compared with the results of the observations in the same ignition position as the ignition position at the time of experiment. This agreement points to the ability of FLACS as CFD tool, to model such complex scenarios even with hydrogen.

Qi Ruifeng et al. (2010) use the ANSYS CFX CFD code to make model LNG vapor dispersion in the atmosphere. The atmospheric conditions, evaporation rate of LNG and pool area, ground surface temperature, turbulence of the source term, and roughness height, and obstacles effect are discussed. An sensitivity analysis was performed to account for uncertainties in simulated results resulting from mesh size and source condition turbulence intensity. The Brayton Fire Training Center also conducted a medium-sized LNG leak test to collect data to validate ANSYS CFX predictions. Comparison of test data with simulated results revealed that CFX was able to account for the dense gas behavior of LNG vapor clouds, and the prediction of wind gas concentrations close to ground was consistent with the test data.

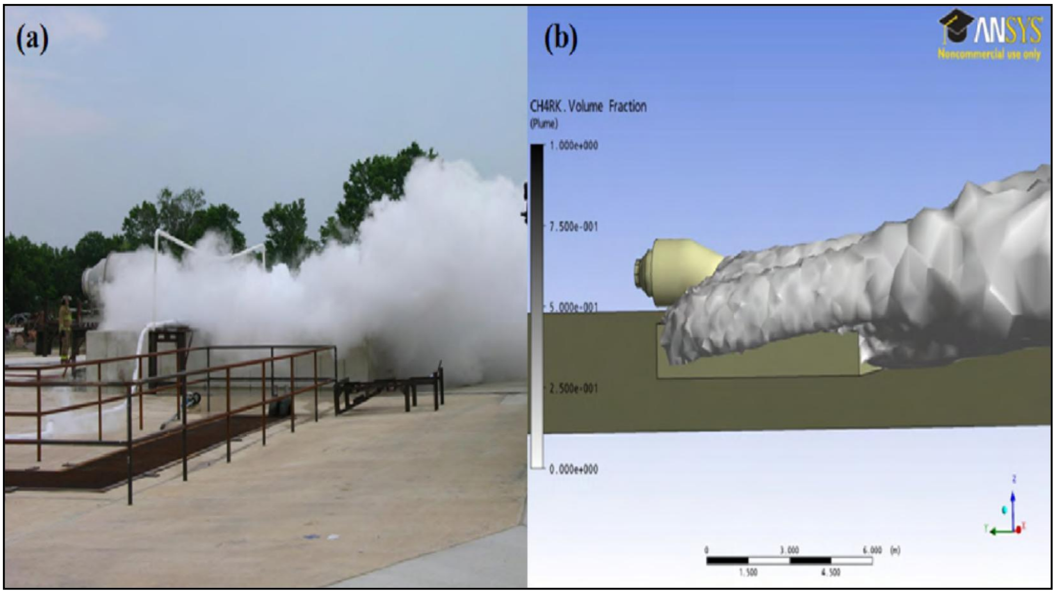

Fig. 3-7 Comparison of the plume shape of on-site photo and the simulation (Qi Ruifeng et al., 2010)

Båfjord (2011) has studied the most suitable location for gas detectors in offshore installations for oil and gas production and evaluated the effects on the functionality and reliability of the gas detection system. Using FLACS, we studied the physical factors that affect the optimum behavior of the exhaust gas with wind speed, wind direction, source of leakage, leakage direction, rate of leakage, gas composition and geometry. Because rapid detection of escape gases is one of the key requirements associated with the gas detection system, the detection time is an important factor in the reliability of the system. Since detection methods hardly share common faults, the combination of different gas detector principles and techniques appears to have a significant influence on the functionality and reliability of the gas detection system.

Choi (2015) studied that leakage or dispersion of gases from underground LNG plants could lead to fire or explosion. In this study, computational fluid mechanics were simulated with dynamic process of gas leakage and dispersion in closed steel spaces. In order to analyze risk assessment factors, such as the ratio of flammable volumes, transient simulations were carried out in different scenarios. Simulation results have time to visualize gas distributions in closed space. Flammable volume ratios have been introduced to quantitatively analyze fire burst possibilities.

Mazzoldi (2008) studied a comparison for leak from CO_2transportation and storage facilities. "Carbon Capture and Storage (CCS) is of interest to the scientific community as a way of achieving significant global reduction of atmospheric CO_2 emission in the medium term. CO_2 would be transported from large emission points (e.g. coal fired power plants) to storage sites by surface/shallow high pressure pipelines. This paper deals with the evaluation of the atmospheric dispersion CFD tool Fluidyn-PANACHE against Prairie Grass and Kit Fox field experiments. "Explanation of turbulence generation and dissipation models used (k −3 and k − l), and comparison with Gaussian model ALOHA for two field experiments. The authors propose to modify the extent to which the model can be measured for acceptability in the high-pressure CO_2 transportation risk assessment, taking into account the overall simplification leading to the use of a constant wind speed and direction within the CFD dispersion model.

Siddiqui et al., (2012) studied "Dense gas dispersion in indoor environment for risk assessment and risk mitigation" .Environmental risks are inherent in the management of a complex chemical process industry. Because dense clouds tend to continue to be at the surface of the earth or at the breathing levels of humans, they are of special interest to the interior of hazmat with higher densities than air. This study proposes a Computer Fluid Dynamics (CFD) model for the interior assessment taking into account accidental releases of continuous small toxic gas (chlorine) releases that have not been detected in the industrial indoor environment. Simulation results show that chlorine gas as dense as a liquid and it flows throughout the floor. At the same time, the concentration at the point off the ground increases slowly, resulting in both stratification and dilution due to the spread of dense gas. Discuss the effects of these diffusion patterns from a risk assessment and risk mitigation perspective.

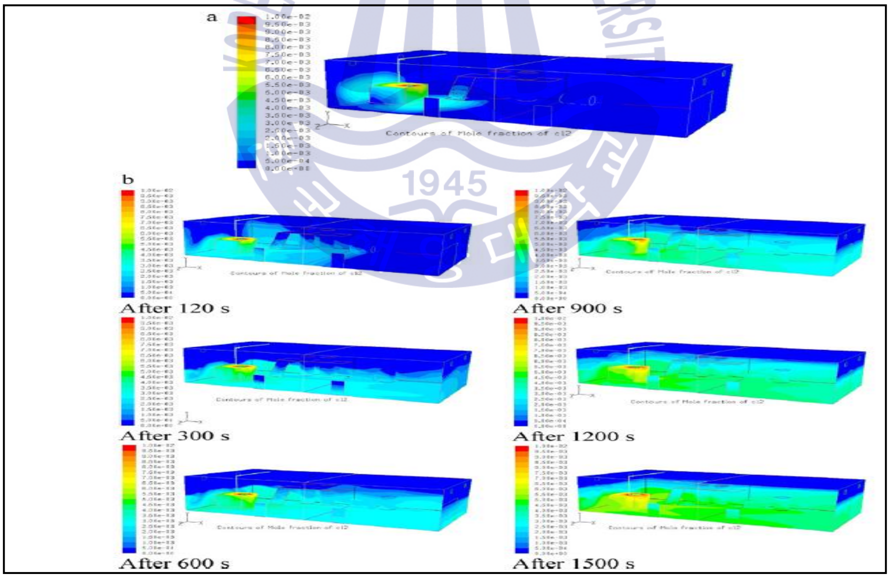

Fig. 3-8 Predicted concentration of chlorine after 50s from release (Siddiqui et al., 2012)

Kim, et al. (2013) studied "CFD simulation in SIC-CVD Process, for the uniform and homogeneous deposition of silicon carbide on these huge components". This requires not only a detailed adjustment of the process variables, but also, more essentially, the gas flow of the CVD reactor is necessary for changing the shape of the samples at the reactor level and for reducing the costs of its owners. In this study, CFD simulations are used to predict the internal distribution of gas rates. Chemical reaction simulation is used to predict the distribution of the concentrations of the reactive gases at the rotational speed of the stage.

Seo, et al. (2014) studied "Numerical Study on the HCFC-123 Leak in Turbo Chiller by using CFD". HCFC-123 is one of the chemicals being considered as a replacement for the chlorofluorocarbons. Using HCFC-123 frequently results in the risk of losing consciousness or dying due to lack of oxygen, and because the steam is heavier than air, it can accumulate in a lower ceiling and cause oxygen to be deficient. CFD was used to investigate the distribution of indoor oxygen concentration when 4 workers died from HCFC-123 gas leakage in the mechanical room of supermarkets in 2011.

Cho (2005) studied thermo-acoustic instability of methane/air flames in an industrial gas-turbine combustor is numerically investigated adopting CFD analysis. The combustor has 37 EV burners, which mix methane and air and then inject it into the chamber. An extended analysis is proposed and numerically tested to determine the instability mechanism within the burner and the passive control method that inhibits the instability.

Jang, et al. (2015) studied accidents in laboratory dealing with chemicals. In the case of a gas explosion or an accident related to leakage of chemical materials, the damage is much greater, so leading to a serious accident. In this paper, 5 gases(CO, NH_3, H_2, CH_4, N_2) are chosen as models because they are commonly used in university laboratories. In the gaseous release scenario, the diffusion process is estimated and analyzed to estimate the extent of the damage by PHAS Tv.6.6. The internal diffusion process is modelled using the CFD code Fluent.

Choi & Kang (2013) studied the methodology to evaluate particle resuspension and dispersion in building environment. To assess indoor particle dispersion, a computational fluid mechanics (CFD) technique was proposed based on the Lagrangian method. The CFD model was validated by comparing simulated results with experimental data, including the distribution of indoor particle concentrations.

Zhang Bo & Chen (2010) studied some major toxic gas release accidents demonstrate the urgent need of a systematic risk analysis method for individuals exposed to toxic gases. A CFD numerical simulation and a combined dose-response model approach were proposed for quantitative analysis of acute toxic gas exposure threats. Finally, this method consists of four steps. First, establish CFD models and monitor points, and second, correct CFD equations, and forecast real-time concentration fields for toxic gas emission and dispersion. Third, the gas concentration estimate is calculated. A case study of hydrogen sulfide emitted from gas charging stations was carried out using a three-dimensional Fluent model. Acute exposure mortality was initially valued as a simplified ideal model, assuming that workers stay in their original exposure locations without moving. Comparison is then made with a more realistic model, assuming the workers begin to evacuate according to the hydrogen sulfide detection system alarms according to a planned course. The two models have the worst case response and the best response effects, respectively, and the analysis results are quite different. The results indicate that the CFD and dose-response combination approaches are good for estimating the mortality rates of individuals exposed to accidental toxic gas releases.

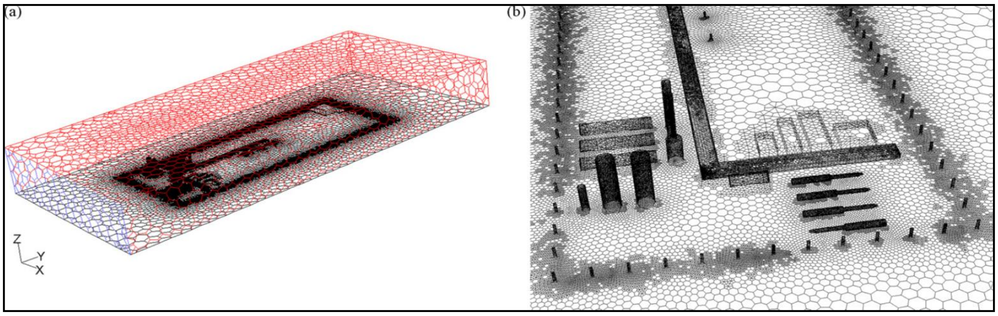

Fig. 3-9 Surface mesh of computational domain (Zhang Bo & Chen, 2010)

3.2 LNG fueled ship literatures

Kumar et al.(2011) studied an eco-friendly cryogenic fuel for sustainable development. As the demand for natural gas has increased rapidly around the world over the past two decades, transportation of natural gas from many parts of the world has become increasingly important. Liquefaction of natural gas provides a safer and more economical alternative to transportation, as well as the storage capacity of natural gas. This article provides an overview of the characteristics of LNG, the current state of LNG, the imports of LNG abroad, and the environmental friendliness of LNG as a motor fuel of natural gas fuels.

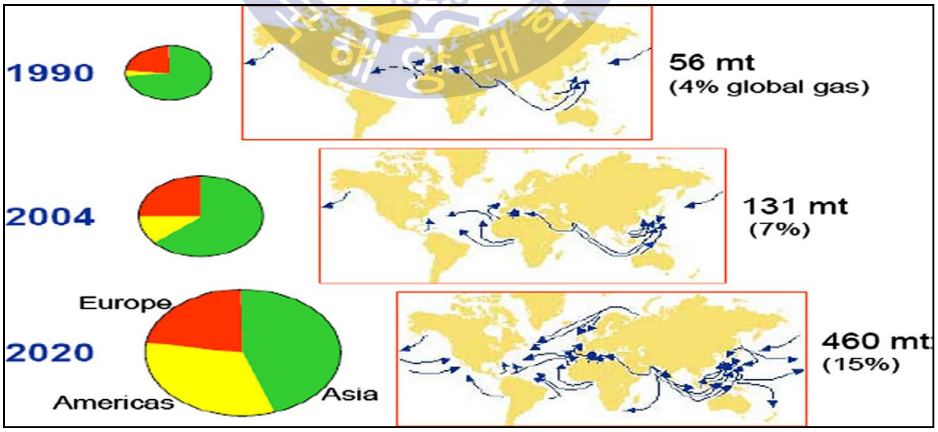

Fig. 3-10 Schematic representation of growing global LNG demand (Kumar et al., 2011)

Kim (2016) studied "Quantitative risk analysis by CFD". Engine room with fuel gas supply system is so limited that it can be damaged in part by hull construction and is crowded enough to endanger sensitive auxiliaries by explosion overpressure. For this reason, an analysis should be performed to assess the structural resistance required to develop new safety codes for vessels using gas or other low flash-point fuels or to mitigate explosion overpressure. Quantitative risk analysis could be performed in various ways, but explosion analysis in particular needs to be carried out by quantitatively calculating gas clouds and gas emissions. In addition, it is essential to use a general purpose chemical process simulator to obtain characteristics information of gas leakage. This paper has explained the overall process required for quantitative risk analysis to satisfy the satisfactory levels of safety of gas-powered vessels.

Lee, et al. (2016) studied "CFD Analysis and Explosion Test of a Crankcase Relief Valve Flame Arrester for LNG-Fuelled Ships". The results of a computational fluid dynamics based feasibility analysis of the crankcase relief valve flame arrester design conducted using ANSYS CFX V14 showed that the inlet and outlet relief valve temperatures differed by 350-700° C. An explosion test was carried out based on European standard EN14797 to evaluate the flame transmission and mechanical integrity of the valve.

Kang (2013) studied "Dispersion Characteristic of Boil off Gas in Vent Mast Exit of Membrane type LNG Carriers". This paper describes the boil off gas dispersion characteristic from a vent mast under cargo tank cooling down conditions of the membrane type LNG carriers.

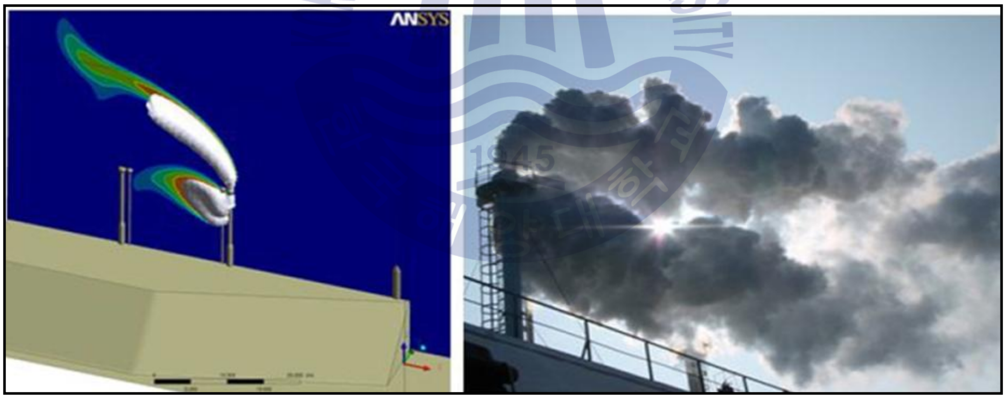

Fig. 3-11 LNG gas dispersion at vent mast of LNG ship (Kang, 2013)

3.3 Various CFD literatures

Kim & Jeong (2014) studied "Aerodynamic Design and Performance Prediction of Rotor Blades in a Single-Stage Axial Fan by using CFD Method". CFD is used to design the rotor blade of the axial flow fan and predicts the aerodynamic performance. Blade profiles initially determined by free vortex method are adapted to the target values of rotor workload with 3D Navier-Stokes solver analysis.

Kim, et al.(2012) studied "Reduction of a Numerical Grid Dependency in High-pressure Diesel Injector Simulation by using the Lagrangian-Eulerian CFD Method". The Lagrangian-Eulerian method is very widely used to simulate liquid spray entering the gas stage. This method can provide simple solutions and a low cost of computation, but the Lagrangian spray model is reported to have a numeric grid dependency resulting in a significant numerical error. To verify the enhanced spray model, compare the calculations with the results of the experiment.

Pontiggia et al., (2009) studied "Hazardous gas dispersion: A CFD model accounting for atmospheric stability classes". Thanks to the growing CPU power today, computational fluid mechanics (CFD) use is also growing rapidly in the industrial risk assessment area and replace integrated models in certain situations, such as when complex terrain or larger obstacles are involved. Nevertheless, commercial CFD codes do not usually provide a specific turbulence model that simulates the stratification effect described as an integrated model with a well-known stability-class approach. In this study, a new approach to take into account atmospheric characteristics in CFD simulations was developed and validated against the available experimental data.

Jin, et al (2009) studied gas turbine engine with CFD code. In compressor and turbine, 2-D NS implicit code is applied with k-ω SST turbulent model. In combustor, 0-D lumped method chemical equilibrium code is adopted according to the limitations. The product is just 10 different types of molecules and air fuel, and is a perfect blend with 100 % combustion efficiency at a constant pressure.

Heo, et al. (2011) studied refrigerant after the expansion valve interchanges the heat at the evaporator. At this time, the state of the gas and liquid flows in two phases, resulting in irregular noise. To avoid noise, two-phase flow patterns should be predicted. In this paper, procedures for predicting a two-phase flow pattern, such as churn flow and annular flow, were proposed using CFD software.

Dan, et al. (2011) studied "The quantitative risk analysis for using alternative mixtures in existing recharging facilities using three types of explosion models" "TNT equivalency model, PHAST and CFD-based FLACS" to manage the risk effectively. Differences in results by model were compared and a practical method was proposed for when and how these models were used.

Kim, et al. (2015) studied "Conjugate Heat Transfer (CHT) Analysis for High Pressure Cooled Turbine Vane in Aircraft Gas Turbine". The CHT code has been verified by a comparison between CFD results and the experimental results of the C3X vanes. The combination of k-ω based SST turbulence model and transition model was applied to solve the flow and thermal field of the fluid zone and the material property of CMSX-4 was adopted to the solid zone.

Lee, et al. (2013) studied "Coupled flow-structure Analyses on the Roots Type Vacuum

Pumps in semiconductor Fabrication Facility". The structural analysis of the pump applies calculated CFD results for internal pressure and temperature distributions. Combined analysis of flow and structure results mainly in the deformation of the pump structure due to heat expansion of the gas in the pump and the deformation impeller and housing can cause severe contact and damage causing mechanical damage.

Lim, et al. (2015) studied "Honeycomb Labyrinth seal leakage characteristic analysis with actual operating conditions on the compressor of Gas Turbine" in order to minimize leakage. Under actual operating conditions of the compressor, a numerical analysis of the honeycomb labyrinth seal was carried out according to pressure, temperature, and rotor speed for CFD. As a result, the leakage rate decreases as the temperature rises. In addition, pressure increased linearly as leakage increased, without affecting the rotational speed.

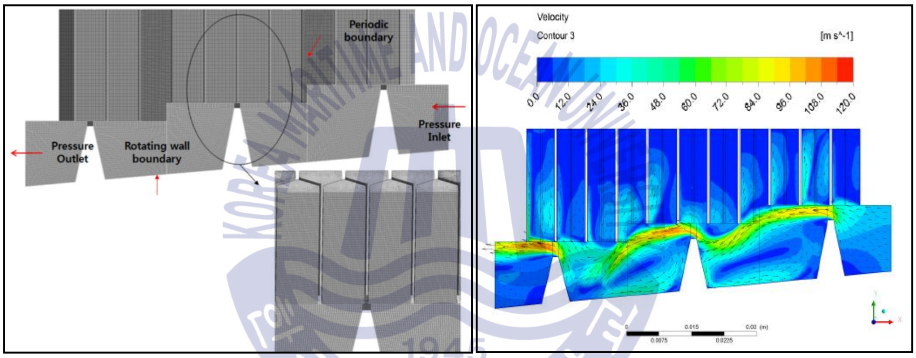

Fig. 3-12 Geometry and velocity contour distribution in Honeycomb Labyrinth seal (Lim, et al., 2015)

Joo, et al. (2015) studied ejector design by using Fluent 6.3 of FVM(Finite Volume Method) CFD techniques to resolve the flow dynamics in the ejector. Effects of the emitters were examined for conditions of operation of geometry and hydraulic properties. Multi-path CFD modeling was carried out to determine the fluid dynamics of the sea water air emitters.

Ha & Sim (2014) studied "Characteristics of Entertainment Flow Rate in a Coanda Nozzle with or without Coaxial Contractor". A MILD(Moderate and Intense Low oxygen Dilution) combustion, effective for NOx reduction, is significantly affected by the recirculation flow of hot exhaust to the combustion furnace. A numerical analysis has been carried out to describe the effect of exhaust gas collection on furnaces with or without coaxial contractors.

Lee, et al. (2015) studied "Cavitation analysis in a centrifugal pump using VOF method". The goal of this paper is to investigate the cavitation problem in the single-stage and double-stage centrifugal pumps. The Volume of Fraction (VOF) method was adopted for the numerical simulations together with Rayliegh-Plesset model for the gas-liquid two-phase flow inside the pump. In order to capture the turbulent phenomena, the standard k-ε turbulence model has been adopted, and the simulations have been done as transient cases. In addition, the motion of the rotating parts was simulated using Multi Reference Frame(MRF) method.

Wie & Kim (2012) studied "Flow Control Fin(FCF) optimization by the computational fluid dynamics(CFD) techniques". The study focused on the performance assessment of FCF attached to the rear part of the ship. The main benefit of the FCF is to increase resistance by producing lift with forward-force components in the foil section and to improve propulsion by providing a consistent speed distribution in the propeller plane. The aim of this study is to assess these functions, to minimize viscous resistance, and to find the optimal FCF shape to equalize the wake up distribution. The results showed that optimized FCF could increase the uniformity of the wake up distribution at the expense of viscous resistance.

Rakibuzzaman, et al. (2015) studied "Cavitation flow of the multistage centrifugal pump". Cavitation can be observed at the front and rear edges of the impeller in the suction area. Head coefficients are measured under different flow operating conditions. The Rayleigh-Plesset cavitation model is applied to do prediction the occurrence of cavitation. The two-phase gas-liquid homogeneous CFD method was adopted to analyze the centrifugal pump performances using two equation transfer turbulence models.

Lee et al. (2015) studied "Flow analysis of the hot gas valve with a pintle" to investigate the effects of numerical methods and the computational area. Three turbulence models were adopted to determine the impact on thrust and temperature distributions. Spallart-Allmaras, RNG k-epsilion, and k-ω SST. The thrust of the hot gas valve is the same in almost all cases, but there is a difference of about 5 % in temperature distribution. In the surrounding areas, differences in temperature distribution with respect to the number of grid are observed.

Kim, et al. (2011) studied "Temperature characteristics of mold transformer for the distribution power system" by using CFD. The model was modelled using coils, cores, insulation, and about 3 MVA rated transformers and was analyzed for temperature distribution in structures with heat fluid. This fluid is assumed to be natural cooling of the transformer cooling system, and it is analyzed as turbulence unless it can be compressed.

Kim, et al. (2011) studied "The combustion phenomena in a sludge incinerator using experimental and numerical method". Temperature and gas concentrations were measured at 33 points to assess mixing and combustion characteristics during heater operation. Numerical simulations were carried out using commercial CFD codes.

Because of the poor mixing performance of flammable materials caused by large, bulky particles of air and flammable material, a large amount of changes in temperature and gas concentration were observed on the freeboard of incinerators. The boundary conditions of CFD simulations were found to be effective in predicting the inadequate mixing and combustion performance of the reactor.

Yi J.S. et al. (2011) studied "Flow characteristics of exhaust gas in a motorcycle muffler". The engine generates 125 cc of displacement. A numerical analysis has been carried out to investigate the exhaust gasses flowing into the motorcycle muffler using CFD. Star-CD S/W is used to analyze three-dimensional stability and transient conditions in the muffler. The Navier-Stokes equation is solved by the SAMPLE and PISO method with Cartesian coordinate system.

Choi, et al. (2011) studied "CFD Study on Aerodynamic Power Output of 6 MW Offshore Wind Farm According to the Wind Turbine Separation Distance". This paper presents aerodynamic output from a 6 MW wind turbine consisting of three sets of 2 MW wind turbines according to separation distances using CFD. Layout designs, including offshore wind power plants and land wind plants, are key contributors to the initial investment, annual energy production and maintenance costs. A full three-dimensional model is used for CFD rather than the actuator disk model with a momentum source for each wind turbine rotor, which is quite technical. The results of this study can be effectively applied to the layout design of offshore wind farms.

Fig. 3-13 Offshore wind farm wake (Choi, et al., 2011)

Park, et al. (2014) studied "Design optimization of the staking line for an electric fan blade using CFD". The purpose of this study is to increase the performance of the primary model fan using design optimization as an electric fan with an axial blade. So as to aerodynamic analysis, computational fluid dynamics is carried out by using of commercial tool "ANSYS-CFX" ver. 14.5. $k-\omega$ SST turbulence model is applied to the

CFD analysis.

Kim, et al. (2011) studied "CFD analysis of the Disk Friction Loss on the centrifugal compressor" to improve the total efficiency of the compressor. In this study, the losses from disk friction due to axial clearance and surface roughness are analyzed and a new empirical equation is proposed to reduce disk friction losses. This should reduce the disk friction losses as defined by the output loss. The rotating reference frame technique and the 2-equation k-ω and SST model by the CFD code "FLUENT" is applied at the steady-state for the centrifugal compressor impeller.

Cho, et al. (2011) studied "Application of CFD in The Analysis of Aerodynamic Characteristics for Aircraft Propellers. "This is to apply non-linear numerical analysis to verify the accuracy and reliability of the prediction of the efficiency characteristics of aircraft propellers. The numerical simulation method incorporated the CFD code, which is based on RANS (Reynolds Averaged Navier-Stocks) equation. The efficiency of the propeller calculated from the numerical analysis is consistent with the efficiency of the wind tunnel experiment. The verification results are analyzed and used to optimize the design and manufacture of aircraft propellers to be studied.

Yoo, et al. (2013) studied "Evaluation of Ventilation Efficiency from Ventilation System and Volume in the Small Facilities Using CFD". In this study, a ventilation system was proposed to effectively improve indoor air quality in small print facilities. We used CFD simulations to analyze the hazardous chemical environment. Through all of these actions, the aim of this study is to propose an evaluation of ventilation system and volume ventilation efficiency that can effectively improve the indoor air quality of small print applications.

Nam, et al (2011) studied "Non-uniform Thermal Comfort in Hybrid Air-Conditioning System with CFD". In this paper, the thermal environment for the human thermal model under the various air conditioning systems, including the hybrid system, and the non-uniform thermal comfort, were combined to use in a typical office, computational fluid dynamics, and heat model.

Lee, et al. (2012) studied "Computations of the dynamic derivatives of three dimensional flight vehicle configurations using CFD". The pitch dynamic derivative is calculated by the pitch sine wave action, whereas the roll damping is based on steady state calculations using a non-person frame method. A 3-D Eulerian solver has been developed that can be executed by both non-reflective and inertial frame for flow calculations.

Cho, et al. (2012) studied "Dispersion Characteristic for Fire Scenarios in an Urban Area Using a CFD-WRF Coupled Model". This study uses computational fluid dynamics models combined with medium-sized weather research and forecasting (WRF) models. To better represent the terrain and building effects, GIS data is used to input CFD models. These results show that it is important to understand the city flow accurately to assess the effects of fire induced pollutants in urban areas. The study also shows that CFD models can be useful for assessing urban environments.

Kim (2011) studied "CFD as a seakeeping tool for ship design". CFD has become a powerful tool that can effectively handle the various free surface flows. As a classification society, the ABS is making significant efforts to implement CFD techniques in evaluating the strength of the latest commercial vessels and high-speed navy vessels. The main objective of this study is to verify CFD techniques as a sea keeping tool for ship design, taking into account fully nonlinear three-dimensional slamming and green water on the deck. The structural load of the large container carrier has been successfully calculated using CFD analyses and verified with the segmented model test measurement.

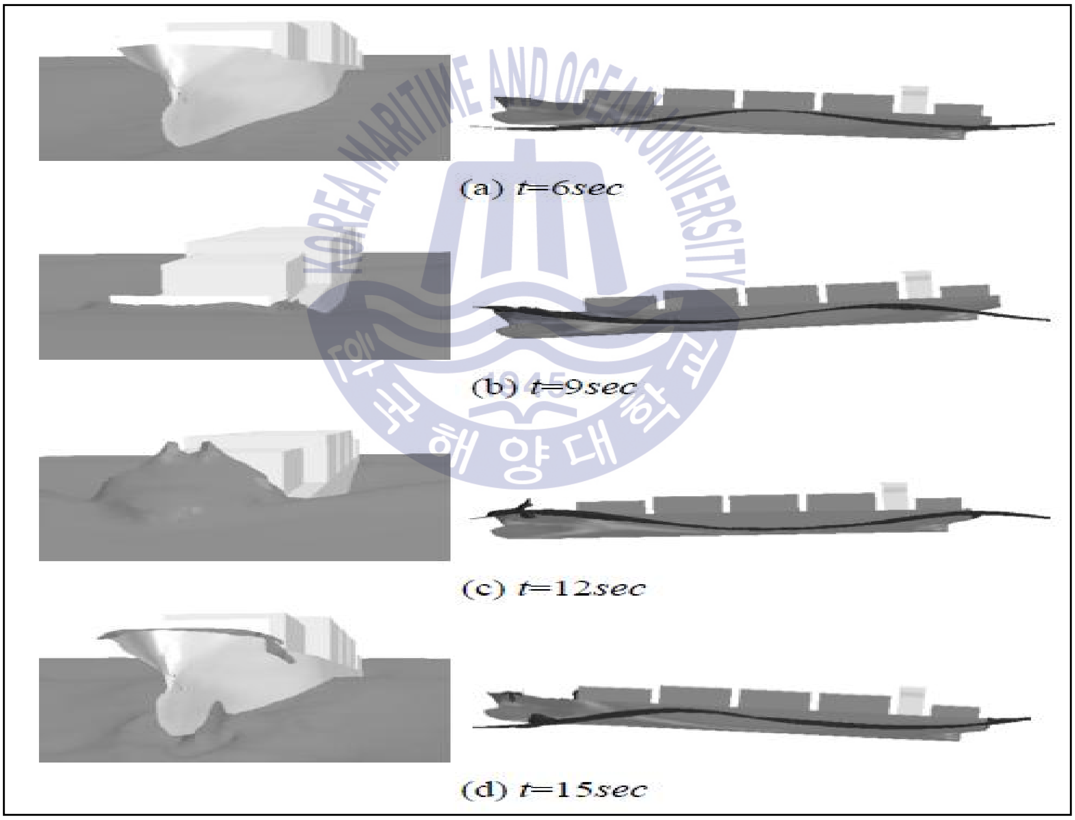

Fig. 3-14 Instantaneous snap shots of nonlinear ship motions at each simulation time (Kim, 2011)

4. Theoretical background

Commercial CFD code is used with ANSYS Fluent release 14.0 version is used to carry out the simulation for this study. This is utilizes the Finite Volume Method (FVM) to discretize the computational equation and domains. Continuity equation, three dimensional momentum, k-ε turbulence model and chemical species are applied.

1) Continuity equation

$$\frac{\partial \rho}{\partial t}+\nabla \cdot (\rho \vec{v})=0$$

$\rho = density\ of\ fluid,\ \vec{v} = velocity\ vector$

2) Momentum equation

$$\frac{\partial (\rho \vec{v})}{\partial t}+\nabla \cdot (\rho \vec{v}\vec{v}) = -\nabla p+\nabla \cdot (\bar{\bar{\tau}})+\rho \vec{g}+\vec{f},\ \bar{\bar{\tau}} = \mu((\nabla \vec{v} + \nabla \vec{v}^{T}) - \frac{2}{3}\nabla \cdot \vec{v} I))$$

$p = pressure,\ \bar{\bar{\tau}} = stress\ tensor,\ \overrightarrow{f} = sum\ of\ the\ body\ force\ \vec{g} = gravity\ of\ vertical\ direction,\ \mu = dynamic\ viscosity$

3) Energy equation

$$\frac{\partial (\rho E)}{\partial t}+\nabla \cdot (\vec{v}(\rho E + p))=\nabla \cdot (K_{eff}\nabla T - \sum_j h_j \vec{J}_j)+(\bar{\bar{\tau}}_{eff}\vec{v}))+S_h$$

$$E = h + \frac{p}{\rho} + \frac{v^2}{2}$$

$S_h =$ $energy\ source\ term,\ E = Total\ energy,\ K_{eff} =$ $effective\ conductivity$

4) k-ε turbulence model

-For turbulent kinetic energy κ

$$\frac{\partial (\rho k)}{\partial t}+\frac{\partial (\rho k u_i)}{\partial x_i}=\frac{\partial y}{\partial x_j}(\frac{\mu_t}{\sigma_k}\frac{\partial k}{\partial x_j})+2\mu_t E_{ij}E_{ij} - \rho\varepsilon$$

-For dissipation ε

$$\frac{\partial (\rho \varepsilon)}{\partial t}+\frac{\partial (\rho \epsilon u_i)}{\partial x_i}=\frac{\partial y}{\partial x_j}(\frac{\mu_t}{\sigma_\varepsilon}\frac{\partial k}{\partial x_j})+C_{1\varepsilon}\frac{\varepsilon}{K}2\mu_t E_{ij}E_{ij} - C_{2\varepsilon}\rho\frac{\varepsilon^2}{k}$$

$u_i = velocity\ in\ correspondiing\ direction,\ E_{ij} = rate\ of\ deformation,\ \mu_t = eddy\ viscosity$

$\sigma_k,\ \ \sigma_\varepsilon,\ and\ \sigma_{2\varepsilon}$ are adjustable constant.

5) Species transport equation

$$\frac{\partial(\rho Y_{i})}{\partial t}+\nabla\cdot(\rho\vec{v}Y_i\ \ )-\nabla\cdot\vec{J}_i+R^i+S^i$$

$R_i = net\ rate\ of\ production\ of\ species\ i\ by\ chemical\ reaction$

$Y_i = local\ mass\ fraction\ of\ each\ species$

$S_i = rate\ of\ creation\ from\ the\ dispersed\ phase\ plus\ and\ user\ defined\ sources$

$J_i = diffusive\ flux\ of\ species\ i$

5. Gas dispersion scenario and computational settings

5.1 CFD code working procedure and turbulence model

Fig. 5-1 shows CFD code working procedure. Gas Leak dispersion modeling is designed with cargo compressor room of 174K ME-GI LNG vessels. The geometry of the compressor room structure and the equipment sizing and piping arrangement are modeled with 1 to 1 scale. Mesh generation between high pressure and low pressure leak scenario is differently designed. High pressure leak is from the discharge pipe of HP Pump/Vaporizer and low pressure leak is from the discharge pipe of VR compressor. In these two cases, leak pressure and temperature and the locations are completely different in order to study the behavior of the different gas dispersion.

Boundary conditions are differently setting between high pressure and low pressure leak. Different input main parameters are leak pressure, leak temperature and operating temperature. Leak rates are decided according to the pinhole size. In case of HP Pump/Vaporizer leak, we are considering the pipe rupture, in case of VR compressor leak, we are not considering the pipe rupture due to leak rate is too much to do carry out the desk top personal computer. Solver setting is applied with k-ε turbulence model & species model (CH_4 and Air) with transient state.

Selection of turbulence models is an important factor in the success of CFD results, typical models and features are as follows.

- Spalart-Allmaras turbulence model

The Spalart-Allmaras model is a single equation for addressing the modelled transport equation for kinematic eddy turbulent viscosity. This model was designed specifically for aerospace applications with flows limited by the walls, and was shown to provide good results for the boundary layer due to backpressure gradient. It is also becoming popular in the field of turbo machinery.

- K-epsilon (k-ε) turbulence model

k-ε turbulence model is the most common model used in CFD to simulate the average flow characteristics for turbulence flow conditions. These are two evaluation models which generally explain turbulence in the form of two PDEs (Transport Equations). The original driving force of the k-ε model was to find an alternative model that improved the mixed-length model and defined the turbulence length in the medium to high complexity flow.

- K-omega (k-ω) turbulence model

k–omega(ω) turbulence model is a commonly used equation used as the closure of the Reynolds-averaged Navier–Stokes equations (or RANS equations). The model attempts to predict turbulence with two partial differential equations, for two variables k and Omega, the first parameter is turbulence kinetic energy (k), and the second variable is heat dissipation rate.

- SST (Menter's Shear Stress Transport)turbulence model

SST is a powerful secondary equation fluid-viscosity turbulence model that is widely used in computational fluid dynamics. The model combines the k-omega turbulence model and K-epsilon turbulence model such that the k-omega is used in the inner region of the boundary layer and switches to the k-epsilon in the free shear flow.

- Reynolds stress equation model (RSM),

The Reynolds Stress Equation model (RSM), called Second Moment-Closures, is the most complete classic turbulence model. In these models, the data viscosity hypothesis is prevented and the individual components of Reynolds stress tensor are calculated directly. These models use Reynolds stress-transfer equations for formulation. They explain the effects of Reynolds ’ stress and the direction of complicated interactions in turbulence. The Reynolds stress model offers significantly higher accuracy than the Eddy-viscosity based turbulence model, while being composedly cheaper than direct numerical simulations and larger eddy simulations.

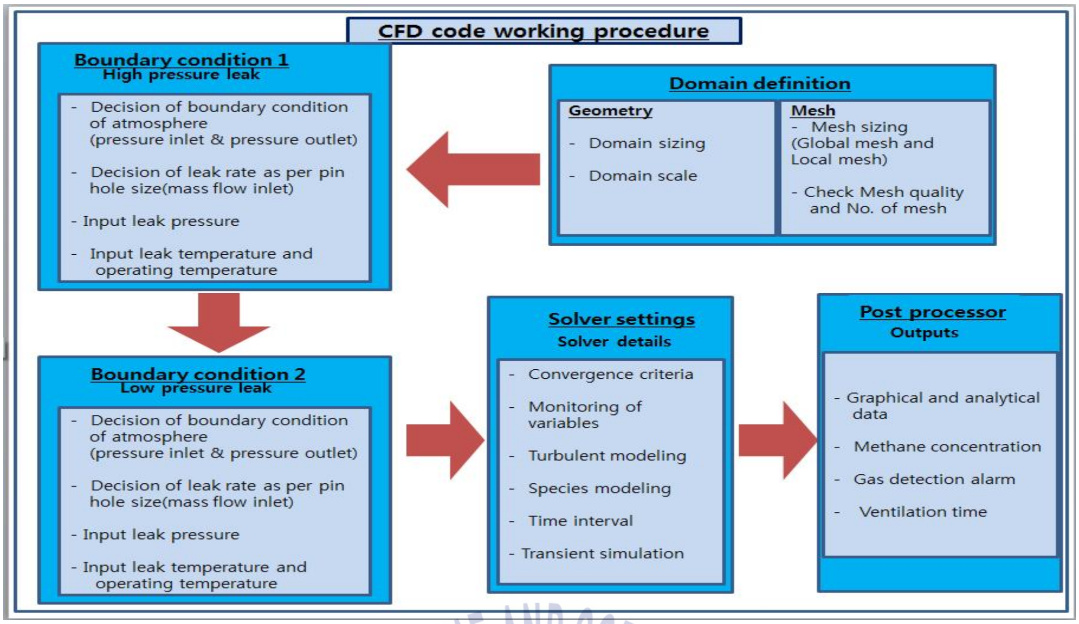

Fig. 5-1 CFD code working procedure

5.2 Leak scenario

Leak scenario is composed of two cases, high pressure leak and low pressure leak. In case of high pressure leak, it is very likely that LNG leak will occur from high-pressure gas pipe lines. Those pipelines are from high pressure pump/vaporizer to main engines and HP Fuel gas compressor to main engines.

High pressure leak scenarios have been chosen at the "high pressure pump/vaporizer" discharge pipe which is located on the first deck far away from the ventilators. "HP Fuel gas compressor" discharge pipe has not been chosen because it is located near the mechanical ventilators. Pressure and temperature at high pressure pipe is 305 bar and 43 ℃.

Low pressure leak scenarios have been decided at the VR compressor discharge pipe which is located on the floor deck different with first deck and positioned at the farthest away from the ventilators. Pressure and temperature at low pressure discharge pipe is 1 bar and -110 ℃.

These potential gas release scenarios are interesting and worthwhile to study because we are considering different gas state not only the cryogenic condition(-110 ℃) at 1 bar but also high temperature condition(43 ℃) at 305 bar differently. Fig. 5-2 and 5-3 show a typical arrangement of cargo handling equipment in cargo compressor room.

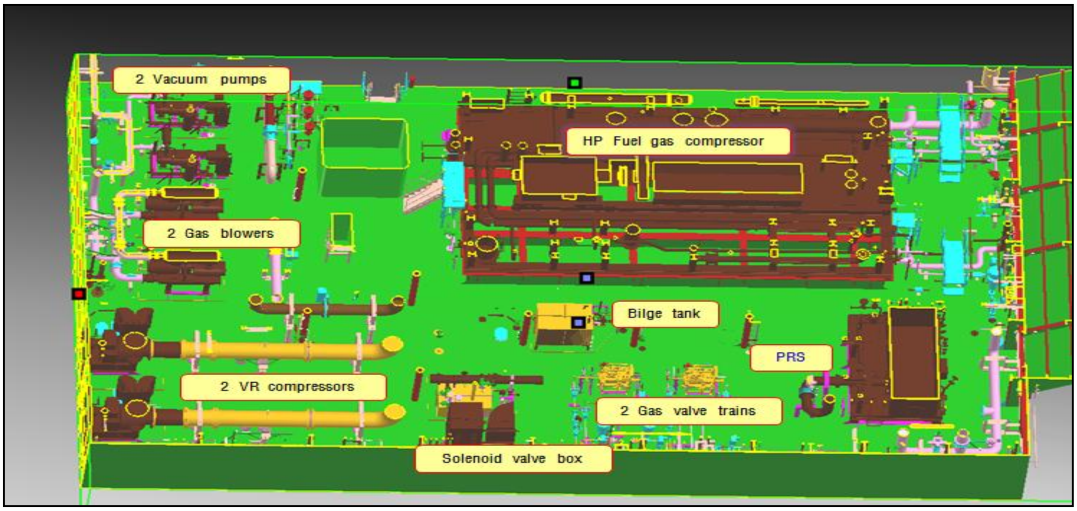

Fig. 5-2 Layout in cargo compressor room on floor deck (Released from DSME)

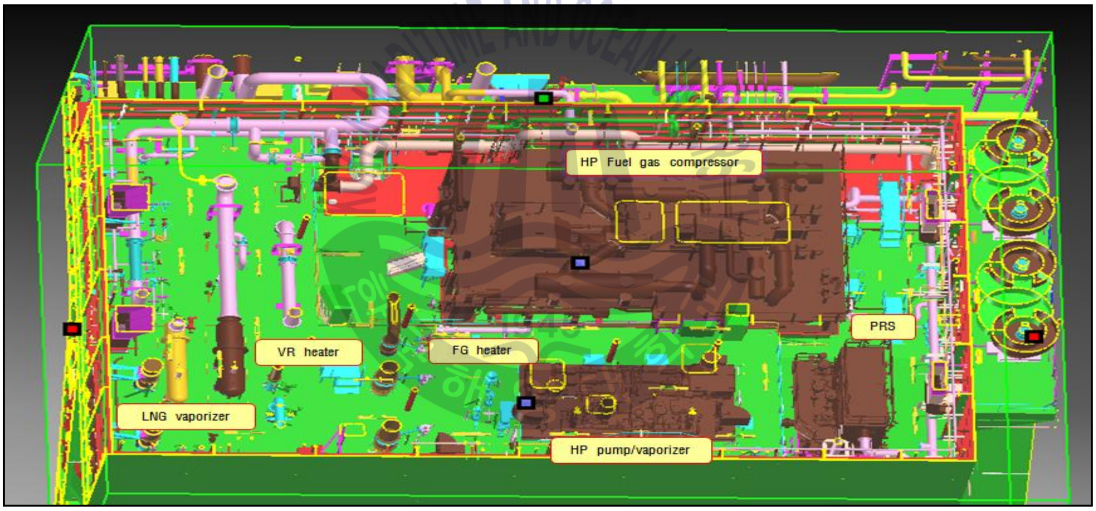

Fig. 5-3 Layout in cargo compressor room on the first deck (Released from DSME)

Leak scenario is according to the different leak mass flow rate as per the pinhole size. Applied formula is the same as (1) and (2).

$$\frac{dm}{dt} = c_d A_h P_0 K \sqrt{\frac{W_g}{\gamma R T}} \quad (1)$$

$\frac{dm}{dt}$ = mass flow rate, $C_d = (0.97), coefficient\ of\ leak,\quad A_h =$ $Area\ of\ crack$ hole, $P_0 = pipe\ internal\ pressure,\ W_g = molecular\ weight,$ $\gamma = specific\ heat\ ration\ (\frac{c_p}{c_v})$, R= $gas\ constant,\quad T = gas\ temperature$

$$K = \gamma\left(\frac{2}{\gamma+1}\right)^{\frac{\gamma+1}{2(\gamma-1)}} \quad (2)$$

Table 5-1 Mass flow rates for high pressure leak

Leak location	Pin hole size	Mass flow rate $\frac{dm}{dt}$(kg/s)	Mass flow rate(kg/h)
Discharge pipe of Hi pressure pump/vaporizer	4.5 mm	0.8	2,880
	5.0 mm	1.0	3,567
	5.6 mm	1.25	4,474

Pinhole sizes are differently assumed as shown on the Table 5-1. Case 3 is rupture case in case of HP Pump/Vaporizer maximum capacity. One(1) of the gas detection sensor which is the nearest point 30% LFL of the total four(4) sets will be alarmed after the gas leak and then leaked gas will be continuously discharged during 10 seconds and stop. Mechanical ventilators are operating always before and after leak and methane gas behavior and ventilation capacity can be monitored. HP pump/Vaporizer is located on the first deck in the middle of cargo compressor room as shown on the Fig. 5-2 and supply the fuel gas to the main engine so discharge gas service temperature is about 40 ° C. So hot gas movement can be studied.

Table 5-2 Mass flow rates for low pressure leak

Leak location	Pin hole size	Mass flow rate $\frac{dm}{dt}$(kg/s)	Mass flow rate(kg/h)
Discharge pipe of Vapor return compressor	100 mm	1.8	6,480
	140 mm	3.5	12,600

Pinhole sizes are differently assumed as shown on the Table 5-2. Pinhole size is assumed to 100 mm and 140 mm, mass flow rate is distinguished from two times between case 1 and case 2. One of the gas detection sensors which are the nearest point 30% LFL of the total four sets will be alarmed after the gas leak and then leaked gas will be continuously discharged during 10 seconds and stop. Mechanical ventilators are operating always before and after leak and methane gas behavior and ventilation capacity can be monitored. Two VR compressors are located farthest from the ventilator outlets in the cargo compressor room floor deck as shown on the Fig. 5-2 and VR compressors discharge gas service temperature is about -110° C. So we can study the cold gas movement.

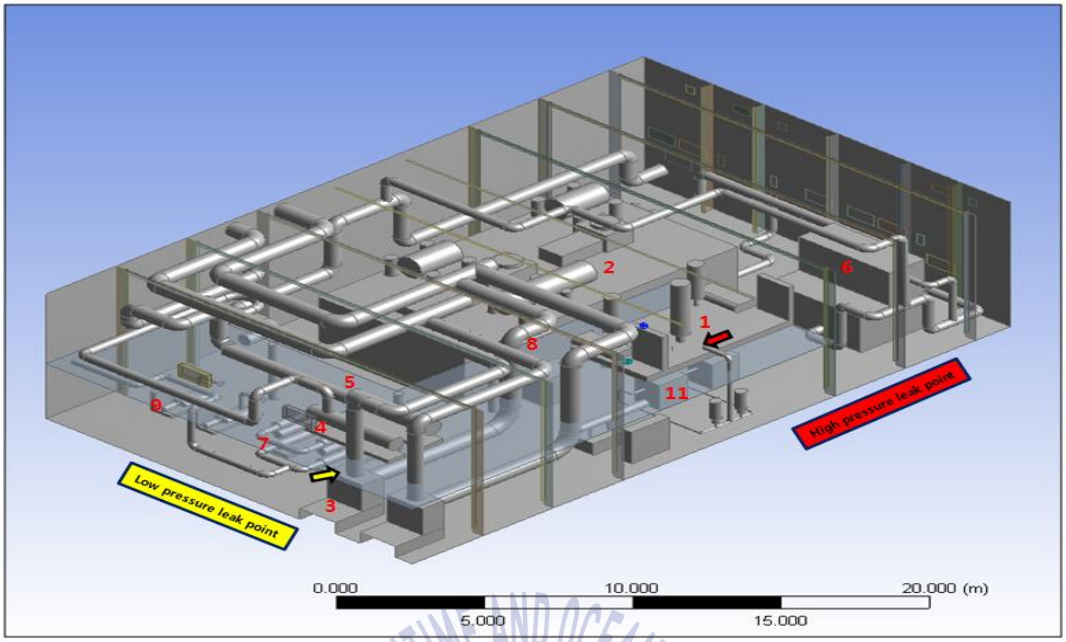

Fig. 5-4 Leak points of HP Pump/Vaporizer discharge pipe and VR Compressor discharge pipe

5.3 Computational domain

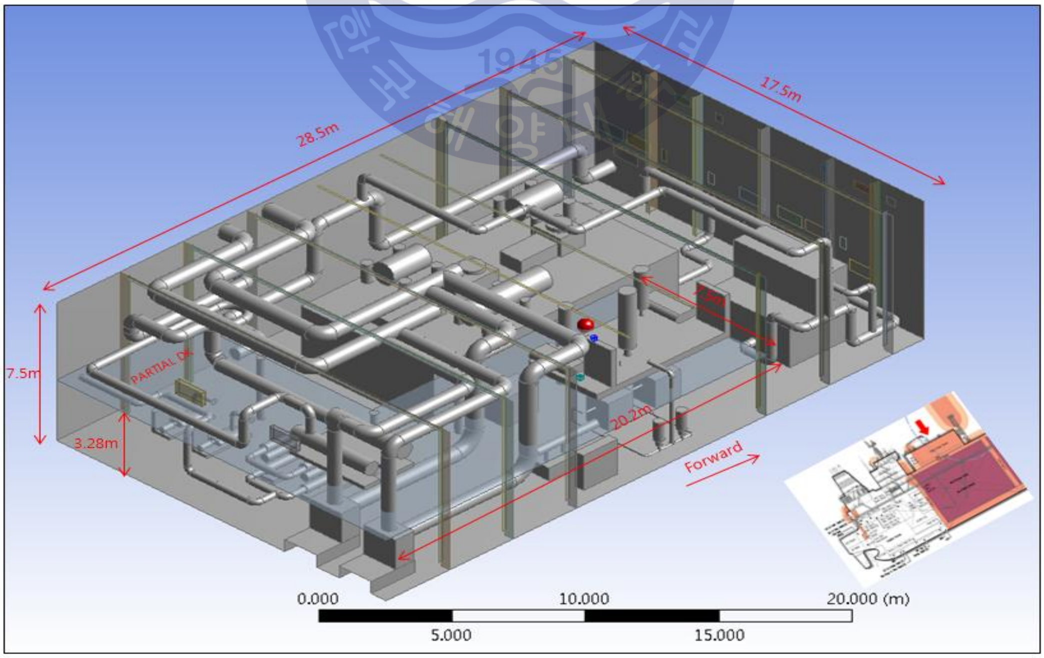

Fig. 5-5 Isometric view of cargo compressor room

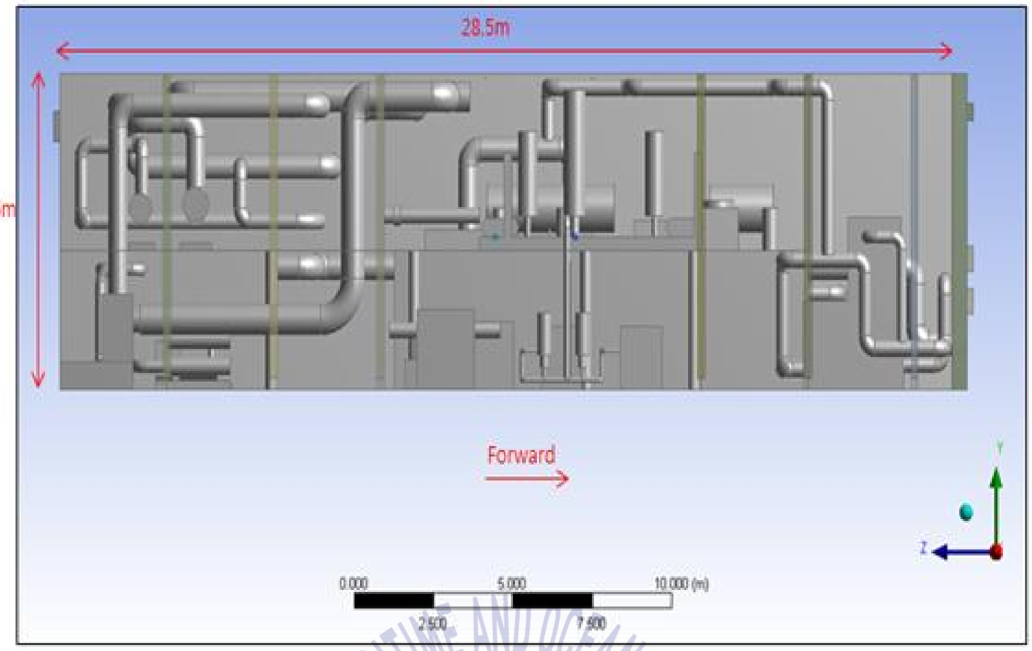

Fig. 5-6 Elevation view of cargo compressor room

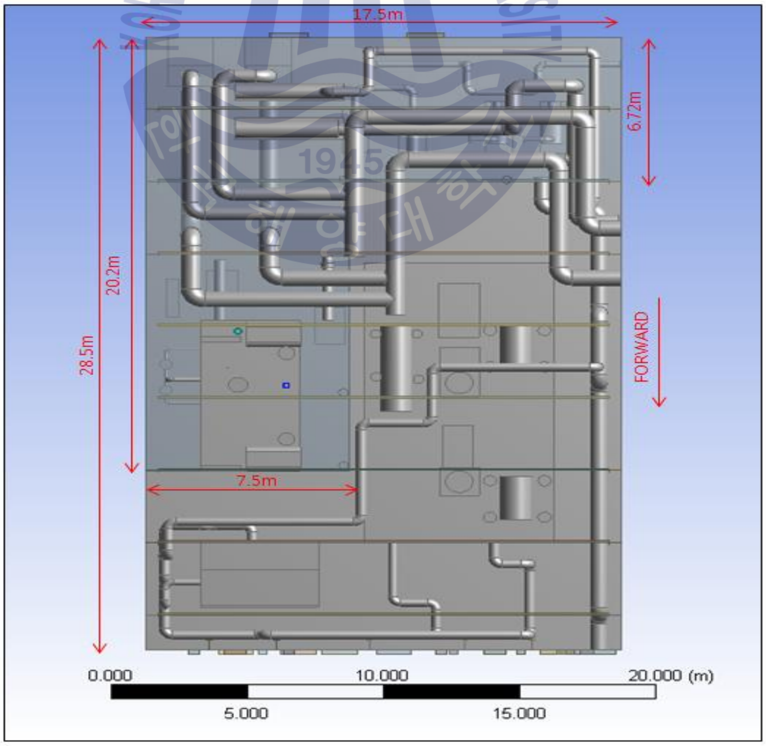

Fig. 5-7 Top plan view of cargo compressor room

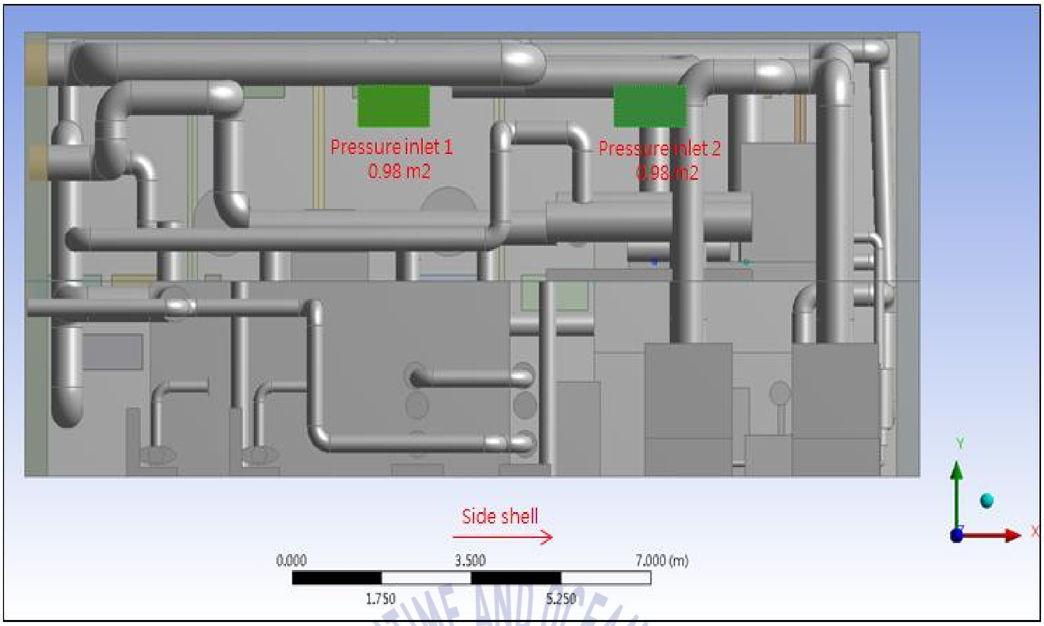

Fig. 5-8 Section view of cargo compressor room(seen from after)

Fig. 5-9 Section view of cargo compressor room(seen from forward)

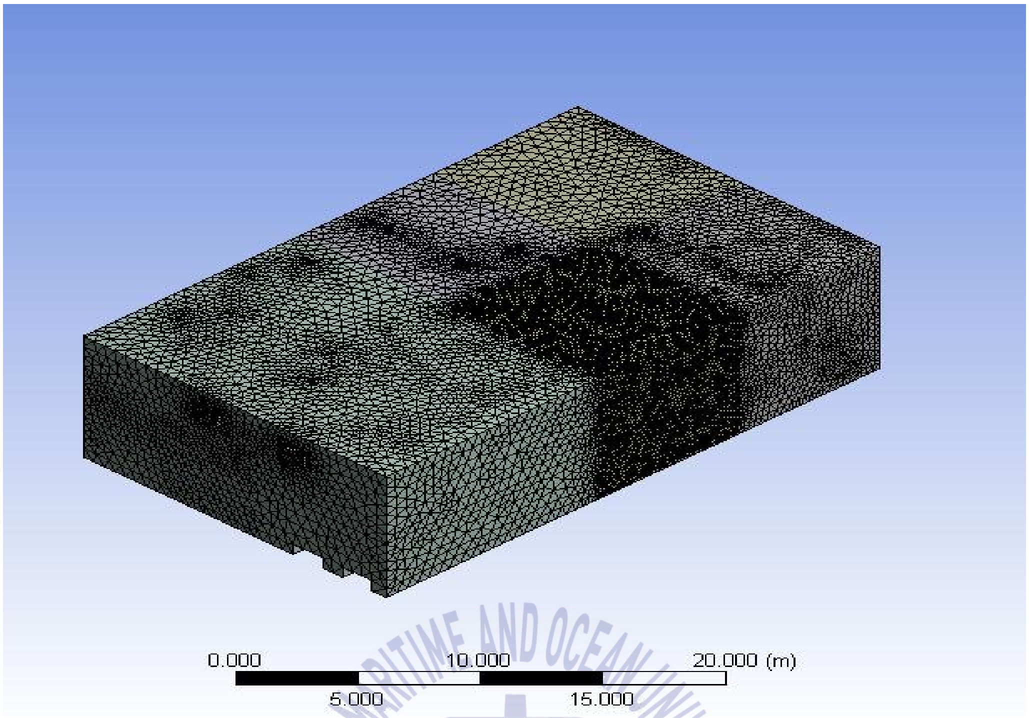

Fig. 5-10 Mesh design of high pressure leak

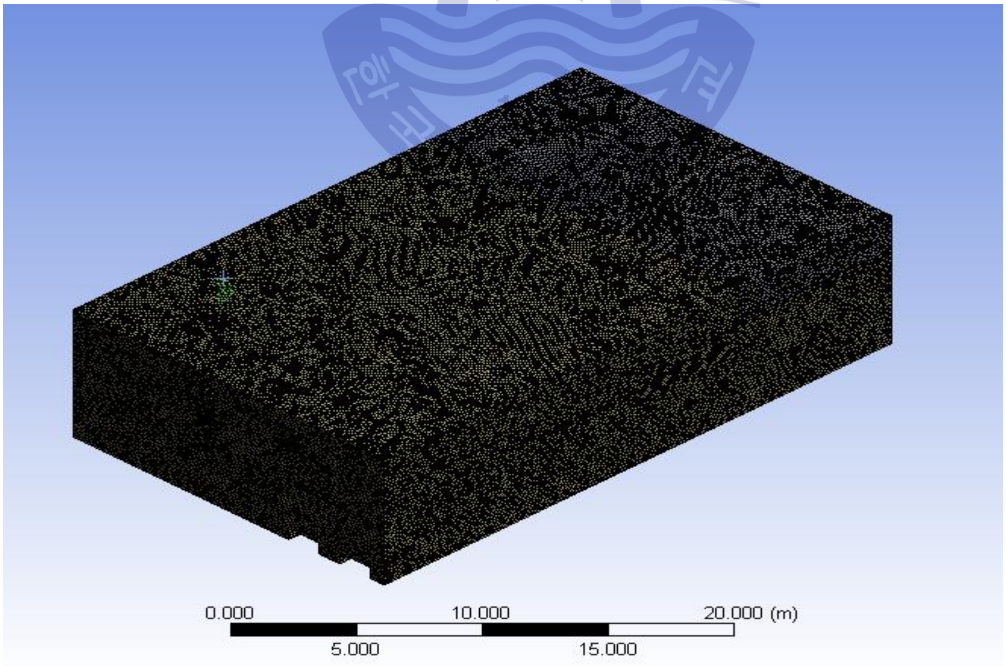

Fig. 5-11 Mesh design of Low pressure leak

5.4 Initial and boundary condition

LNG gas dispersion simulation is carried out in cargo compressed room in accordance with pinhole size, boundary condition is set to two(2) pressure in' at natural vents, seventeen(17) 'pressure out' at mechanical ventilators and 'mass-flow- inlet" at leak points.

5.4.1 Physical properties

To do gas dispersion simulation, actual LNG gas physical properties are used.

5.4.2 Mass flow rate

$$\frac{dm}{dt} = c_d A_h P_0 K \sqrt{\frac{W_g}{\gamma R T}}$$

Table 5-3 Mass flow rate for pinhole size variation at 305 bar

Pin hole size	Mass flow rate $\frac{dm}{dt}$(kg/s)	Mass flow rate (kg/h)
4.5 mm	0.80	2,880
5.0 mm	1.00	3,600
5.6 mm	1.25	4,500

Table 5-4 Mass flow rate for pinhole size variation at 1 bar

Pin hole size	Mass flow rate $\frac{dm}{dt}$(kg/s)	Mass flow rate (kg/h)
100 mm	1.8	6,480
140 mm	3.5	12,600

$\frac{dm}{dt}$ = mass flow rate, $C_d = (0.97), coefficient\ of\ leak$, $A_h = Area\ of\ crack\ hole$, $P_0 = pipe\ internal\ pressure$, $W_g = molecular\ weight \gamma = specific\ heat\ ration\ (\frac{c_p}{c_v})$, R$= gas\ constant$, $T = gas\ tmperature$

$$K = \gamma(\frac{2}{\gamma+1})^{\frac{\gamma+1}{2(\gamma-1)}}$$

Table 5-5 Numerical condition

Cargo compressor room size(meter)	Kind of Grid & size	Boundary condition	Type of Leak	Numerical setting
Width x Depth x Height (28.5x17.5x7.5)	Tetrahedron mesh 1,437,630 element 263,163 nodes	- Leak Gas : CH_4 - Pressure in : 101,325 Pa - Pressure out : 100,626 Pa - Mass flow in : 305 bar - Leaked gas temperature: 45 ℃ - Room temperature: 25 ℃ - Leak rate 1) 0.8 Kg/s, 2) 1.0 Kg/s, 3) 1.25 Kg/s	High pressure leak	- Density based - k- ε turbulence model, Realizable, - Scalable wall functions
	Tetrahedron mesh 1,941,574 element 365,724 nodes	- Leak Gas : CH_4 - Pressure in : 101,325 Pa - Pressure out : 100,626 Pa - Mass flow in : 1 bar - Leaked gas temperature: -110 ℃ - Room temperature: 10 ℃ - Leak rate 1) 1.8 Kg/s, 2) 3.5 Kg/s,	Low pressure leak	

5.5 Solution method

When performing time dependent simulation, the convergence criterion of residual was set as 0.00001. The simulation was executed with two computers. One is 3.50 GHz Intel® Xenon processor and the other is 64.0 GB of RAM and 3.40 GHz Intel® Core(TM) i7-6800K processor and 64.0 GB of RAM. The execution time for this paper is approximately one month with two(2) work stations to achieve a converged simulation.

5.6 Mesh validation and Courant number

Mesh validation was performed at the optional point(14, 7, 12) with different mesh size 0.02, 0.025 and 0.03 m. Mesh size was adopted to 0.025 m as useful value.

Table 5-6 Methane concentration as per mesh size

Time(seconds)	CH4 ppm(0.02 m)	CH4 ppm(0.025 m)	CH4 ppm(0.03 m)
1.0	56,800	56,700	56,900
1.5	38,760	38,760	40,900
2.0	35,290	35,300	35,800
2.5	34,400	34,400	35,100
3.0	33,390	33,400	34,400
3.5	32,100	32,100	33,300
4.0	30,210	30,210	31,940
4.5	27,130	27,140	29,660
5.0	22,250	22,250	22,260

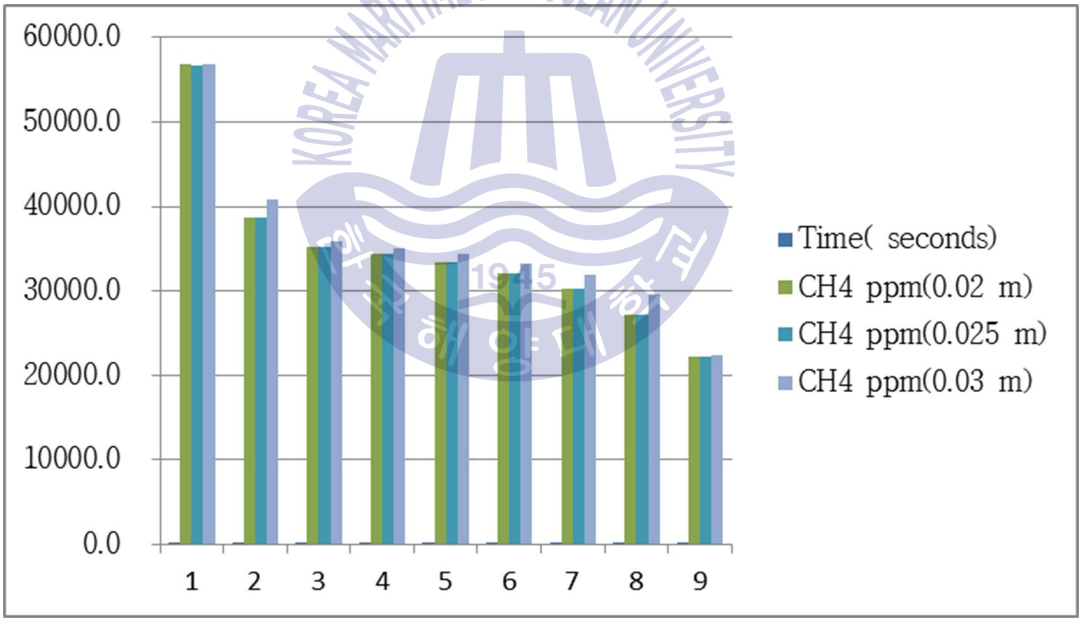

Fig. 5-12 Methane concentration as per mesh size

In addition to mesh validation, to make a convergence of the CFD simulation, Courant number setting is very important, it is defined as follows.

$$Courant\ \ Number = \frac{u\Delta t}{\Delta x} \leq Cmax$$

Where the dimensionless number is called the Courant number,

- u is the magnitude of the velocity
- Δt is the time step
- Δx is the length interval

In mathematics, the Courant number condition is a necessary condition for convergence while solving certain partial differential equations numerically by the method of finite differences. Unsteady calculation is a sequence of processes for finding the answer every time step. Therefore, it must be converged every time step. if it is not possible to converge in the current step, the analysis results of the next step are incorrect because the correct answer is used to calculate the results. For time step size, although it is not possible to determine it exactly in a certain way, it is conceptually advantageous to determine the time step size by which the flow moves to one cell. For mathematical convergence, Courant number condition must be met. Courant number setting for high pressure leak was set to adjust from 0.0001 to 5 by solution steering menu in Fluent.

6. Results and discussions

6.1 High pressure gas leak

Table 6-1-1 shows the leak flow rate, gas detection alarm time after the leak starting from the Hi pressure pump/vaporizer, CH_4 volume fraction after 10 seconds and CH_4 volume fraction at 508 seconds as final transient flow calculation. Gas leak was continued during 10 seconds after the gas alarm and stop. And after mechanical ventilators only is operated without gas leak. The first gas detection alarm is monitored at the No.1 location for all three cases. The highest CH_4 volume fraction at 10 seconds after alarm is monitored at the case 3 as the fuel gas supply rupture case. Final measuring at 508 seconds is monitored without flammable concentration all measuring values are below 6,500 ppm.

Table 6-1-1 Mass flow rate for each scenario of high pressure leak

Case	Pin hole Size	Leak flow rate	Gas detection alarm point (CH4 volume fraction at gas detection point 1)	CH4 volume fraction at 10 seconds after alarm	CH4 volume fraction at final measuring time (at 508 seconds)
1	4.5 mm	0.87 kg/s	4 seconds (27,190 ppm)	14 seconds 22,444 ppm	5,296 ppm

2	5.0 mm	1.0 kg/s	3.5 seconds (26,516 ppm)	13.5 seconds 20,661 ppm	6,345 ppm
3	5.6 mm	1.25 kg/s	3 seconds (32,775 ppm)	13 seconds 29,052 ppm	6,156 ppm

Fig. 6-1-1 shows that the location of gas detection sensors. Four sets of infrared gas detection sensor are installed near the underneath of the ceiling at 500mm below. The location of the four sensors is positioned left and right in the direction of the vent side in the cargo compressor room.

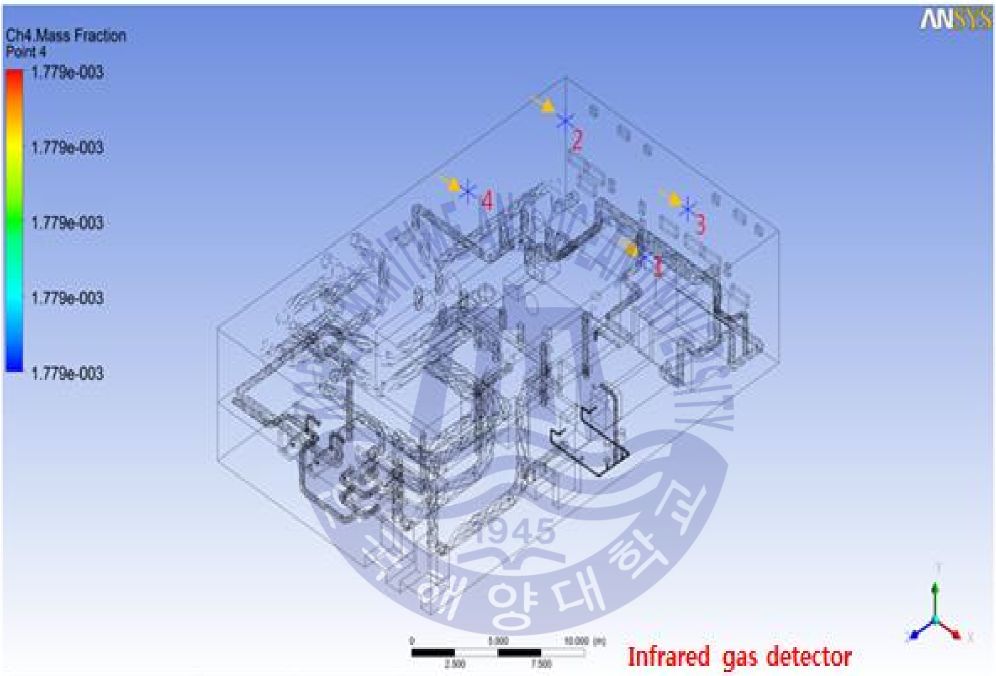

Gas detection sensor location	X (m)	Y(m)	Z(m)
1 Location	13	7	6.5
2 Location	2	7	2
3 Location	12	7	2
4 Location	2	7	10

Infrared gas detector

Fig. 6-1-1 Gas detectors and locations

These locations were optionally decided by the agreement with the ship-owner and shipbuilder without the CFD analysis. Applied infrared gas detectors are point detectors for gas concentration monitoring potentially hazardous environment with less than response time 4.5 second.

Fig. 6-1-2, 6-1-3 and 6-1-4 show that the gas dispersion simulation. Gas cloud is made by CH4 volume fraction. Volume fraction 5% ~ 15% is flammable limits, gas detection is alarmed at 0.015 of 30% of LFL(0.05). So gas cloud behavior is seen between 0.015 and 0.15. Gas alarm time according to the leak flow rates are nearly the same at point 1, case 3 is one second faster than others. Gas cloud shapes for three cases are not so much different.

Fig. 6-1-5, 6-1-6 and 6-1-7 show that the gas dispersion simulation after 10 seconds from gas detection alarm. All cases are monitored with similar gas behavior. Gas cloud is vertically positioned from the pinholes surface of the pipe and dispersed to the ceiling and the walls. Their sizes are proportional to the leak flow rate. CH_4 concentration is higher near the leak area and lower far away. The shape of gas cloud which is located far from the leak place is lower positioned than the leak area and gas cloud is accumulated to the ventilator direction.

Fig. 6-1-8, 6-1-9 and 6-1-10 show that gas leak simulation after 10 seconds from gas detection alarm on xy plan. CH_4 concentration contours are proportional to the leak flow rate. CH_4 concentration is higher near the leak area and lower far away.

Fig. 6-1-11, 6-1-12 and 6-1-13 show that gas leak simulation after 10 seconds from gas detection alarm on xy plan from 7 meter above the floor. CH_4 concentration contours are proportional to the leak flow rate. CH_4 gas is widely spread from the leak place and CH_4 is accumulated to the ventilator direction.

Fig. 6-1-14, 6-1-15 and 6-1-16 show that CH_4 volume fraction contour at 508 seconds seen from height 7m. The value of the highest concentration area is 10,230 ppm at the right corner of the compressor room ceiling. Comparing with three cases, CH_4 contour shapes are similar. The values of case 1 are the lowest than others. Since Case 3 leak rate is much more than other cases, so CH_4 concentration is the highest, Case 1 leak rate is the smallest than others.

Fig. 6-1-17, 6-1-18 and 6-1-19 show that CH_4 contour at 508 seconds from height 4m. The value of the highest concentration area is 9,157 ppm in front of the high pressure fuel gas compressor. Comparing with three cases, CH_4 contour shapes are similar. Case 1 value is 6,864 ppm and is the lowest value compared to other cases. Since Case 3 leak rate is much more than other cases, so CH_4 concentration is the highest, Case 1 leak rate is the smallest than others.

Fig. 6-1-20, 6-1-21 and 6-1-22 show that gas CH_4 contour at 508 seconds from height 1 m. The value of the highest concentration area is 10,060 ppm around vapor return compressors. Comparing with three cases, CH_4 contour shapes are similar. Case 1 value is 7,557 ppm and is the lowest value compared to other cases. Since Case 3 leak rate is much more than other cases, so CH_4 concentration is the highest, Case 1 is the smallest than others.

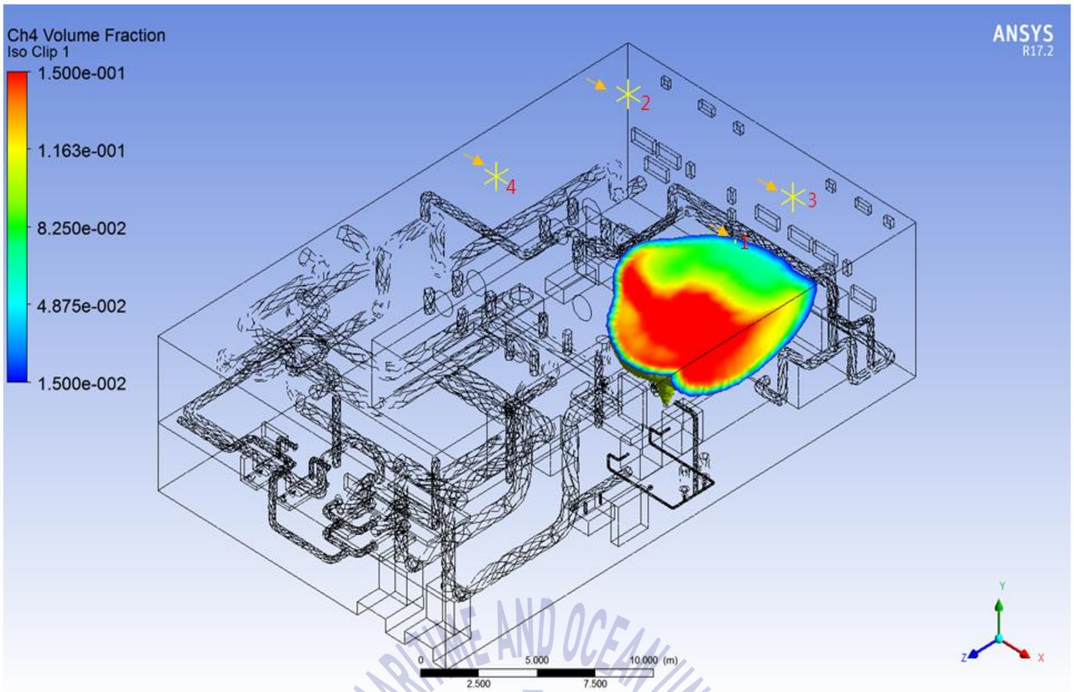

Fig. 6-1-2 Case 1, Gas detection alarm at 4 seconds

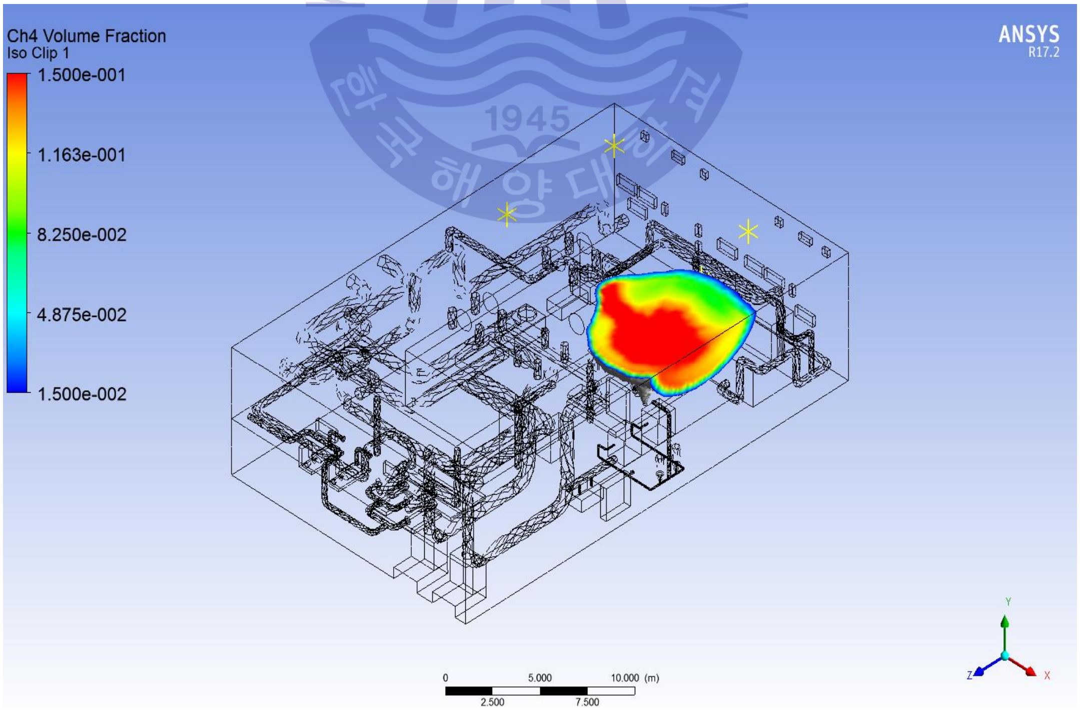

Fig. 6-1-3 Case 2, Gas detection alarm at 3.5 seconds

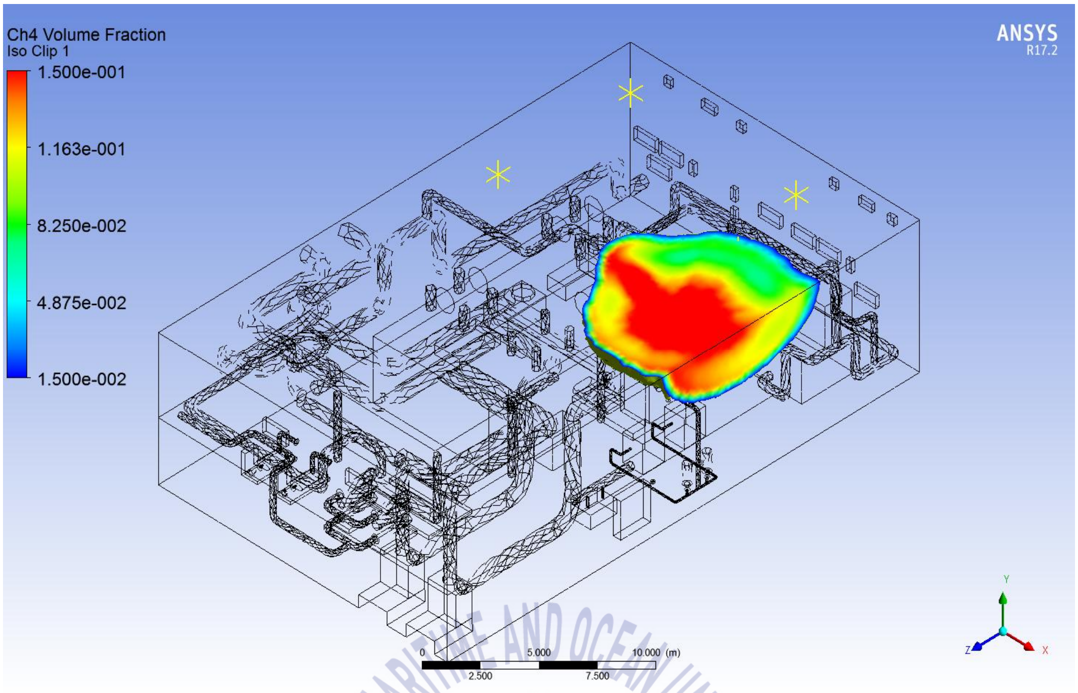

Fig. 6-1-4 Case 3, Gas detection alarm at 3 seconds

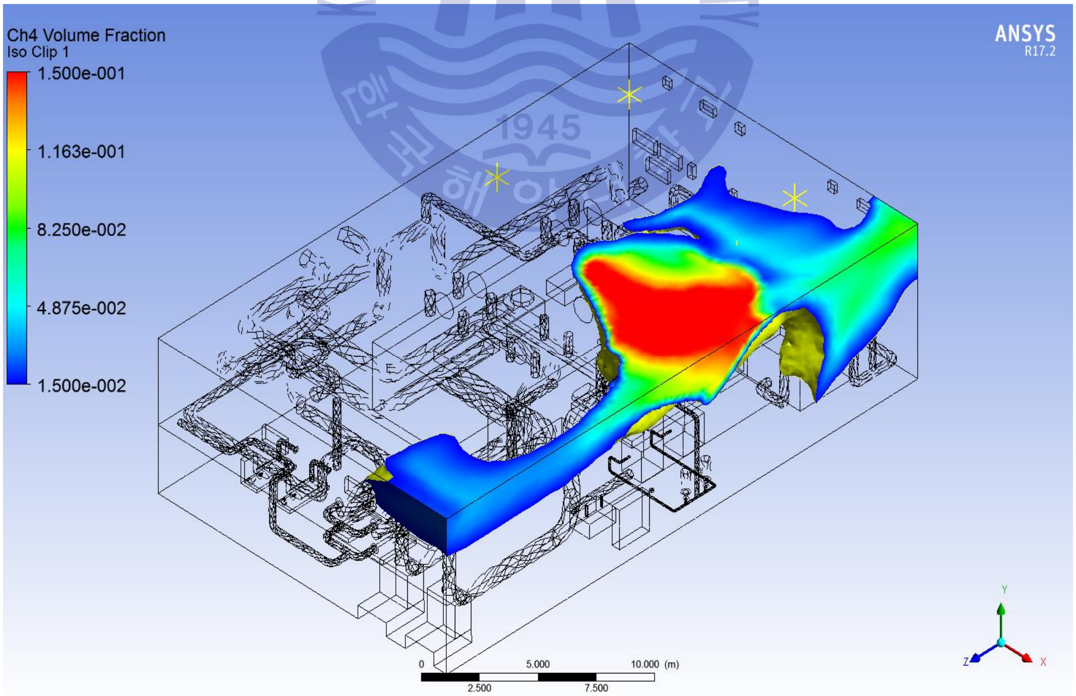

Fig. 6-1-5 Case1, After 10 seconds from gas detection alarm (14 seconds)

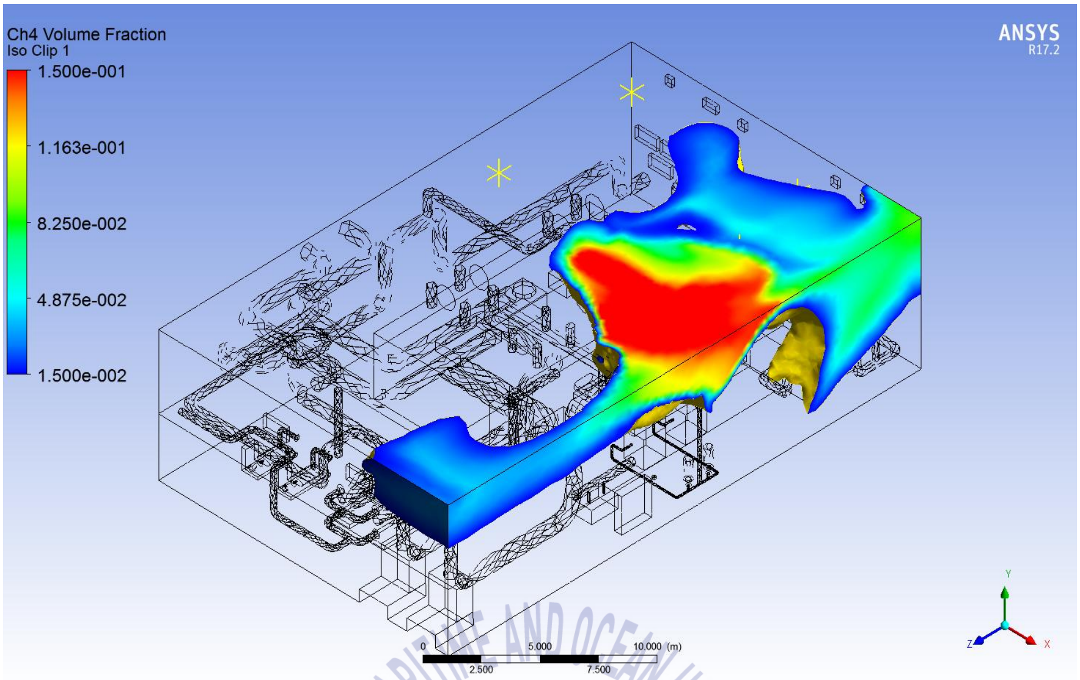

Fig. 6-1-6 Case 2, After 10 seconds from gas detection alarm(13.5 seconds)

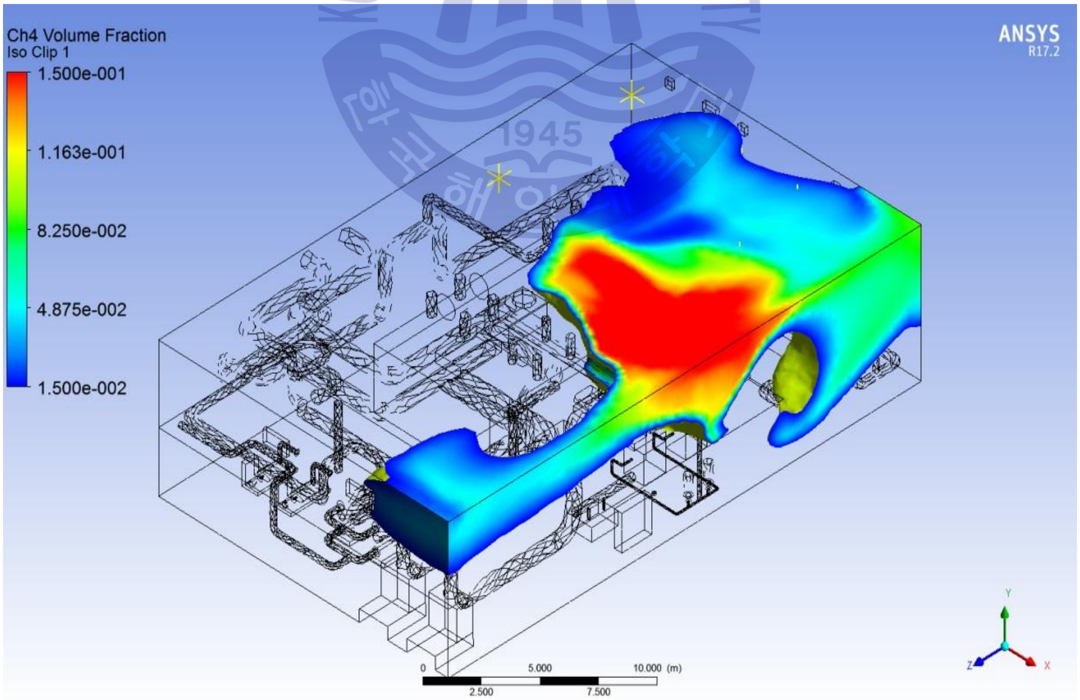

Fig. 6-1-7 Case 3, After 10 seconds from gas detection alarm(13 seconds)

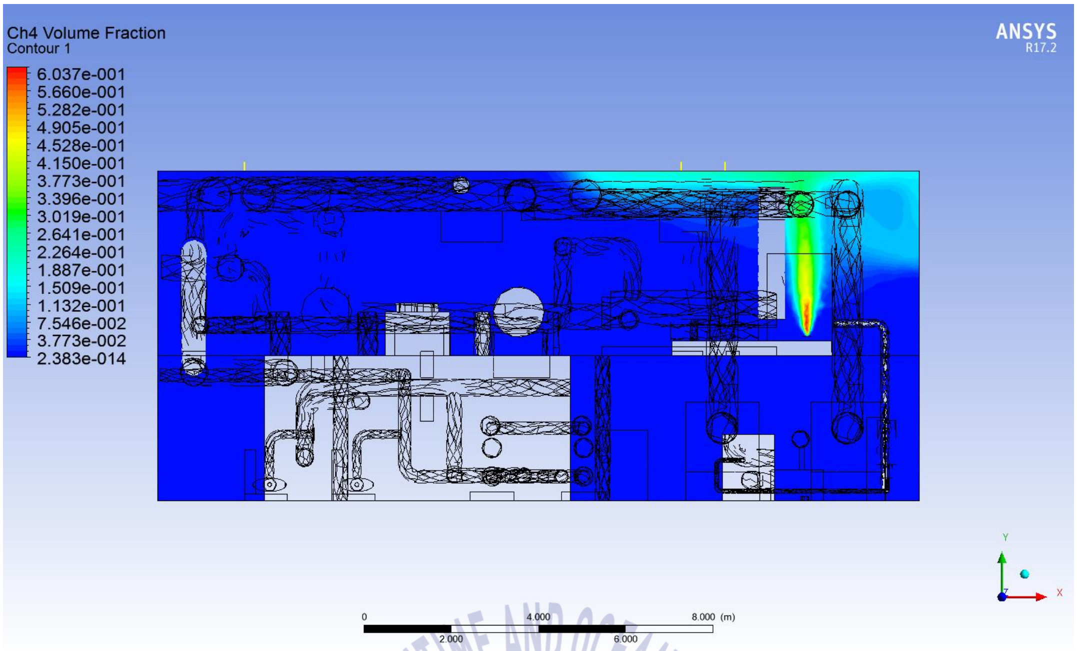

Fig. 6-1-8 Case1, After 10 seconds from gas detection alarm(14 seconds) (xy plan)

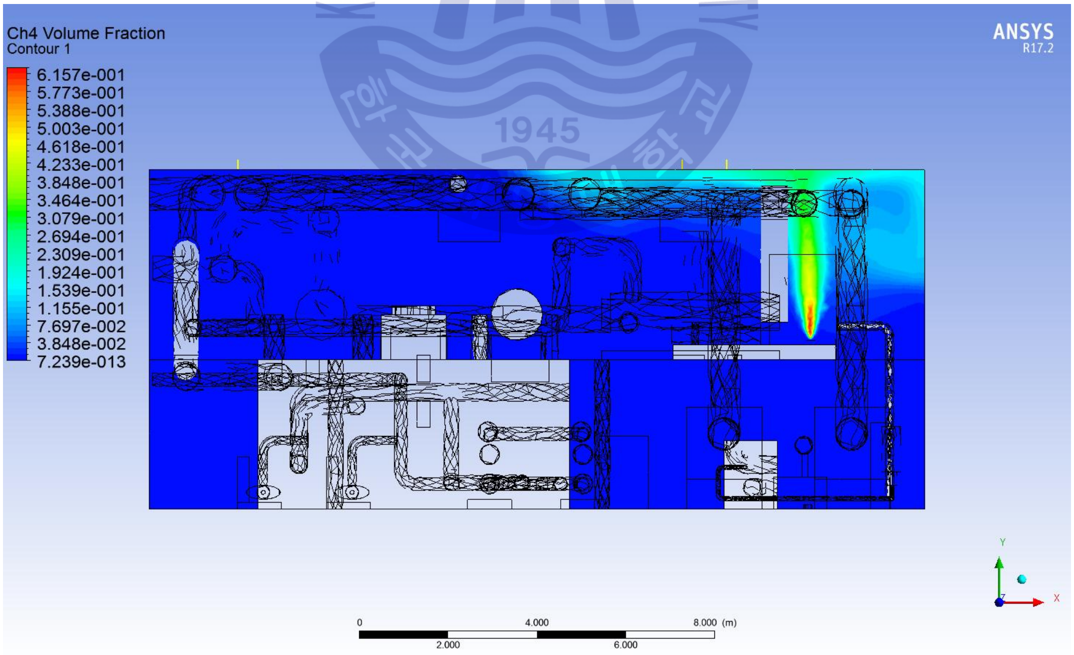

Fig. 6-1-9 Case2, After 10 seconds from gas detection alarm(14 seconds) (xy plan)

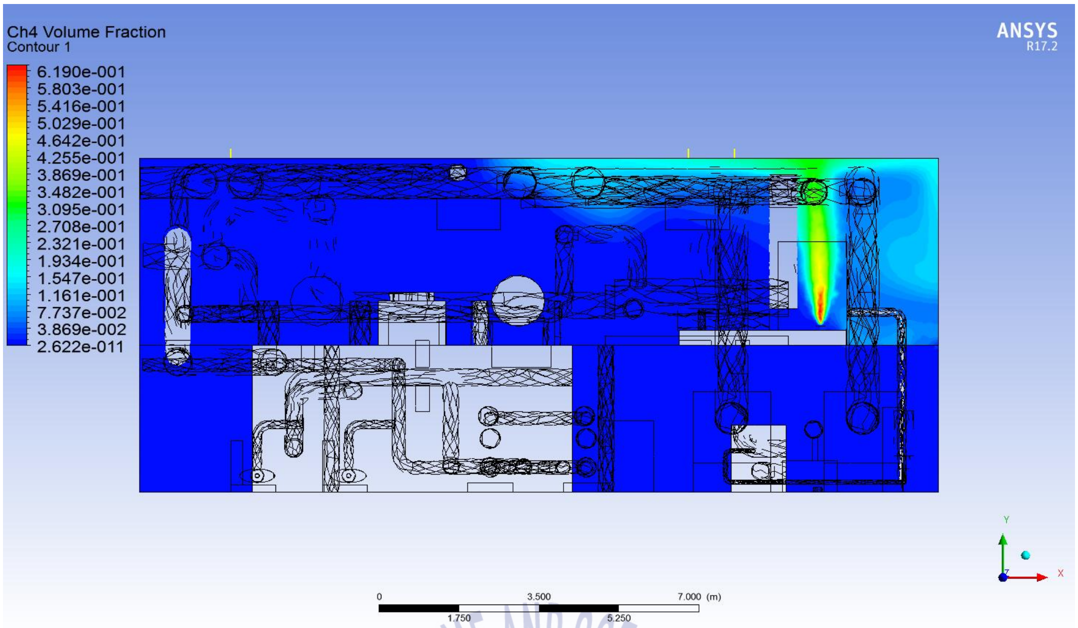

Fig. 6-1-10 Case3, After 10 seconds from gas detection alarm(13 seconds) (xy plan)

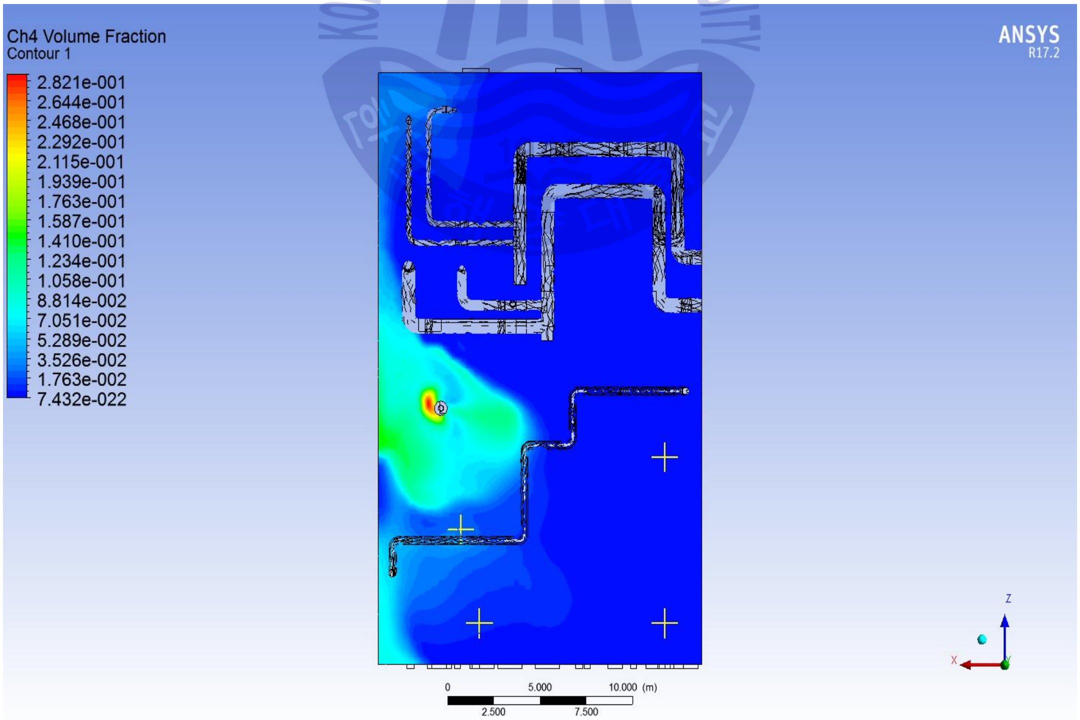

Fig. 6-1-11 Case1, After 10 seconds from gas detection alarm (yz plan)

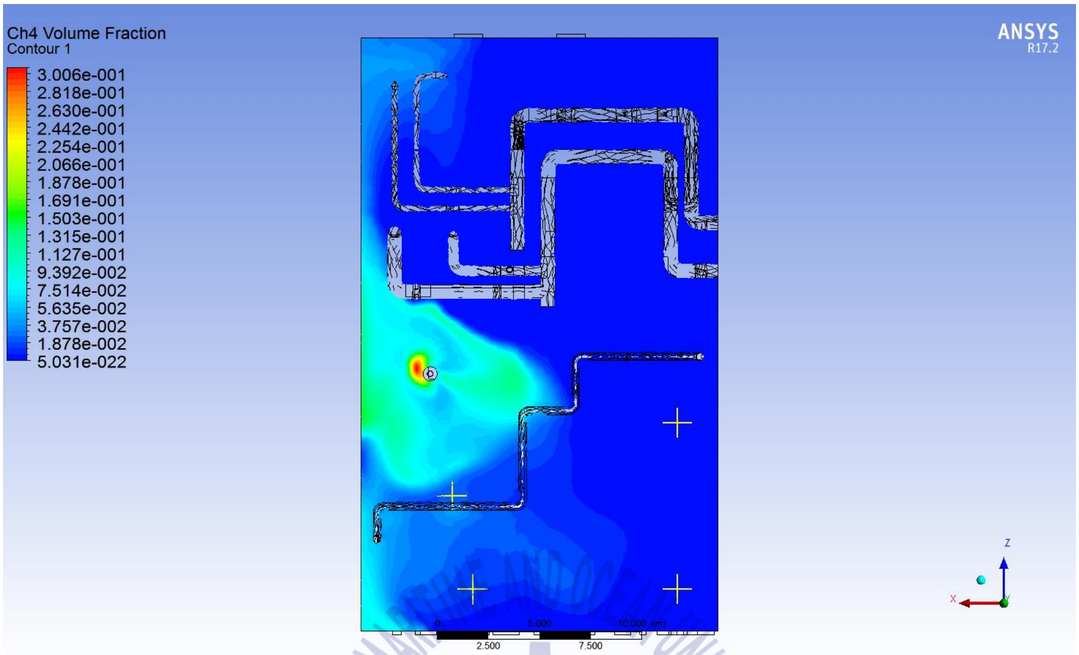

Fig. 6-1-12 Case2, After 10 seconds from gas detection alarm (yz plan)

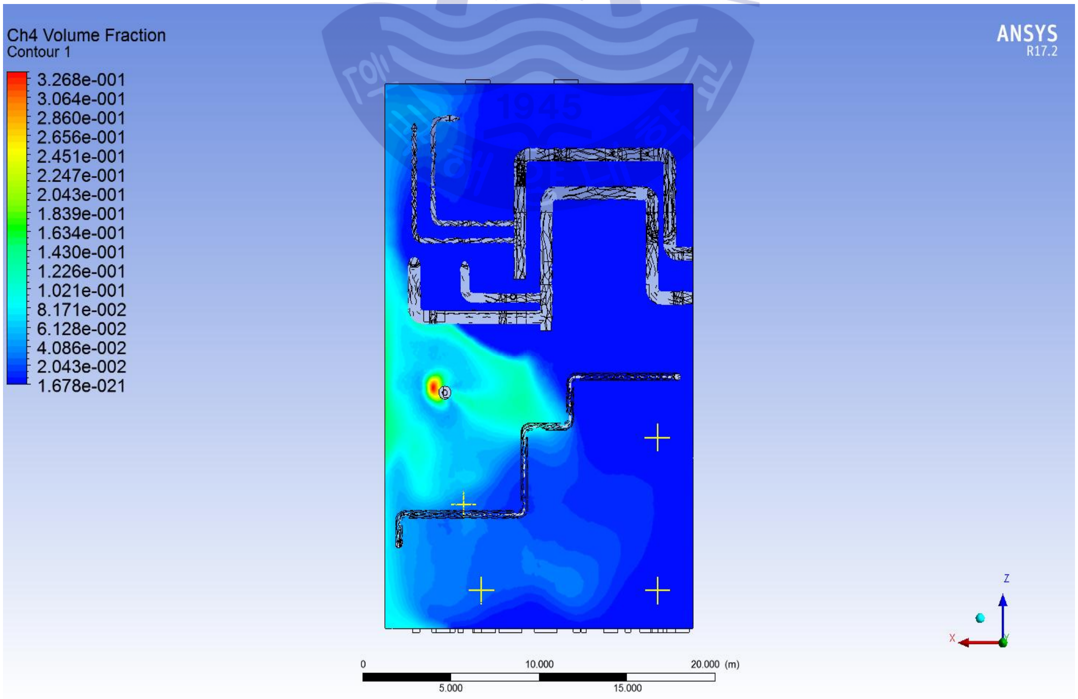

Fig. 6-1-13 Case3, After 10 seconds from gas detection alarm(yz plan)

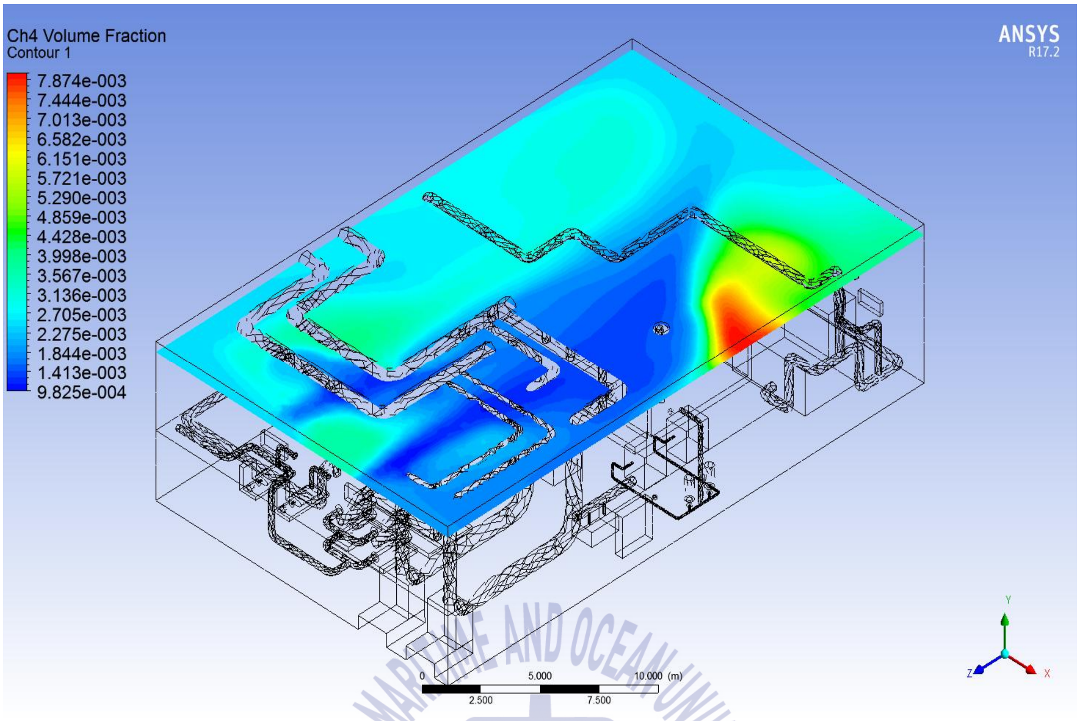

Fig. 6-1-14 Case 1, CH_4 volume fraction at 508 seconds (height 7m)

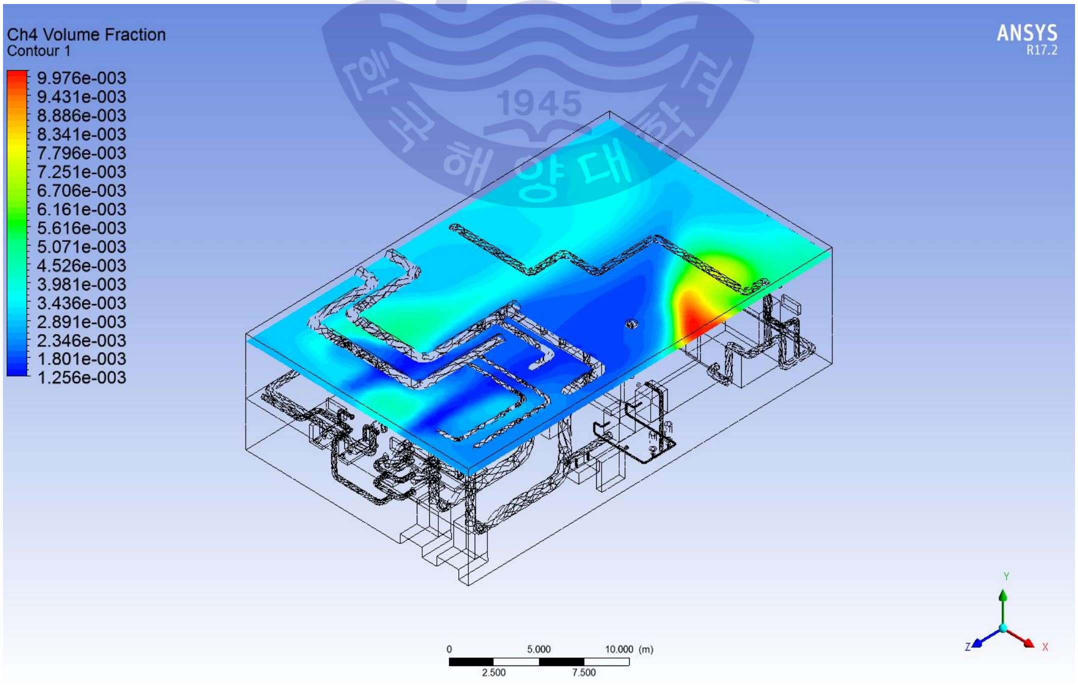

Fig. 6-1-15 Case 2, CH_4 volume fraction at 508 seconds (height 7m)

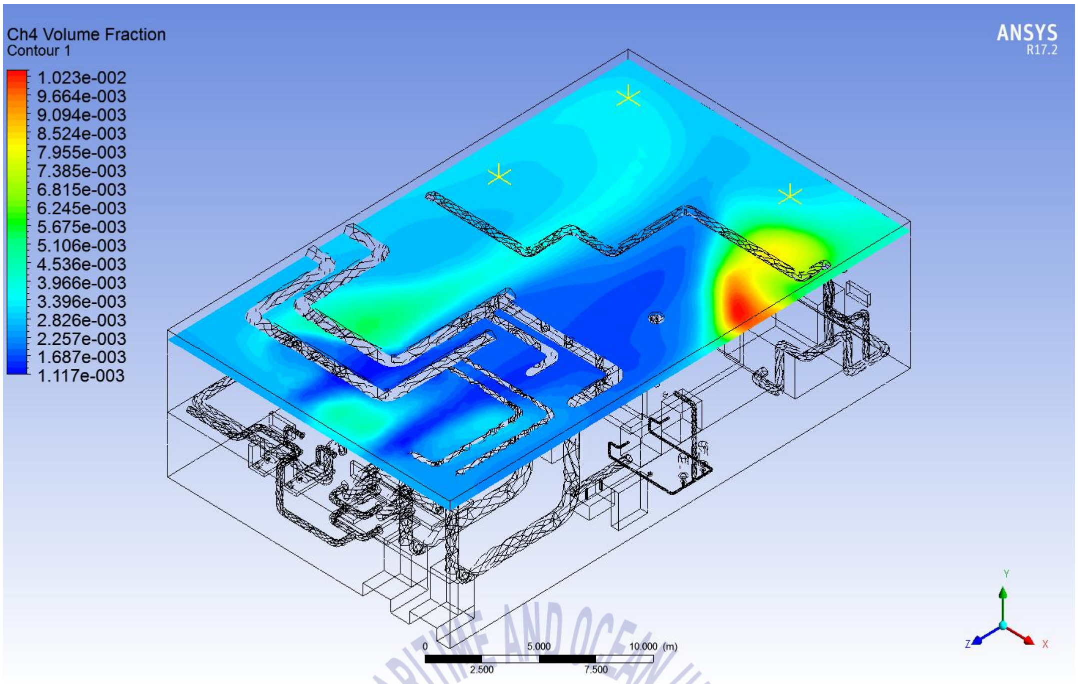

Fig. 6-1-16 Case 3, CH_4 volume fraction at 508 seconds(height 7m)

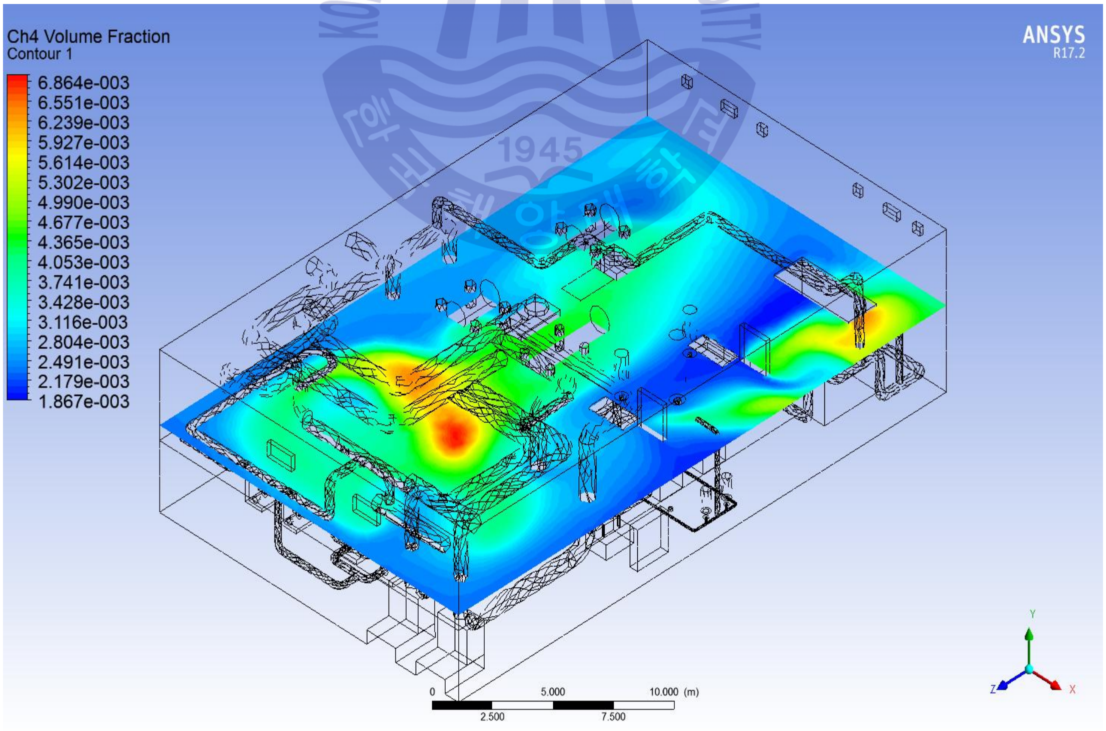

Fig. 6-1-17 Case 1, CH_4 volume fraction at 508 seconds (height 4m)

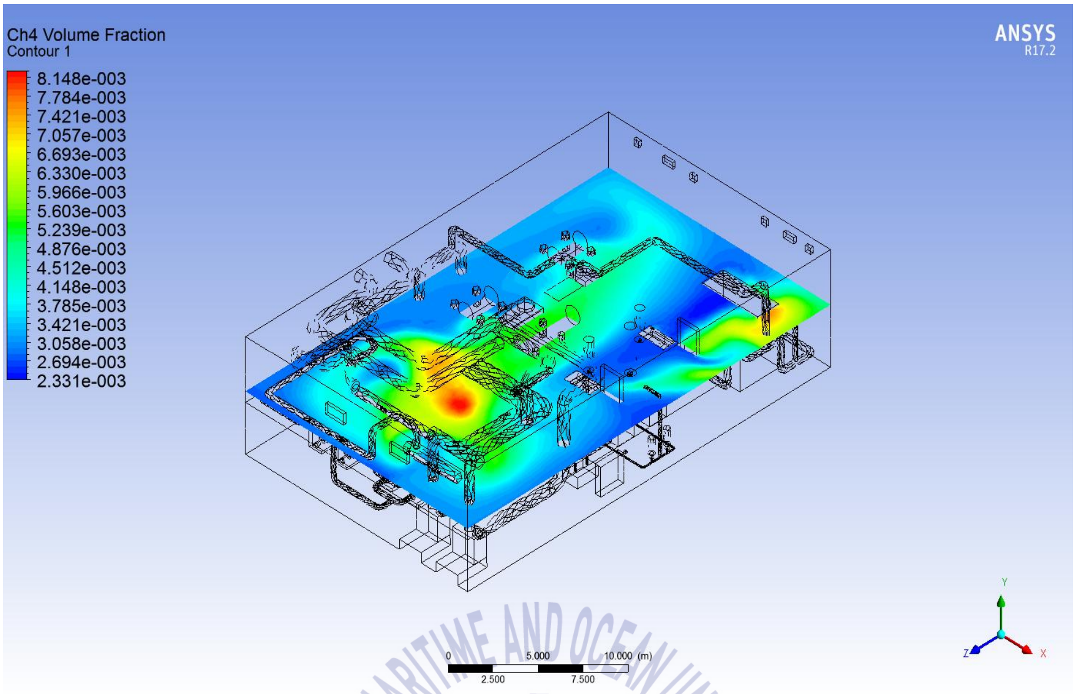

Fig. 6-1-18 Case 2, CH_4 volume fraction at 508 seconds (height 4 m)

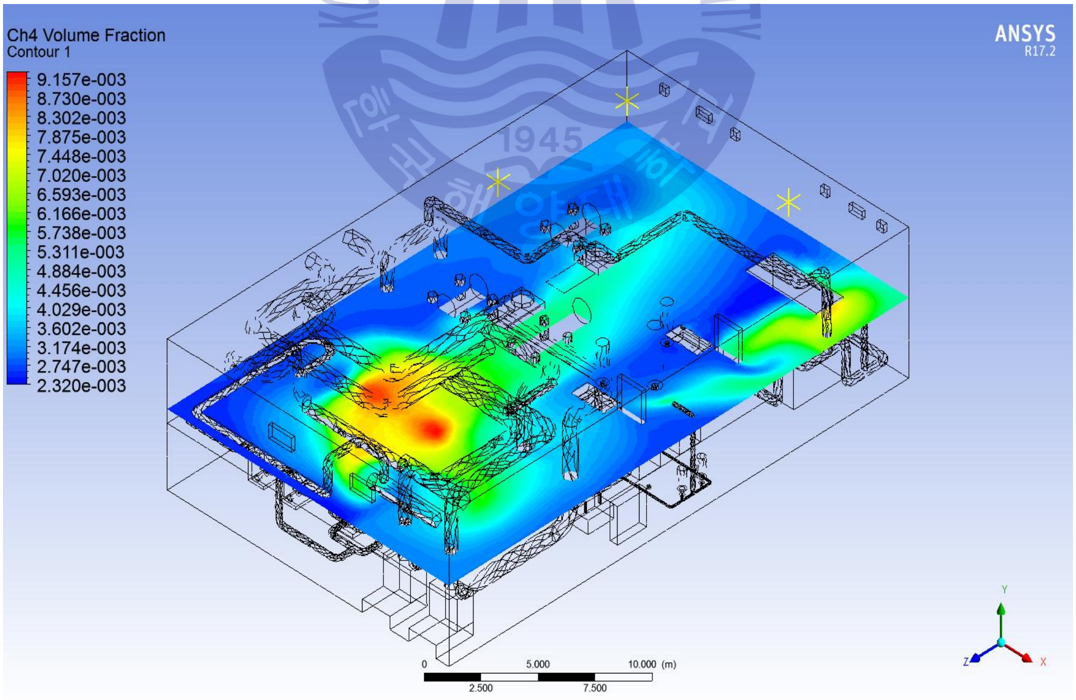

Fig. 6-1-19 Case 3, CH_4 volume fraction at 508 seconds(height 4 m)

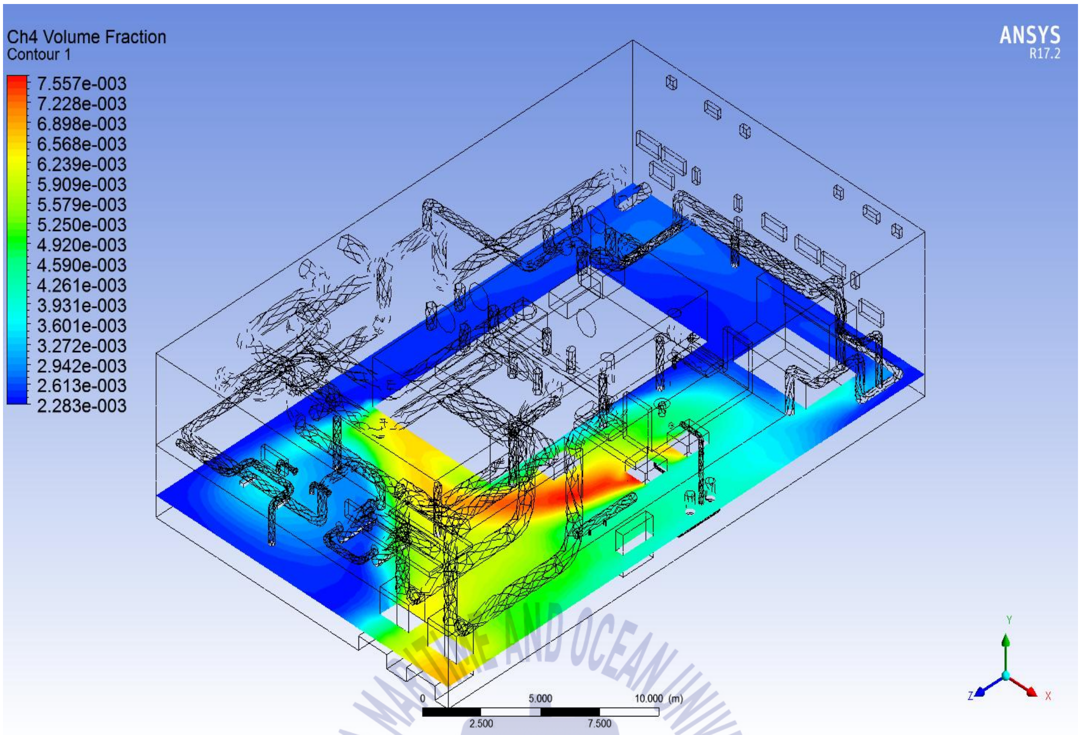

Fig. 6-1-20 Case 1, CH_4 volume fraction at 508 seconds (height 1 m)

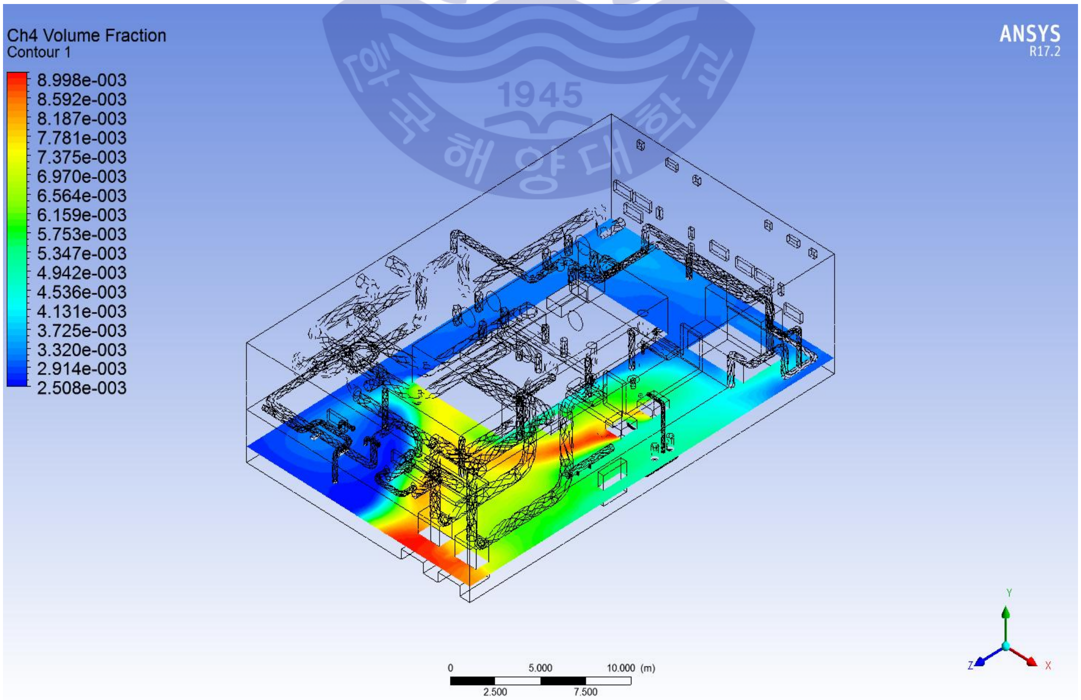

Fig. 6-1-21 Case 2, CH_4 volume fraction at 508 seconds (height 1 m)

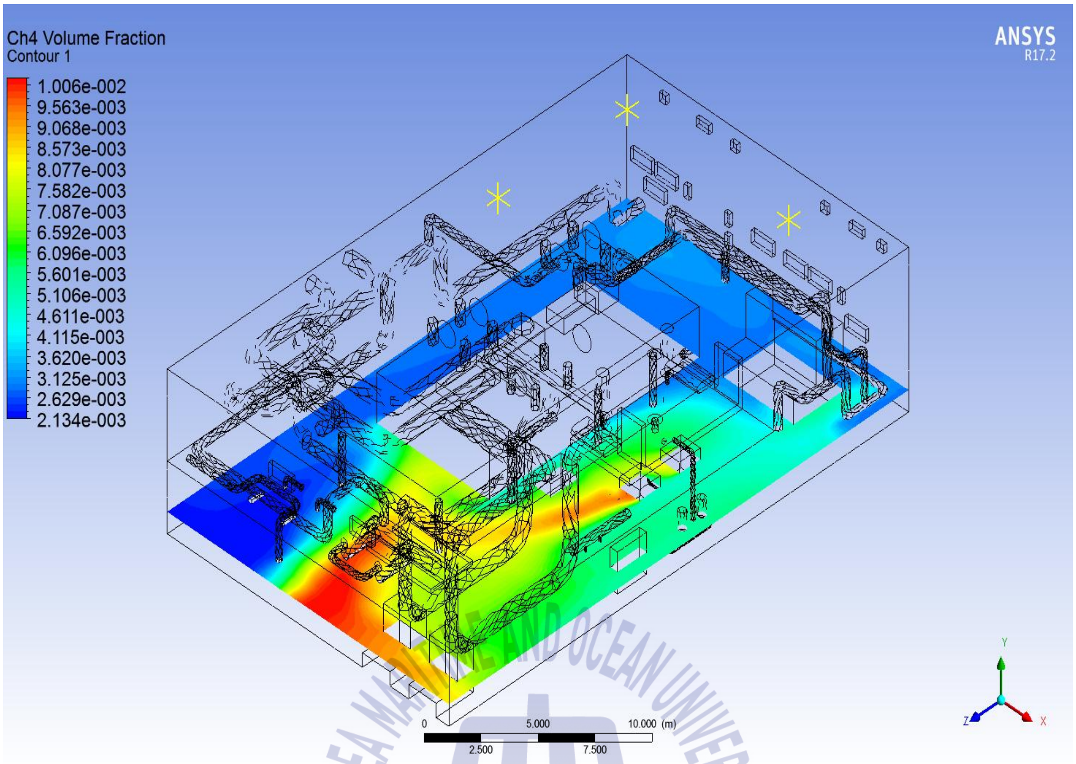

Fig. 6-1-22 Case 3, CH_4 volume fraction at 508 seconds (height 1 m)

Table 6-1-2 is CH_4 volume fraction variation from 2.5 seconds to 508 seconds at gas detection point 1 for each case. Gas alarm is sounded at 4 seconds, 3.5 seconds and 3 seconds, gas leak is continuing until 10 seconds. And then leak is stopping and mechanical ventilator is still operating until 508 seconds.

Fig. 6-1-23, 6-1-24 and 6-1-25 show that CH_4 volume fraction variation at gas detection point 1. Gas detection points are total four sets, the gas cloud is captured at the first alarm point for each case. Maximum methane gas concentration for three cases is below 60,000 ppm. Since leak stops, methane gas concentrations are dramatically decreasing below 6,500 ppm at 508 seconds

Fig. 6-1-26, 6-1-27 and 6-1-28 show that velocity vector movement at various plan. The highest velocity vector is at the HP Pump/Vaporizer discharge pipe and the vector movements are verified from the pressure inlets to the pressure outlets.

Table 6-1-2 CH_4 volume fraction(ppm) variation at gas detection point 1

Time (seconds)	Case 1 (ppm) (CH4 volume fraction)	Time (seconds)	Case 2 (ppm) (CH4 volume fraction)	Time (seconds)	Case 3 (ppm) (CH4 volume fraction)
2.5				2.5	2397
3		3	3087	3	32775
3.5	5043	3.5	26516	3.5	59198
4	27190	4	53233	4	52667
4.5	44054	4.5	54243	4.5	49699
5	48882	5	50012	5	46898
5.5	46985	5.5	46253	5.5	45207
6	44229	6	44369	6	44701
6.5	42324	6.5	43321	6.5	44177
7	40433	7	41028	7	42429
7.5	38117	7.5	37765	7.5	39731
8	35426	8	34493	8	36728
8.5	32341	8.5	31510	8.5	33928
9	29122	9	28467	9	31652
9.5	26197	9.5	25166	9.5	29476
10	24117	10	22390	10	26995
10.5	23192	10.5	20643	10.5	24775
11	22604	11	19839	11	23583
11.5	21660	11.5	19643	11.5	23512
12	20536	12	19589	12	24402
12.5	19822	12.5	19554	12.5	26197
13	19964	13	19786	13	29052
13.5	20928	13.5	20661	13.5	31192
19.5	47072	18	46950	18	47542
28	45224	28	51193	23	36922
38	28573	38	38924	28	43985
48	25388	48	31970	33	44281
58	22444	58	28928	43	42674
68	21196	68	26765	53	40503
78	20304	78	25166	63	38134
88	19643	88	23388	73	35761
98	19143	98	23388	83	33329
108	18732	108	22675	93	31069
158	16513	158	19804	103	29069
208	13787	208	16244	153	22836
258	11162	258	13104	203	18177
308	9342	308	10928	253	14738
358	8134	358	9901	303	11918
408	7303	408	8837	353	10117
458	6327	458	7610	403	9000
508	5296	508	6345	453	7592
				508	6156

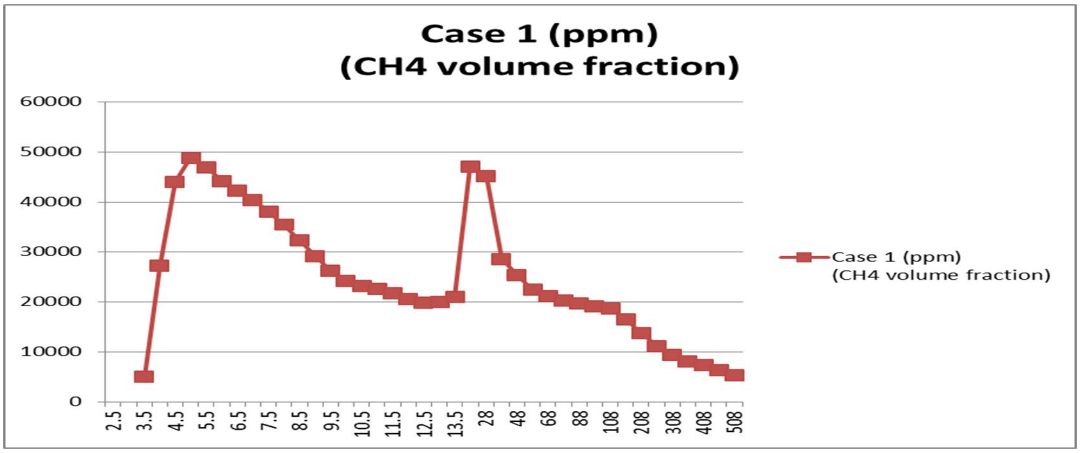

Fig. 6-1-23 Case 1, CH_4 volume fraction variation at gas detection point 1

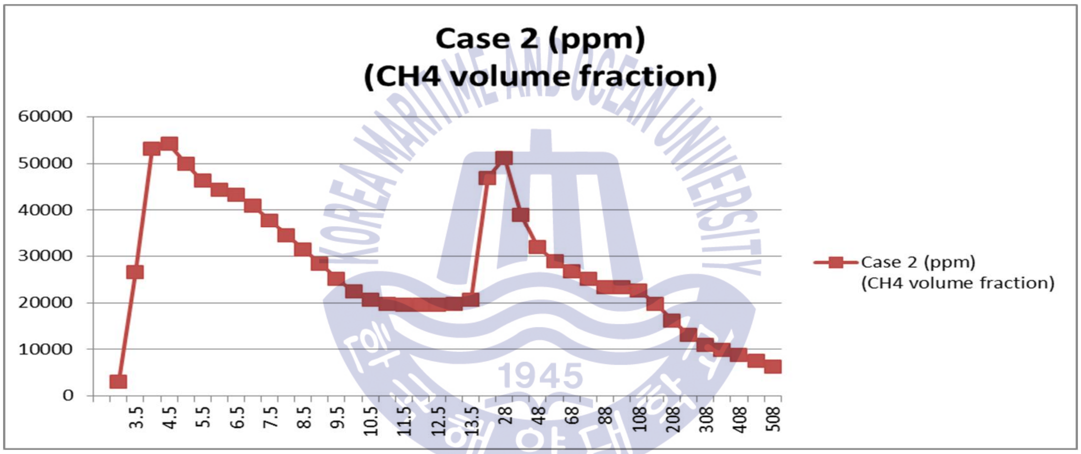

Fig. 6-1-24 Case 2, CH_4 volume fraction variation at gas detection point 1

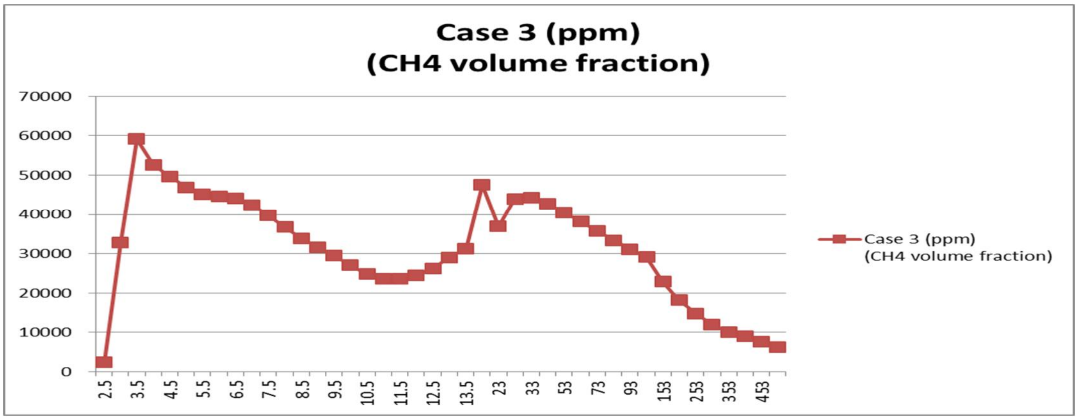

Fig. 6-1-25 Case 3, CH_4 volume fraction variation at gas detection point 1

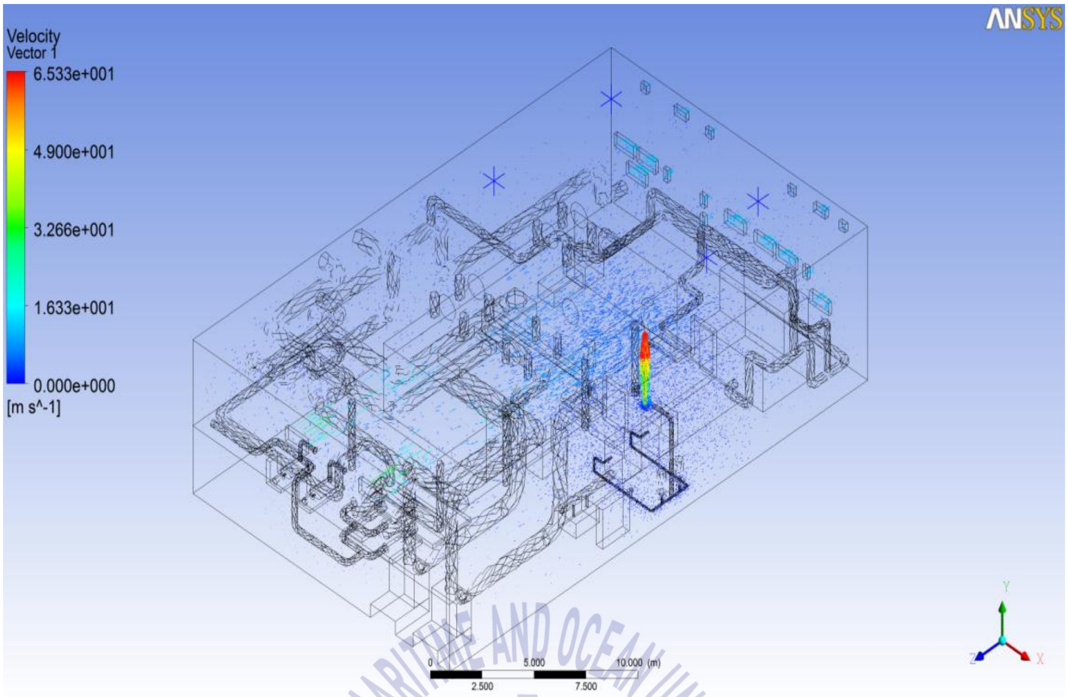

Fig. 6-1-26 Velocity vector movement at 3-dimensional space

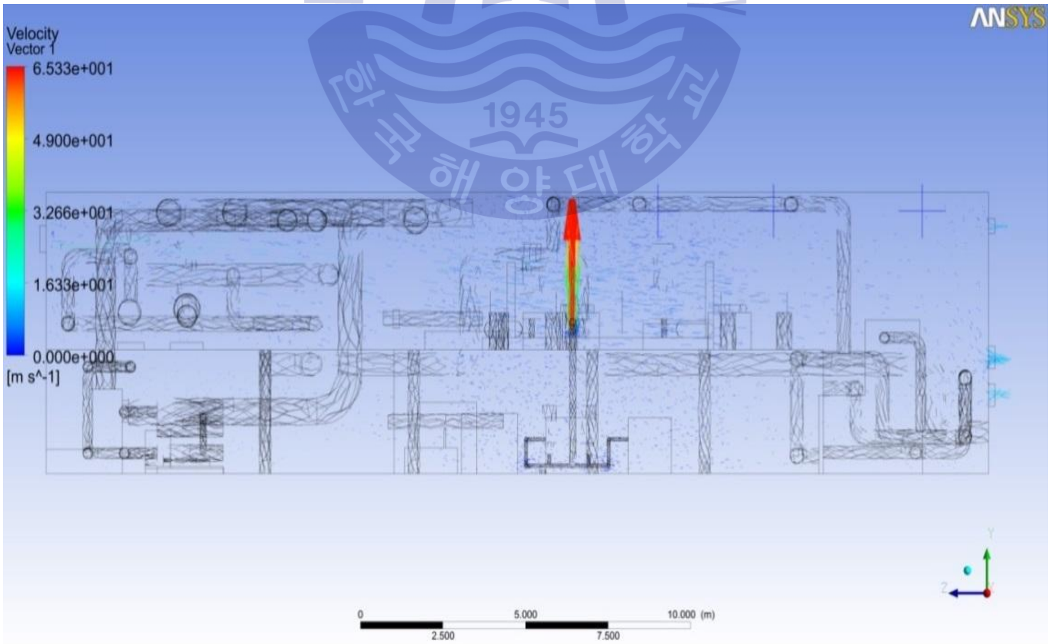

Fig. 6-1-27 Velocity vector movement at Y-Z plane

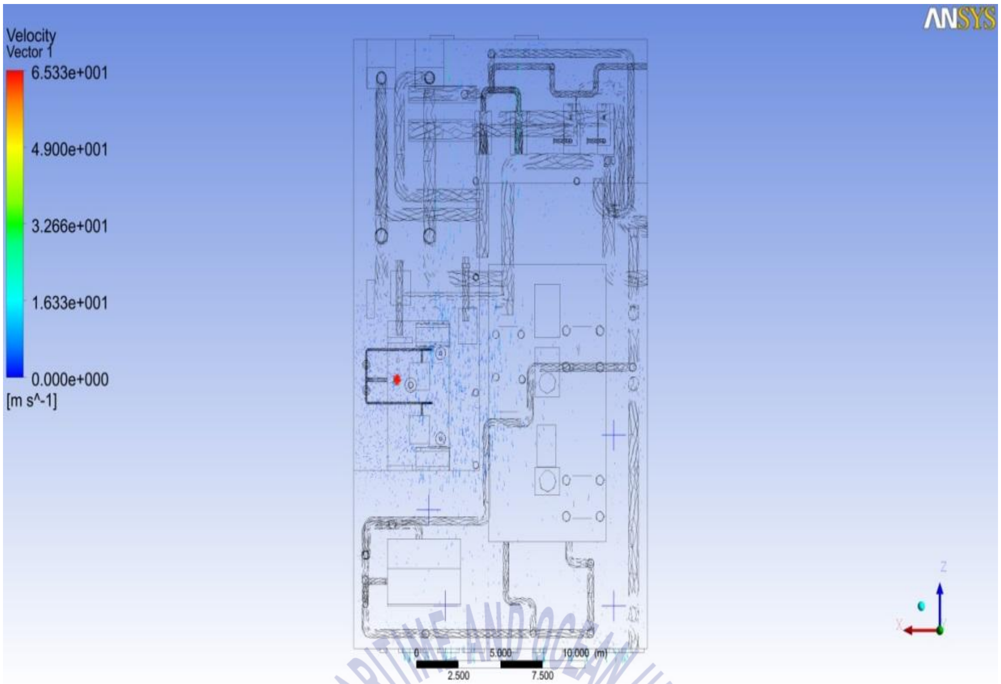

Fig. 6-1-28 Velocity vector movement at X-Z plane

6.2 Low pressure gas leak

Table 6-2-1 shows mass flow rate for each scenario of low pressure leak, gas detection alarm time after the leak starting from the VR compressor discharge pipe, CH_4 volume fraction after 10 seconds and CH_4 volume fraction at 2,312 and 4,697 seconds as final transient flow calculation. Gas leak was continued during 10 seconds after the gas alarm and stop. And after mechanical ventilators only is operated without gas leak. The first gas detection alarm is monitored at the No.1 location for case 1 and case 2. CH_4 volume fraction is monitored at 10 seconds after alarm at the four gas detection points. Final measuring at 2,312 and 4,697 seconds for each case is monitored without flammable concentration and all measuring values are below 9,000 ppm, and No.4 gas detection point for case 1 is 11,216 ppm. Leak flow rate of case 2 is two(2) times more than case 1, it take nearly two(2) times to ventilate CH_4 for all gas detection points comparing final measuring time between case 1 and case 2. Transient calculation of case 2 is 2,385 seconds much more than case 1.

Table 6-2-1 Mass flow rate for each scenario of low pressure leak

Case	Pinhole Size	Leak flow rate	Gas detection point	Gas detection alarm point CH4 volume fraction	CH4 volume fraction at 10 seconds after alarm	CH4 volume fraction at final measuring time Case 1 : at 2,312 seconds Case 2 : at 4,697 seconds
1	100 mm	1.8 kg/s	1	**80 seconds** (16,244 ppm)	(18,928 ppm)	(5,260 ppm)
			2	(12,547 ppm)	(16,172 ppm)	(8,783 ppm)
			3	(9,270 ppm)	(12,457 ppm)	(7,068ppm)
			4	(8,765 ppm)	(11,720 ppm)	(11,216ppm)
2	140 mm	3.5 kg/s	1	**65 seconds** (16,746 ppm)	(22,194 ppm)	(4,011 ppm)
			2	(6,707 ppm)	(19,053 ppm)	(6,707 ppm)
			3	(5,224 ppm)	(13,894 ppm)	(5,224 ppm)
			4	(5,875 ppm)	(10,424 ppm)	(8,693 ppm)

From Fig. 6-2-1 to Fig. 6-2-24 show 2D/3D plot of CH_4 volume fraction according to Table 6-2-1. Gas detection points and gas cloud assuming is the same as applied with high pressure leak as already described. Monitored two cases gas behavior is similar movement. Gas cloud is vertically positioned from the pinholes surface of the pipe and dispersed to the ceiling and the walls. Leak point is located at the first deck under and gas temperature inside pipe is -110° C. So comparatively heavier gas than high pressurized leak gas with temperature 43° C at 305 bar cannot be easily dispersed to other spaces and dense high flammable gas is found under the first deck which is farthest from the ventilators. Gas cloud behavior is captured from the gas detection alarm to the 10 seconds after gas leak. Their sizes are proportional to the leak flow rate.

Gas cloud of case 1 at 900 seconds and case 2 at 1,320 seconds show that all cargo compressor room space is greater than gas alarm value 30% LFL (Lower Flammable Limits) with CH_4 volume fraction between 15,000 and 150,000 ppm. Flammable gas cloud for two cases between 50,000 and 150,000 ppm at 500 seconds and 900 seconds is shown on Fig. 6-2-17 and 18, flammable gas cloud is shown on the farthest from the mechanical ventilators.

It is confirmed that the gas detection points are needed for these areas. All two cases reach to 30% LFL(15,000 ppm) within 65 and 80 seconds each from the leak starting, CH_4 gas dispersed to 10 seconds after alarm. The values of Case 1 and Case 2 are significantly decreased after 900 seconds and 1,320 seconds each. CH_4 concentration shown on the Fig. 6-2-19 and 6-2-20 at 7 meter, Fig. 6-2-21 and 6-2-22 at 4 meter and Fig. 6-2-23 and 6-2-24 at 1 meter are all lower values of 14,000 ppm.

Fig. 6-2-1 and 6-2-2 show that the gas dispersion simulation at 30 seconds after gas leak starting. Gas clouds are made by 0.015 to 0.15. Gas alarm is not started and gas clouds are moving from leak point to the ventilator direction. Comparing the two cases, Gas cloud volume for case 2 is much more than case 1, CH_4 concentration under the first deck is much denser.

Fig. 6-2-3 and 6-2-4 show that the gas dispersion simulation at 50 seconds after gas leak starting. Gas alarm is not started and gas clouds are moving from leak point to the ventilator direction. Comparing the two cases, gas cloud volume for case 2 is much more than case 1 and propagates deck under near to the gas detection sensor location 1.

Fig. 6-2-5, 6-2-6 show that the gas dispersion simulation at the first gas alarm point. Gas cloud as volume fraction is from the 0.015 to 0.15. The values are the same as 15,000 ppm to 150,000 ppm. Gas alarm is set to 15,000 ppm. Comparing Case 1 and Case 2 gas alarm time, Case 1 is alarmed at 80 seconds at point 1 and Case 2 is alarmed at 65 seconds at point 1. The gas cloud movement is similar because gas alarm is occurred at the same gas detector positions.

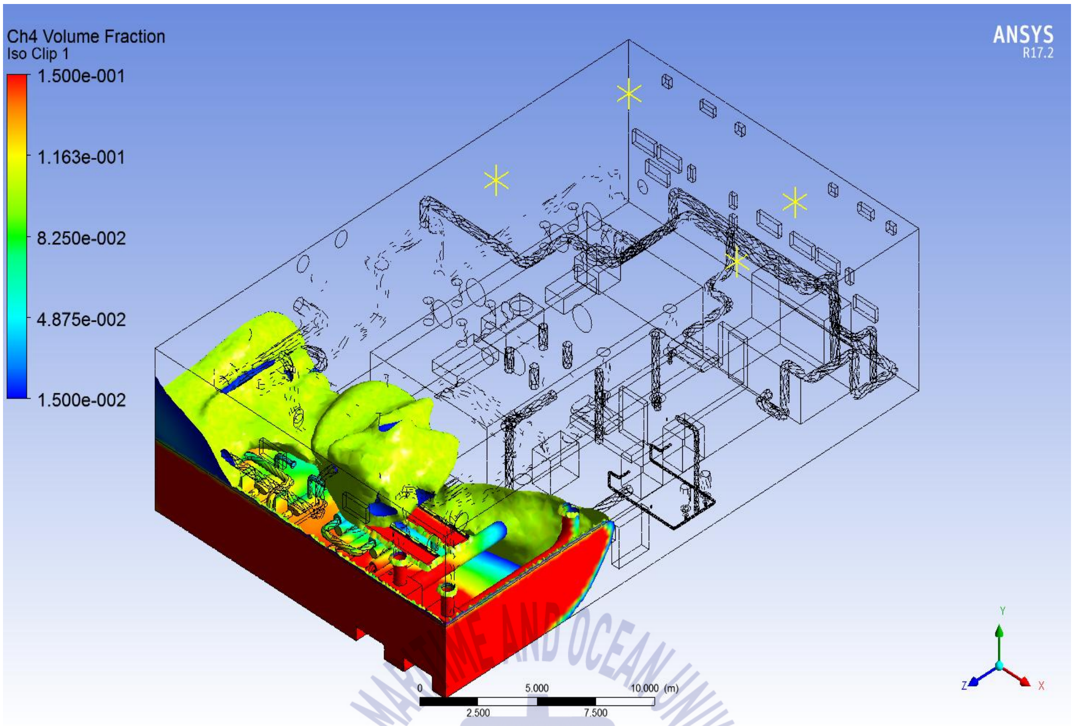

Fig. 6-2-1 Case 1, Gas cloud at 30 seconds(15,000~150,000 ppm)

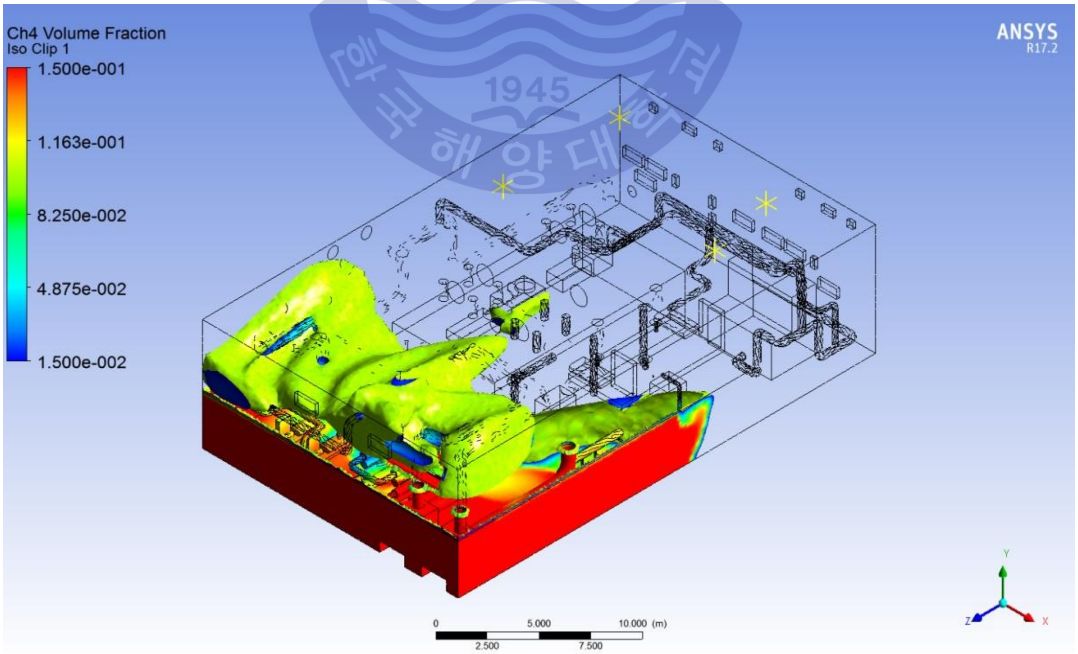

Fig. 6-2-2 Case 2, Gas cloud at 30 seconds(15,000~150,000 ppm)

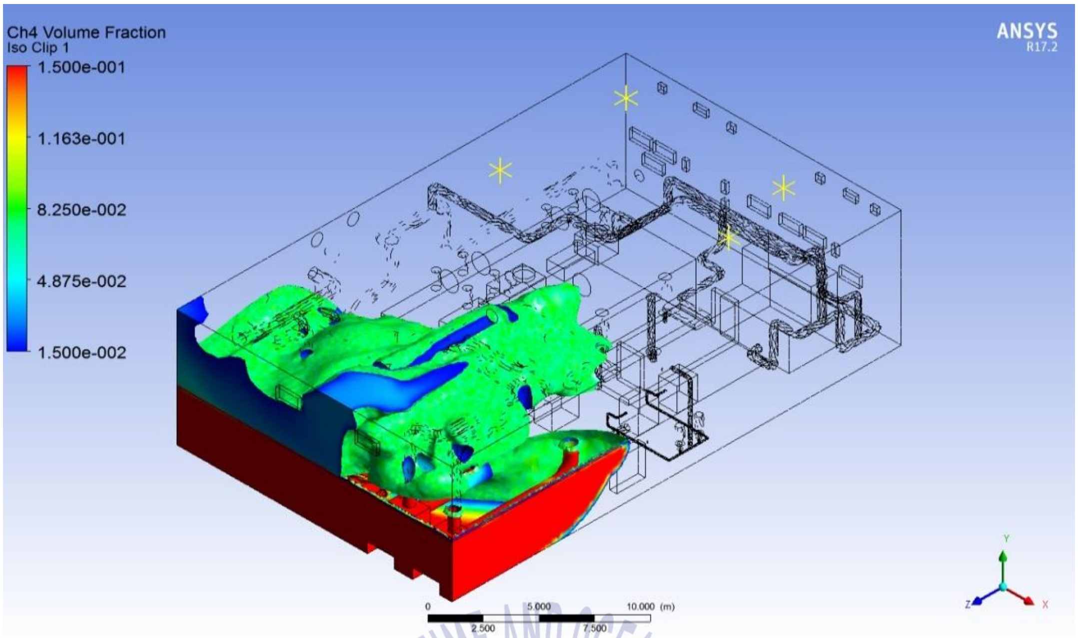

Fig. 6-2-3 Case 1, Gas cloud at 50 seconds(15,000~150,000 ppm)

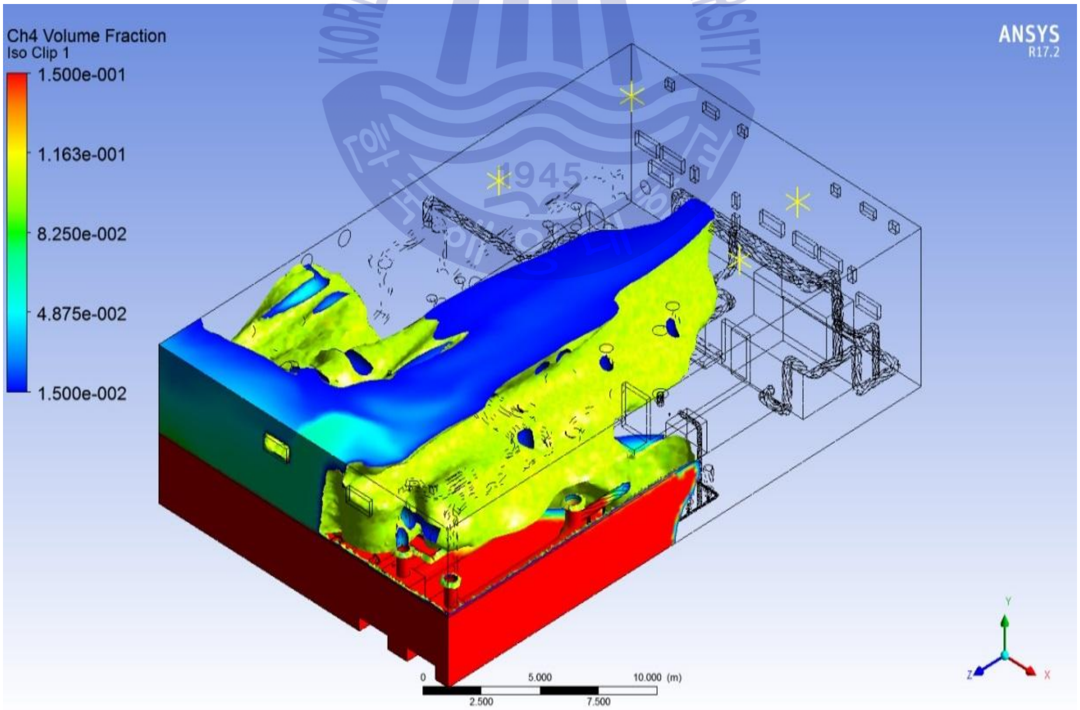

Fig. 6-2-4 Case 2, Gas cloud at 50 seconds(15,000~150,000 ppm)

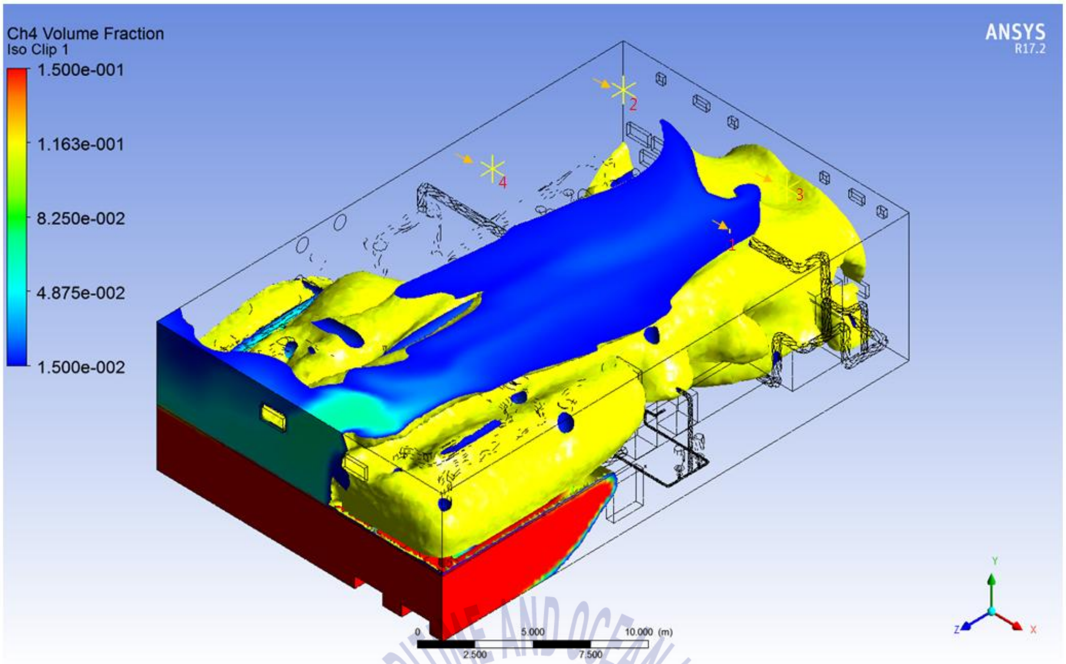

Fig. 6-2-5 Case 1, Gas detection alarm at 80 seconds(at point1)

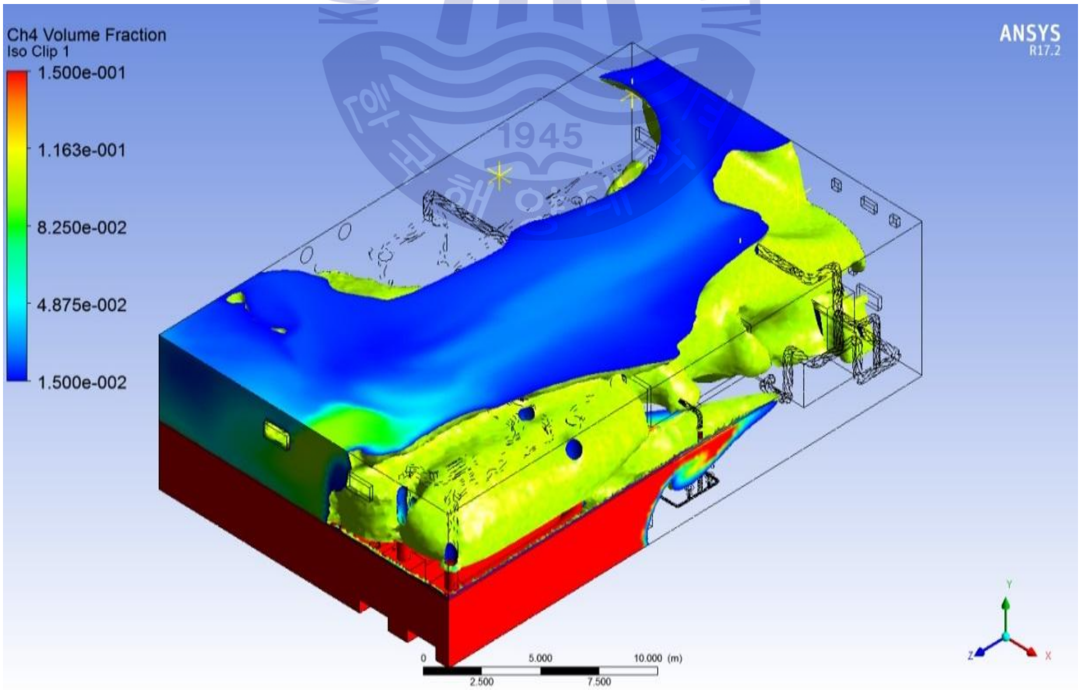

Fig. 6-2-6 Case 2, Gas detection alarm at 65 seconds(at point1)

Fig. 6-2-7, 6-2-8 show that the gas dispersion simulation at yz plan for two(2) cases. Although Case 2 alarm time is shorter than case 1, CH_4 concentration is higher than case 1. Comparing Case 1 and Case2 under the first deck area, CH_4 concentration of Case 2 is more widely propagated than Case 1.

Fig. 6-2-9 and 6-2-10 show that the gas dispersion simulation after 10 seconds from gas detection alarm. The gas cloud for two cases is similar but Case 2 more propagated than Case 1 even if leak time is less than 15 seconds. CH_4 concentration is higher near the leak area and lower far away.

Fig. 6-2-11 and 6-2-12 show that the gas dispersion simulation at yz plan for two(2) cases. Although Case 2 gas leak time is shorter than case 1 as much as 15 seconds, CH_4 concentration is higher than case 1 comparing with the first deck under part and whole area in the compressor room.

Fig. 6-2-13 and 6-2-14 show that the gas dispersion simulation at xz plan for two(2) cases. Gas simulations are captured 7 meter above base line, CH_4 concentration of Case 2 is higher than case 1 comparing with the whole area in the compressor room.

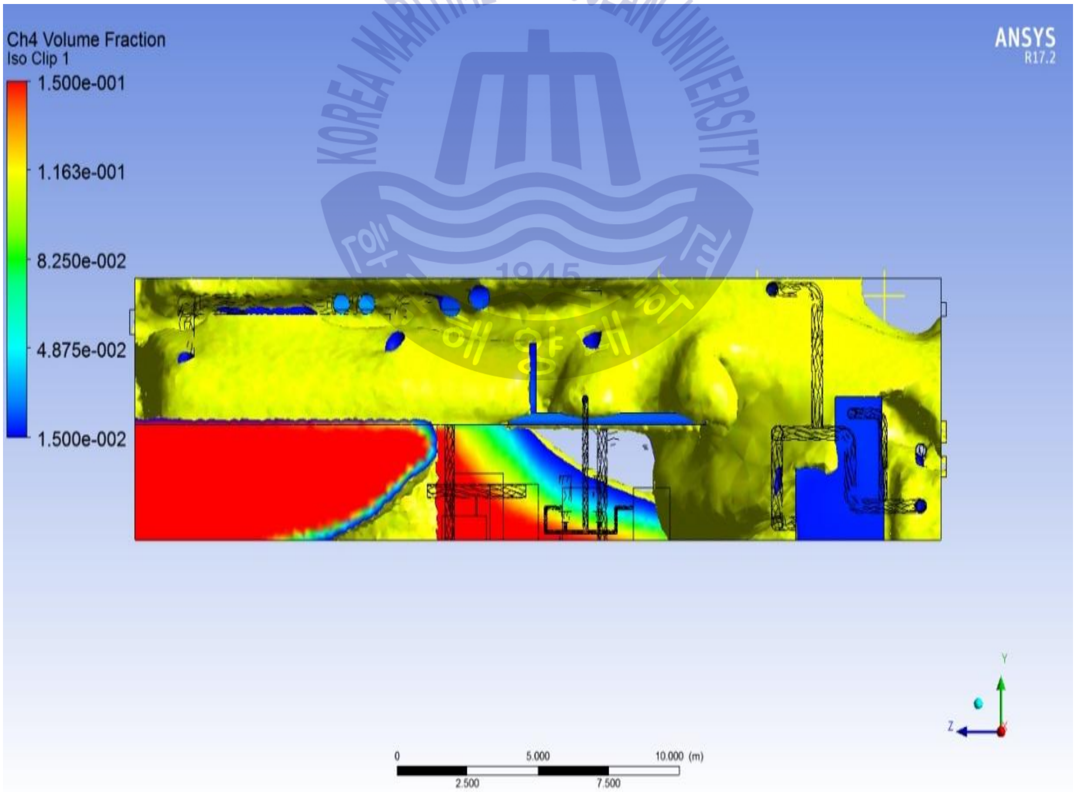

Fig. 6-2-7 Case 1, Gas detection alarm at 80 seconds(yz plan)

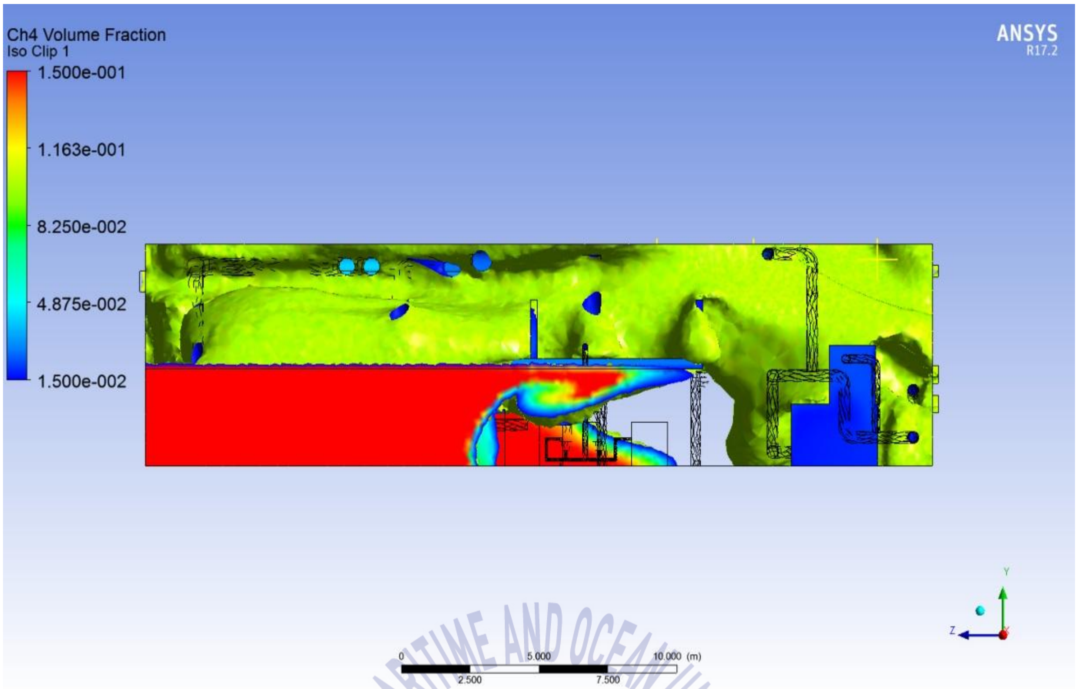

Fig. 6-2-8 Case 2, Gas detection alarm at 65 seconds(yz plan)

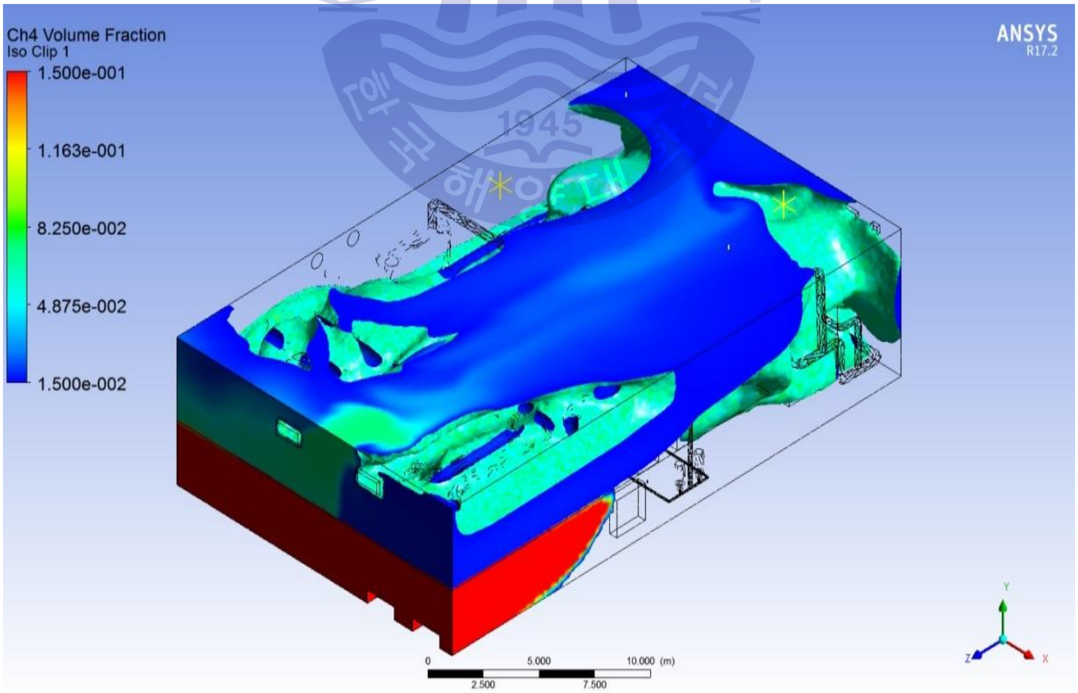

Fig. 6-2-9 Case 1, 10 seconds after gas detection alarm(at 90 seconds)

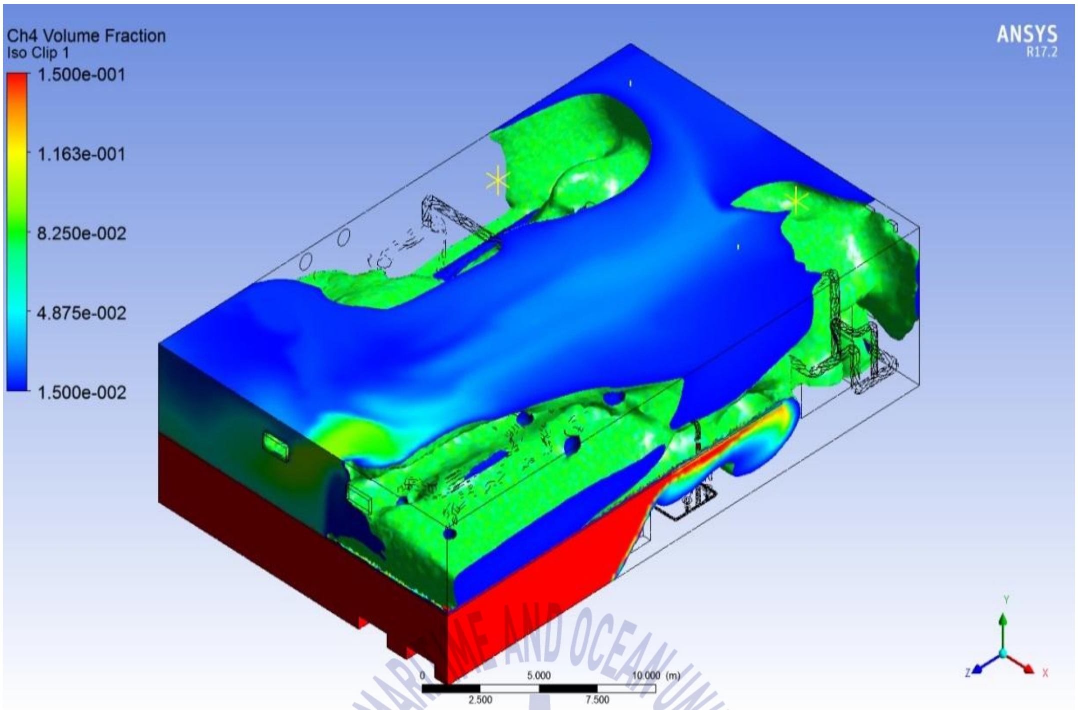

Fig. 6-2-10 Case 2, 10 seconds after gas detection alarm(at 75 seconds)

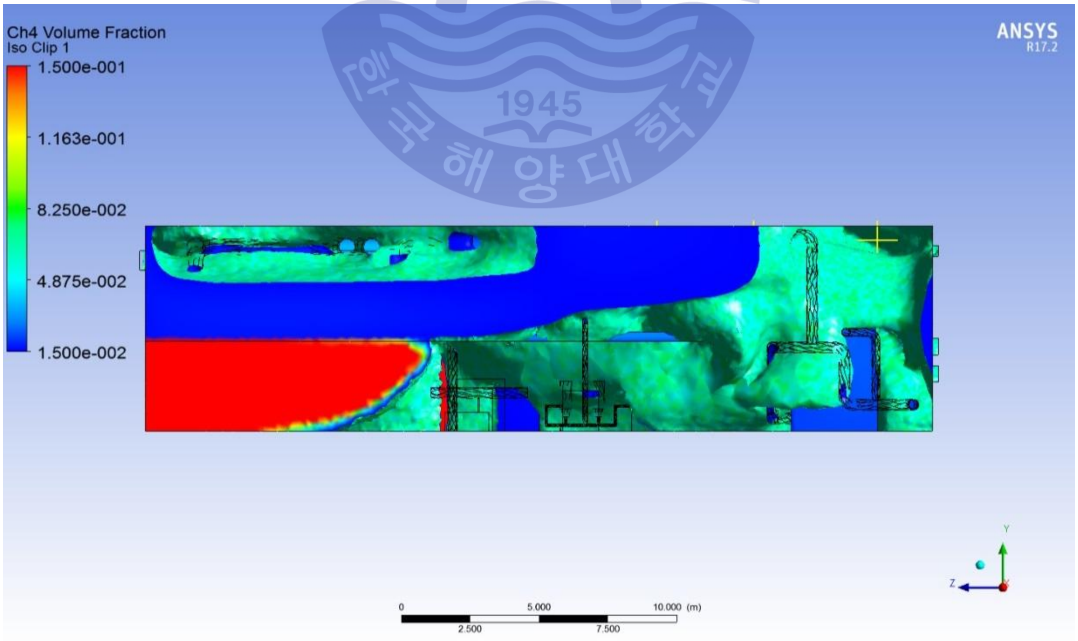

Fig. 6-2-11 Case 1, 10 seconds after gas detection alarm(yz plan)(at 90 seconds)

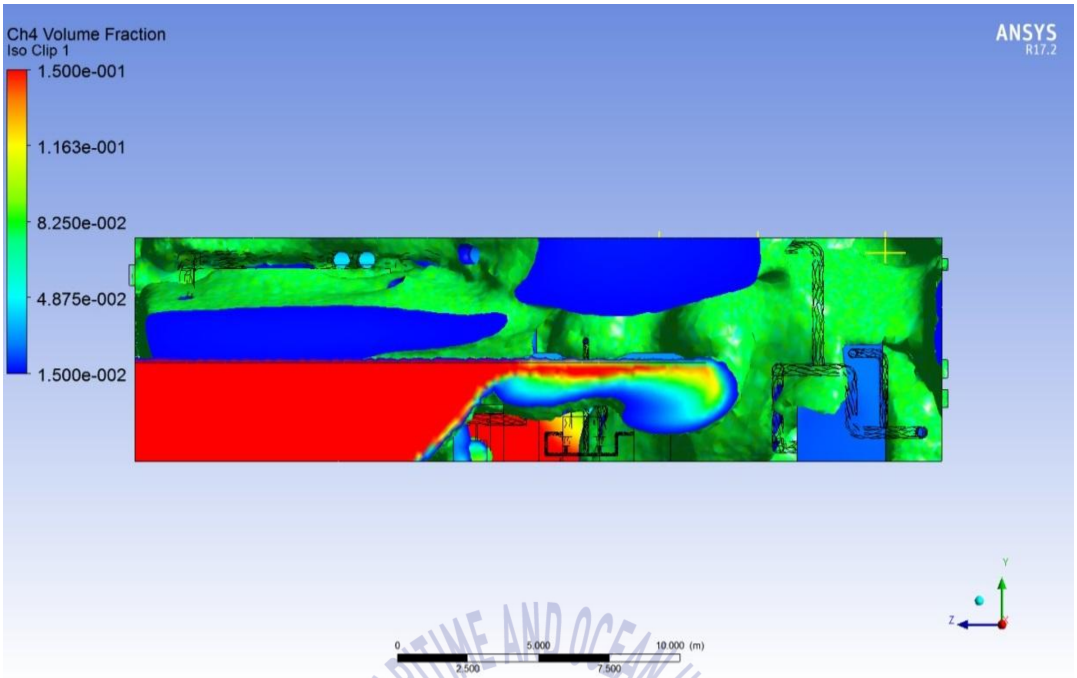

Fig. 6-2-12 Case 2, 10 seconds after gas detection alarm(yz plan)(at 75 seconds)

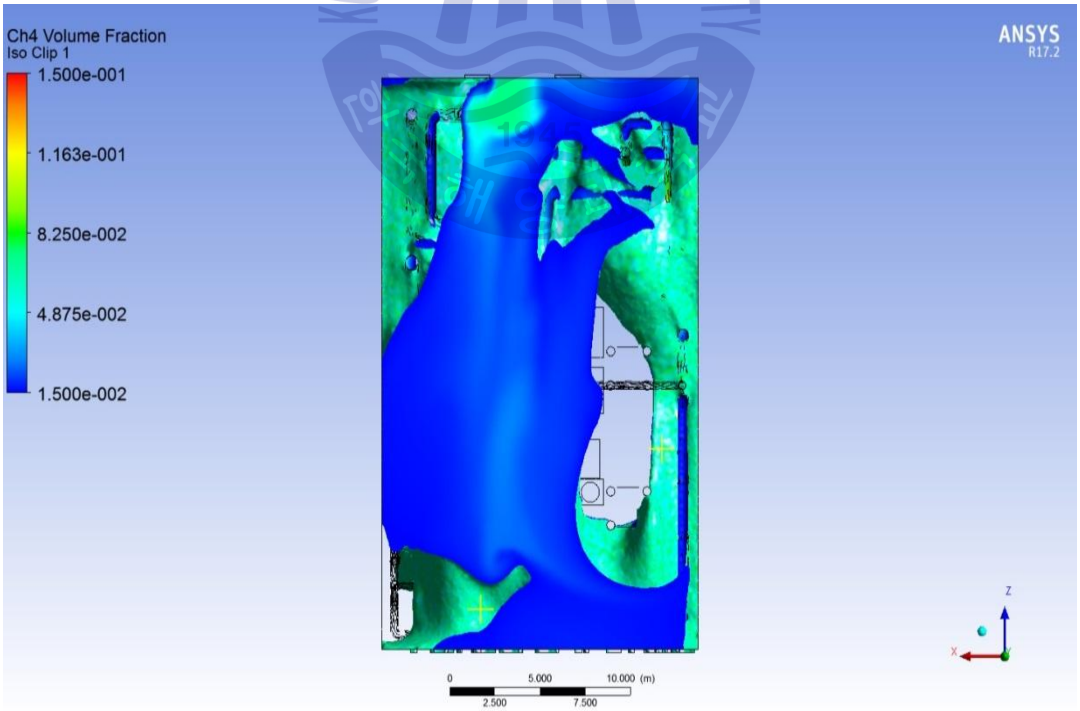

Fig. 6-2-13 Case 1, 10 seconds after gas detection alarm(xz plan)(at 90 seconds)

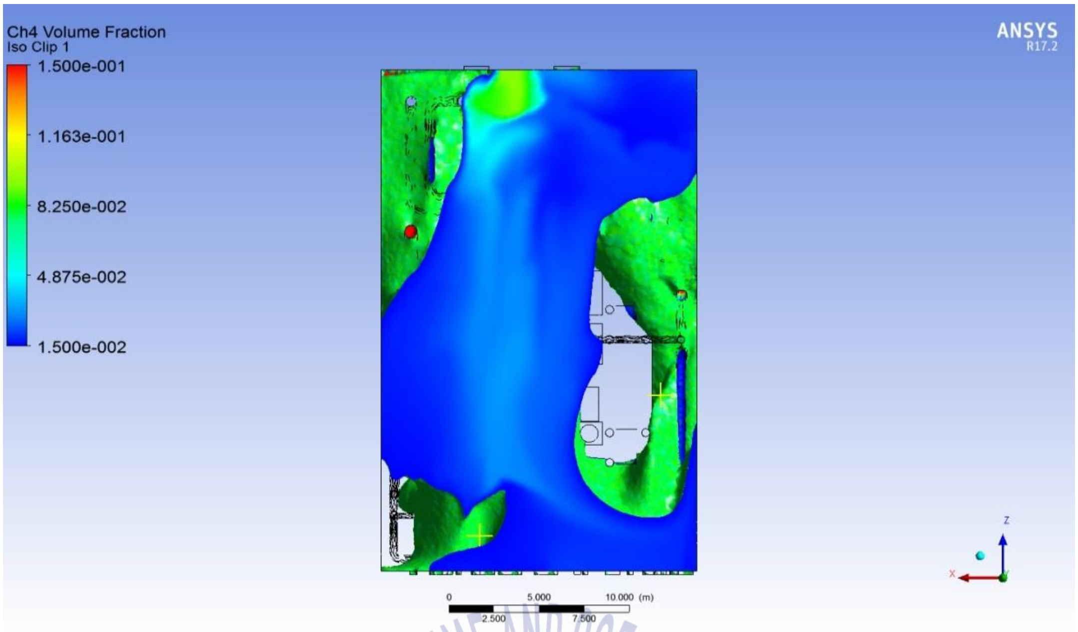

Fig. 6-2-14 Case 2, 10 seconds after gas detection alarm(xz plan)(at 75 seconds)

Fig. 6-2-15 and 6-2-16 show that the gas dispersion simulation at 900 seconds and 1,320 seconds. Most part of the cargo compressor room is greater than gas alarm value 30% LFL (Lower Flammable Limits) with CH_4 volume fraction between 15,000 and 150,000ppm.

Fig. 6-2-17 and 6-2-18 show the flammable gas cloud between 50,000 and 150,000 ppm. Flammable gas cloud is shown on the farthest areas from the mechanical ventilators. We confirm that the gas detection points are additionally needed.

Fig. 6-2-19 and 6-2-20 show that gas CH_4 volume fraction contours at 2,312 seconds and 4,697 seconds seen from height 7m. The value of the highest concentration area is at the left side of the compressor room near the ceiling. Comparing with two cases, CH_4 contour shapes are similar, right side of the compressor room is more ventilated than left side.

Fig. 6-2-21 and 6-2-22 show that gas CH_4 volume fraction contours seen from height 4m. The value of the highest concentration area is 11,780 ppm and 8,995 ppm each at the upper part of the high pressure fuel gas compressor. CH_4 contour shapes are similar, right side of the compressor room is more ventilated than left side.

Fig. 6-2-23 and 6-2-24 show that gas CH_4 volume fraction contour seen from height 1m. The value of the highest concentration area is 11,180 ppm and 8,324 ppm each in front of the fuel gas compressor. CH_4 contour shapes are similar. We confirm the biggest high pressure fuel gas compression the compressor room effect on the ventilation.

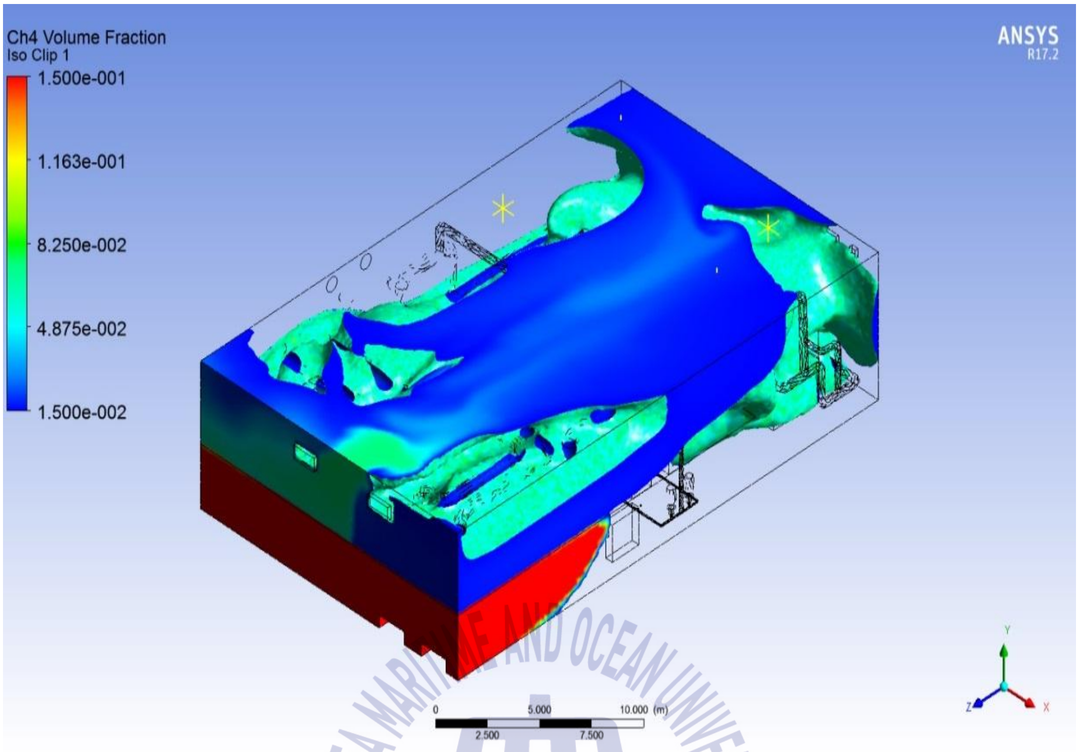

Fig. 6-2-15 Case 1, Gas cloud at 900 seconds(15,000~150,000 ppm)

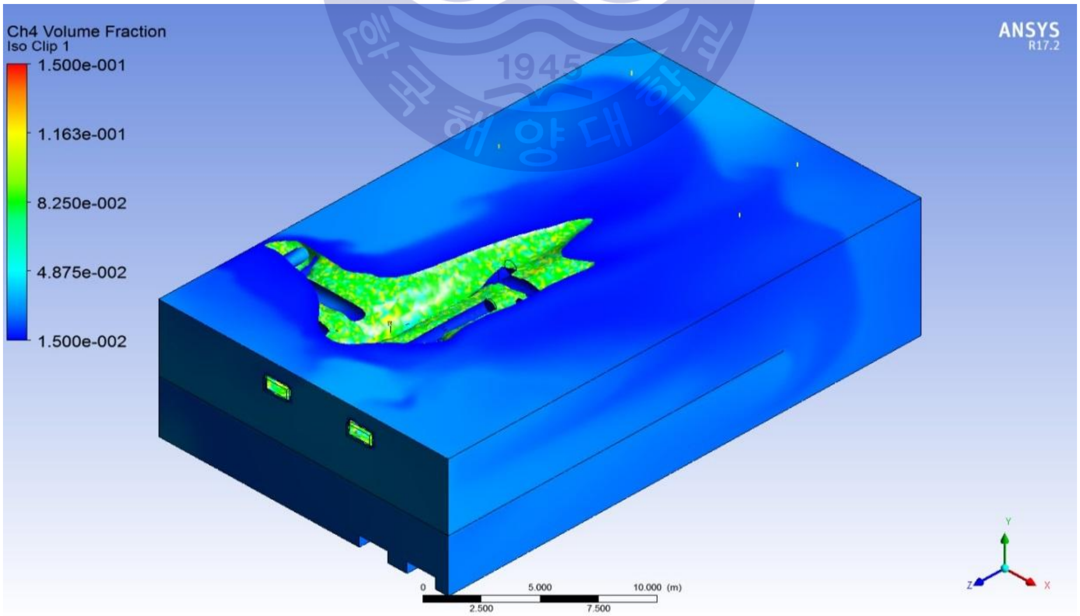

Fig. 6-2-16 Case 2, Gas cloud at 1320 seconds(15,000~150,000 ppm)

Flammable gas clouds for two cases between 50,000 and 150,000 ppm at 500 seconds and 900 seconds show on the Fig. 6-2-17, 18. Flammable gases are remaining on the farthest area from the mechanical ventilators. These area are additional gas detection points are needed.

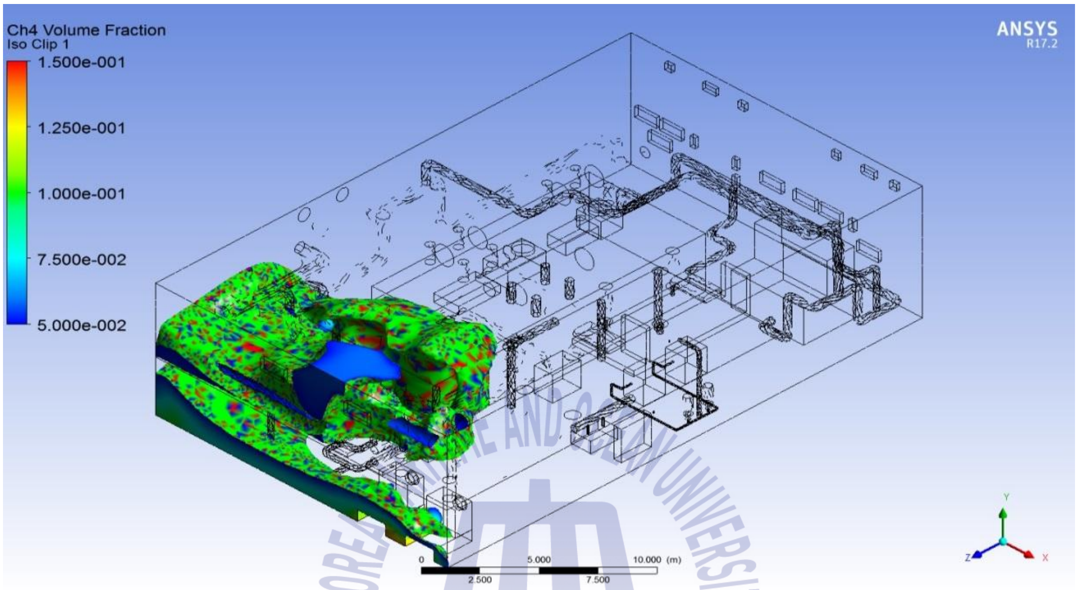

Fig. 6-2-17 Case 1, Gas cloud at 500 seconds(50,000~150,000 ppm)

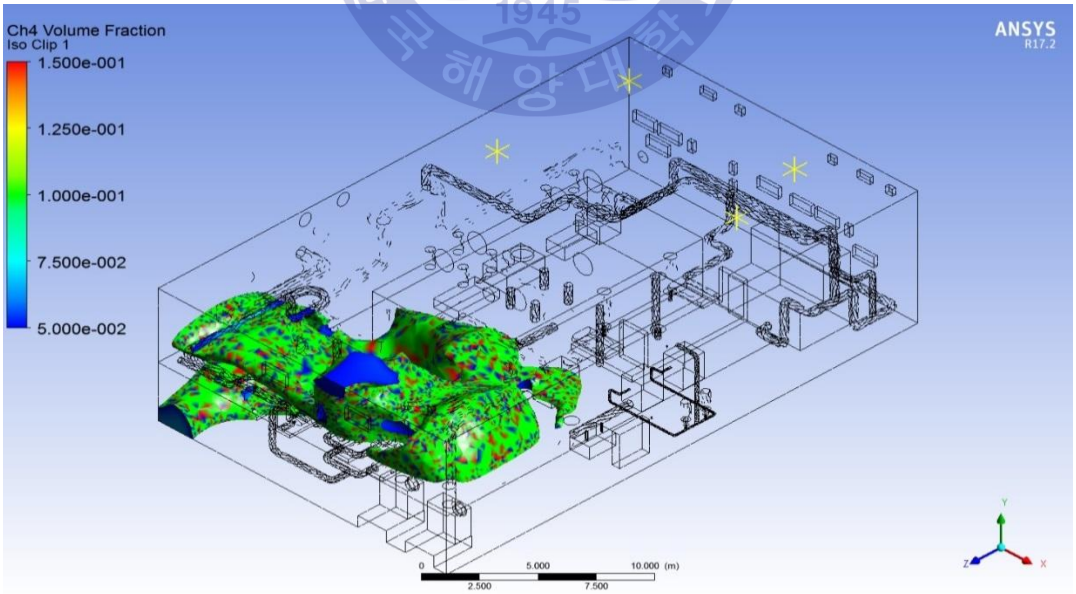

Fig. 6-2-18 Case 2, Gas cloud at 900 seconds(50,000~150,000 ppm)

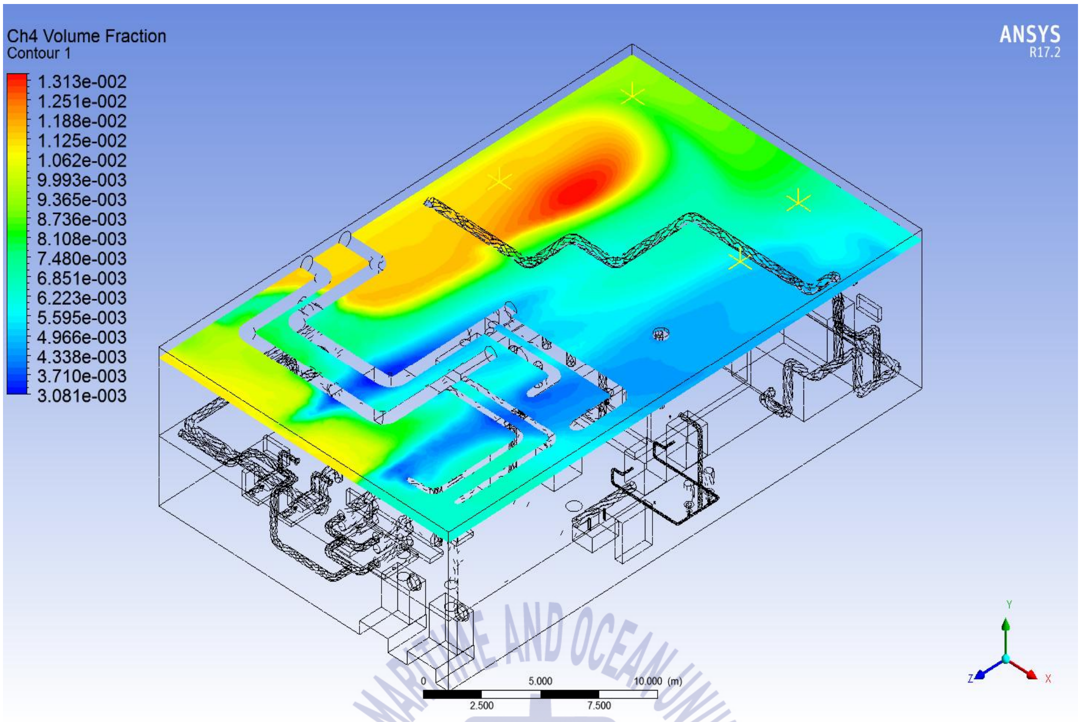

Fig. 6-2-19 Case 1, CH_4 volume fraction at 2,312 seconds (height 7m)

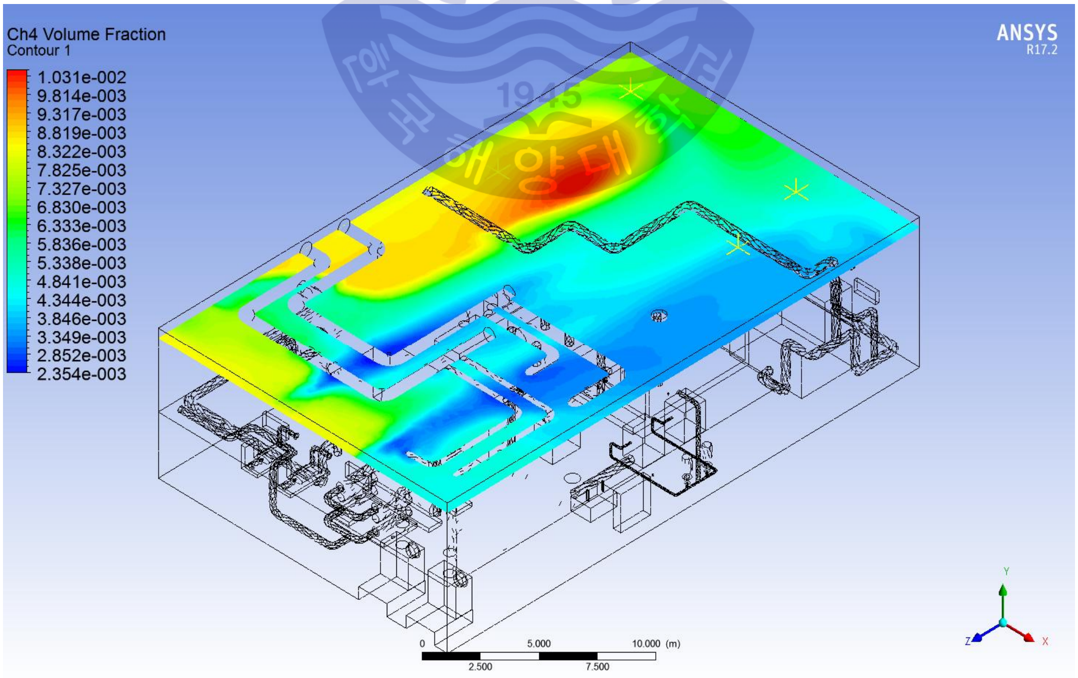

Fig. 6-2-20 Case 2, CH_4 volume fraction at 4,697 seconds (height 7m)

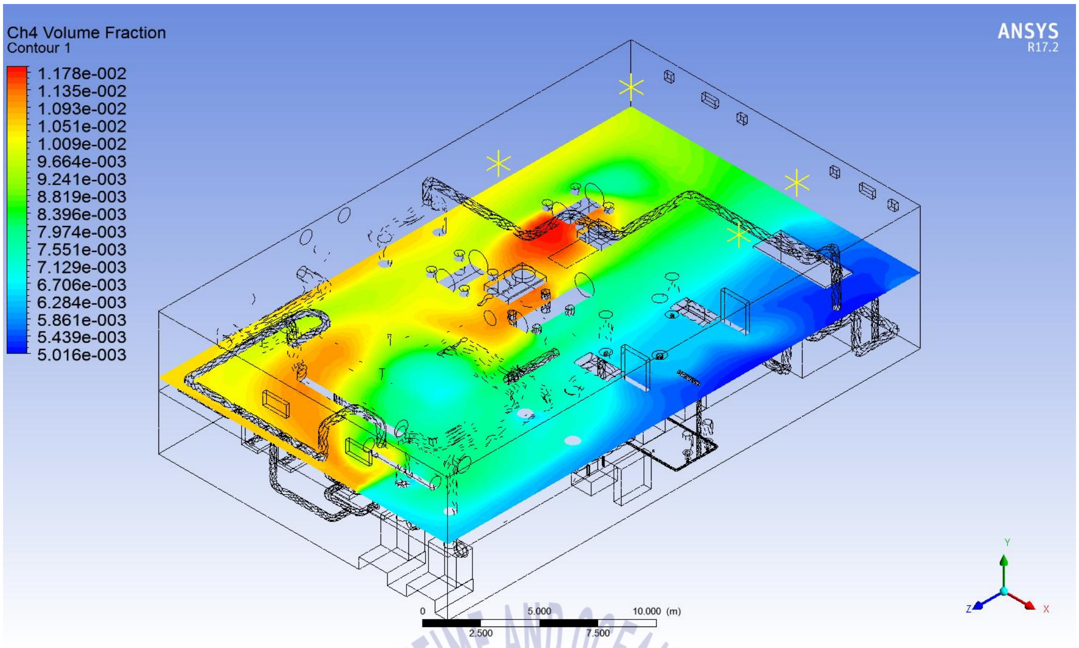

Fig. 6-2-21 Case 1, CH_4 volume fraction at 2,312 seconds (height 4m)

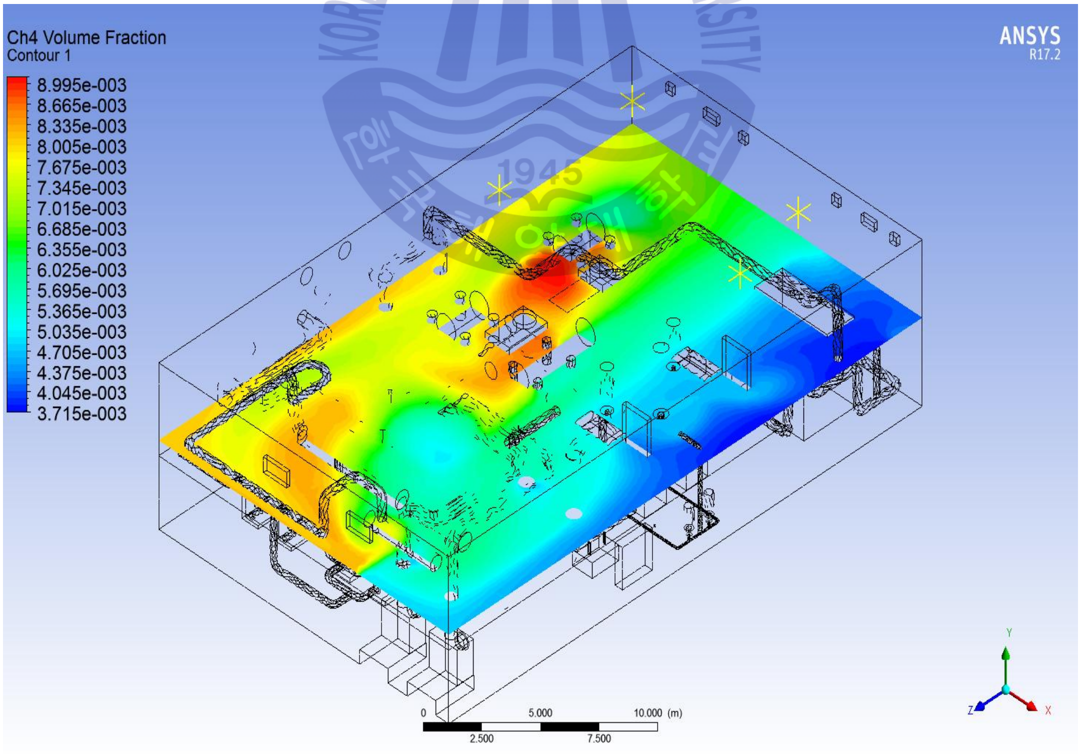

Fig. 6-2-22 Case 2, CH_4 volume fraction at 4,697 seconds (height 4m)

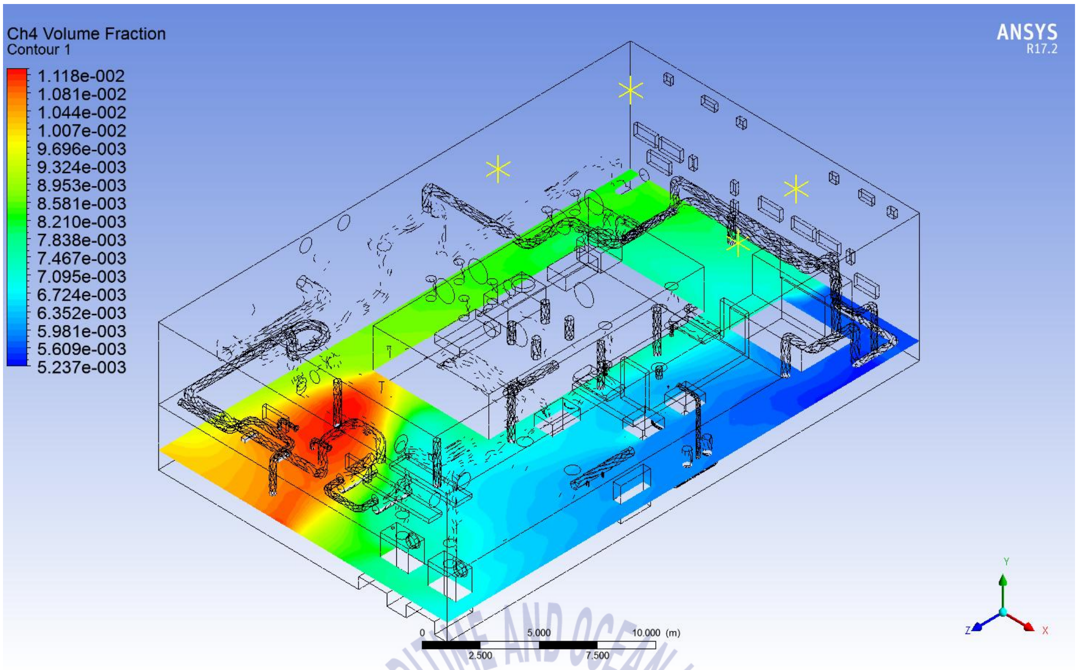

Fig. 6-2-23 Case 1, CH_4 volume fraction at 2,312 seconds (height 1m)

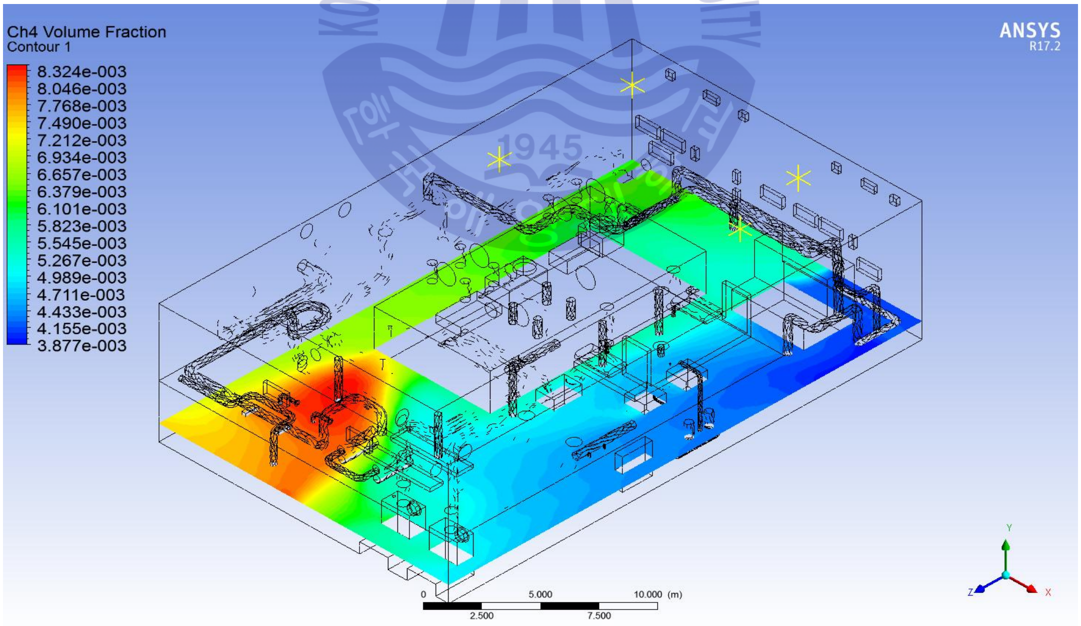

Fig. 6-2-24 Case 2, CH_4 volume fraction at 4,697 seconds (height 1m)

Case 1 and Case 2 reach 30% LFL(15,000 ppm) within 80 and 65 seconds each from the leak starting, there are no flammable gas cloud for monitored gas detection points, and after CH_4 concentration gradually decreased. Case 1 and Case 2 on Fig. 6-2-25 and 26 made by Table 6-2-2 and 3, the values are significantly decreased after 900 seconds and 1,320 seconds. CH_4 concentration all measuring values at final time are below 9,000 ppm, and No.4 gas detection point for case 1 is 11,216 ppm. No more flammable gas clouds and the ventilation effect were confirmed at a quantitative value.

Table 6-2-2 Case 1, CH_4 volume fraction variation at gas detection points1, 2, 3 & 4

Time (seconds)	No.1 (ppm) (CH4 volume fraction)	No.2 (ppm) (CH4 volume fraction)	No.3 (ppm) (CH4 volume fraction)	No.4 (ppm) (CH4 volume fraction)
20	854	1726	872	636
40	3232	2488	3141	1980
60	10171	7231	6671	6201
80(Alarm)	16244	12547	9270	8765
90	18928	16172	12457	11720
105	20536	17641	14307	13122
120	20714	17927	14971	13410
135	21071	18034	15617	13661
150	21249	18392	16029	13912
165	21606	18714	16244	14182
180	21963	18964	16549	14451
195	22319	19107	16781	14738
210	22497	19429	17140	14989
240	23210	19911	17855	15617
270	23744	20357	18571	16244
300	23922	20857	19107	16889
330	24277	21249	19822	17533
360	24811	21784	20179	18034
390	24989	22319	20518	18750
420	24989	22853	20893	19286
450	24989	23388	21249	19822
480	24811	23922	21784	20357
510	24633	24455	22141	20893
540	24099	24811	22497	21535
600	22853	25522	22853	22586
660	21428	25877	22853	23566
720	19822	26055	22497	24455
780	18392	25699	21963	24989
840	16960	24633	21071	25344
900	15796	23388	20000	25344
960	14810	21998	18928	24989
1080	13374	19286	17283	23566
1200	12295	17497	15778	21784
1320	11036	16692	14433	20446
1440	10135	15760	13266	19286
1560	9234	14451	12295	18392
1680	8513	13302	11396	17229
1800	7899	12115	10496	15886
1920	7249	11324	9595	14630
2040	6526	10496	8693	13374
2160	5803	9595	7971	12475
2280	5441	8874	7249	11396
2312	5260	8783	7068	11216

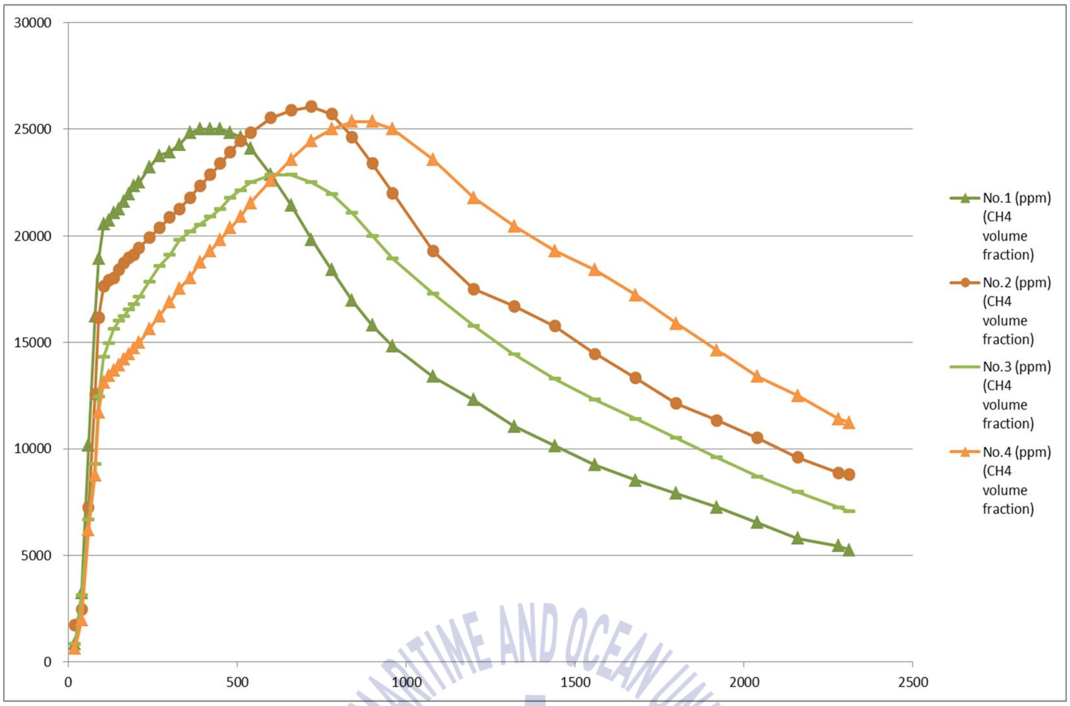

Fig. 6-2-25 Case1, CH_4 volume fraction variation at gas detection points

Table 6-2-3 Case 2, CH_4 volume fraction variation at gas detection points 1, 2, 3 & 4

Time(seconds)	No.1 (ppm) (CH4 volume fraction)	No.2 (ppm) (CH4 volume fraction)	No.3 (ppm) (CH4 volume fraction)	No.4(ppm) (CH4 volume fraction)
20	0	416	0	765
40	2934	3685	4016	4373
60	14164	11468	8874	4699
65	16746	6707	5224	5875
75	22194	19053	13894	10424
80	23121	20268	14523	12924
90	23138	20232	15742	12978
105	23245	20322	16316	13230
120	23388	20464	16692	13463
135	23548	20625	16889	13697
150	23655	20714	17050	13930
165	23815	20946	17175	14182
180	24099	21107	17283	14415
195	24348	21249	17372	14666
210	24455	21428	17444	14899
270	25486	22016	18589	15796

Time(seconds)	No.1 (ppm) (CH4 volume fraction)	No.2 (ppm) (CH4 volume fraction)	No.3 (ppm) (CH4 volume fraction)	No.4(ppm) (CH4 volume fraction)
330	27244	22729	21410	16781
390	28821	23619	22747	17766
450	30609	24793	23334	18767
510	30909	25824	23512	19714
600	30556	27457	24331	21107
720	31987	28591	25362	23121
960	27137	31086	28502	27616
1080	23975	31086	28307	29264
1200	21303	30839	26836	30467
1320	19178	29813	25255	30945
1440	17748	27297	23690	30503
1560	16889	24135	22266	29264
1680	16172	22141	21035	27669
1800	15366	21214	19893	26143
1920	14505	20607	18893	24900
2040	13661	19982	18034	23922
2160	12888	19196	17390	23281
2280	12151	18320	16674	22640
2400	11468	17515	15939	21963
2535	10766	16710	15079	21071
2655	10189	16029	14253	20179
2775	9631	15348	13427	19250
2895	9108	14666	12673	18338
3015	8621	14002	11936	17462
3255	7737	12691	10532	15850
3495	6924	11468	9306	14397
3735	6183	10334	8260	13086
3975	5550	9270	7339	11846
4425	4536	7574	5912	9793
4697	4011	6707	5224	8693

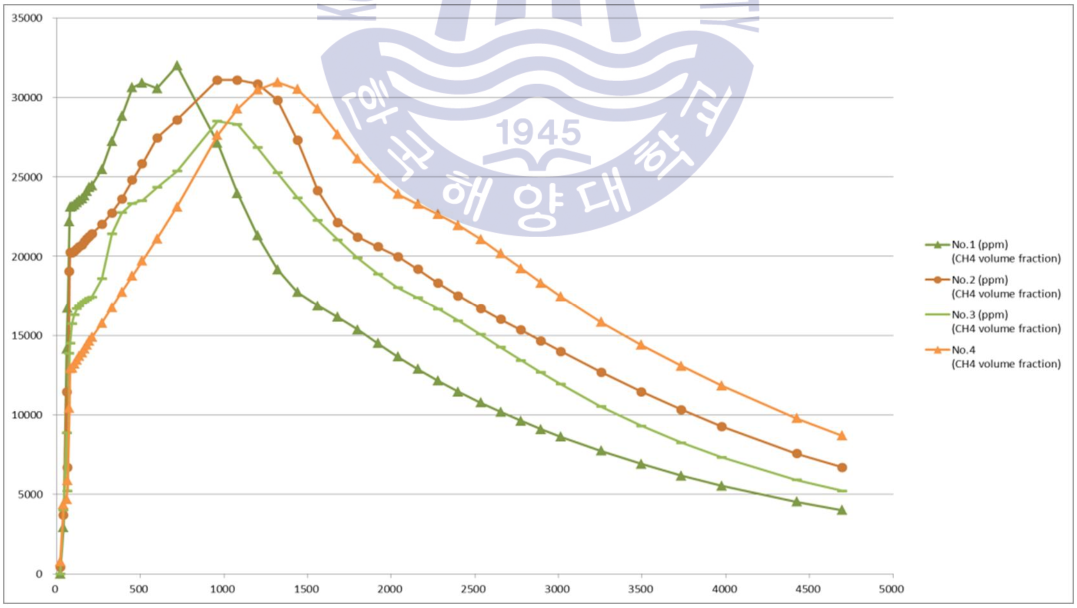

Fig. 6-2-26 Case 2, CH_4 volume fraction variation at gas detection points

Fig. 6-2-27, 6-2-28 and 6-2-29 show that velocity vector movement at various plan. The highest velocity vector is VR compressor discharge pipe and the vector movements are verified from the pressure inlets to the pressure outlets.

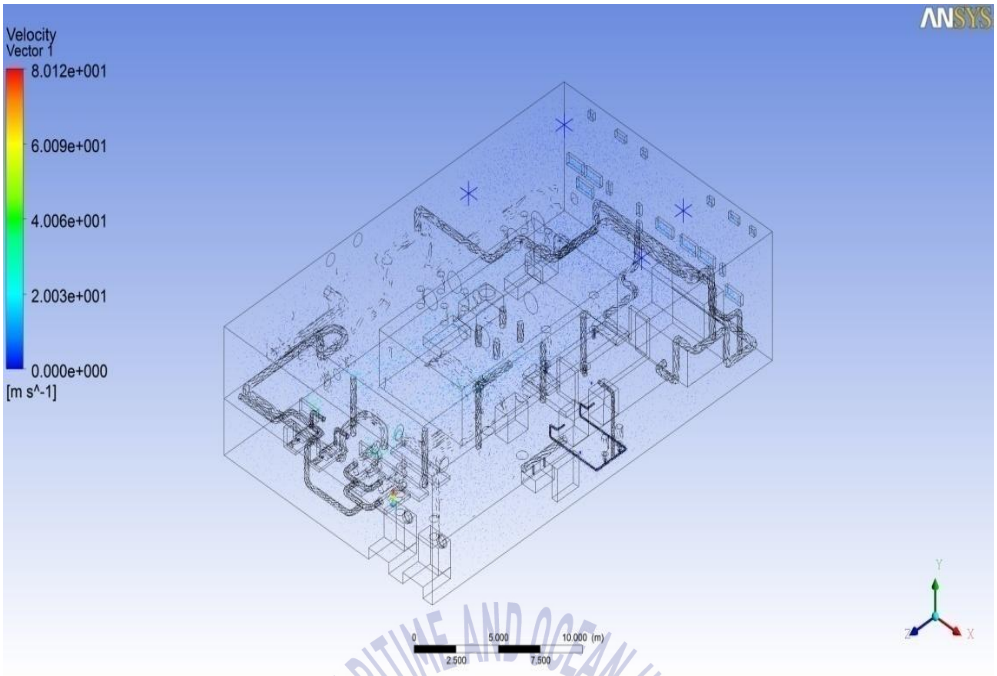

Fig. 6-2-27 Velocity vector movement at 3-dimensional space at 123 seconds

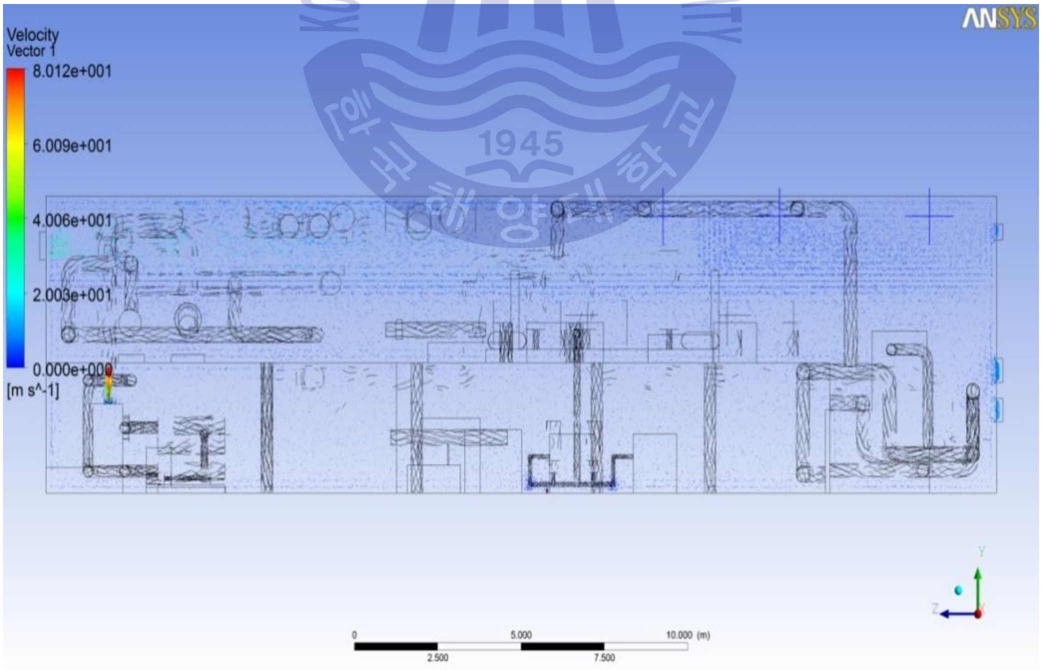

Fig. 6-2-28 Velocity vector movement at yz plan

Fig. 6-2-29 Velocity vector movement at xz plane

6.3 Virtual monitor points

Fig. 6-3-1 shows virtual monitor points in cargo compressor room. Total 140 virtual points are selected except actual existing gas detection point 1, 2, 3 and 4. Virtual monitor points to X-direction are 5, Y-direction 4 and Z-direction 7 for analyzing the CH_4 concentration, numbering of virtual monitor points is from 5 to 144. Naming to Z-direction is from A to G, total 20 virtual monitor points are composed of the each 7 X-Y plane.

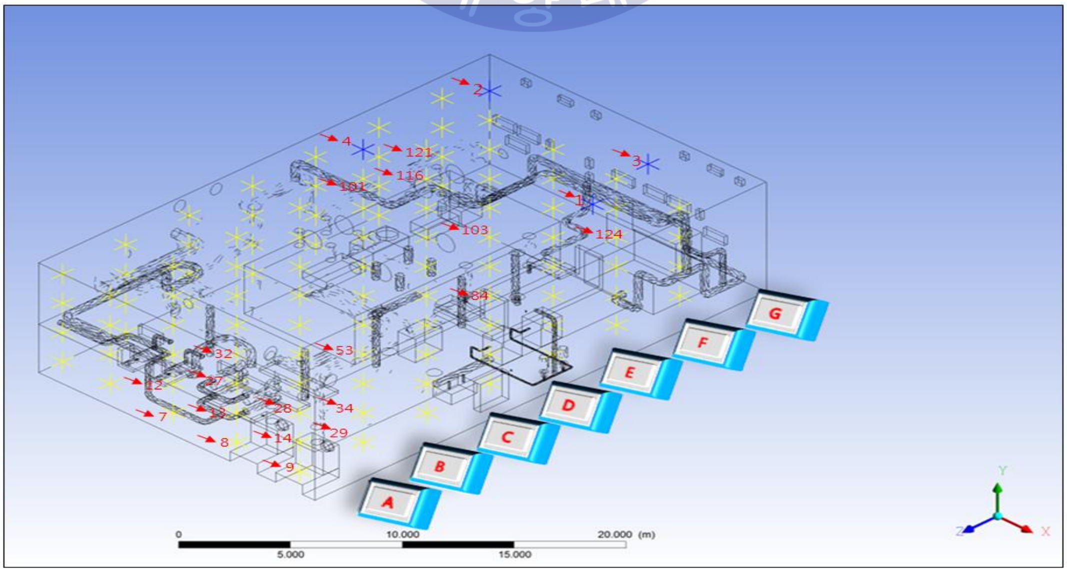

	N(x,y,z)	N(x,y,z)	N(x,y,z)	N(x,y,z)
A	5(1,1,28)	10(1,3,28)	15(1,5,28)	20(1,7,28)
	6(4,1,28)	11(4,3,28)	16(4,5,28)	21(4,7,28)
	7(8,1,28)	12(8,3,28)	17(8,5,28)	22(8,7,28)
	8(12,1,28)	13(12,3,28)	18(12,5,28)	23(12,7,28)
	9(16,1,28)	14(16,3,28)	19(16,5,28)	24(16,7,28)
B	25(1,1,24)	30(1,3,24)	35(1,5,24)	40(1,7,24)
	26(4,1,24)	31(4,3,24)	36(4,5,24)	41(4,7,24)
	27(8,1,24)	32(8,3,24)	37(8,5,24)	42(8,7,24)
	28(12,1,24)	33(12,3,24)	38(12,5,24)	43(12,7,24)
	29(16,1,24)	34(16,3,24)	39(16,5,24)	44(16,7,24)
C	45(1,1,20)	50(1,3,20)	55(1,5,20)	60(1,7,20)
	46(4,1,20)	51(4,3,20)	56(4,5,20)	61(4,7,20)
	47(8,1,20)	52(8,3,20)	57(8,5,20)	62(8,7,20)
	48(12,1,20)	53(12,3,20)	58(12,5,20)	63(12,7,20)
	49(16,1,20)	54(16,3,20)	59(16,5,20)	64(16,7,20)
D	65(1,1,16)	70(1,3,16)	75(1,5,16)	80(1,7,16)
	66(4,1,16)	71(4,3,16)	76(4,5,16)	81(4,7,16)
	67(8,1,16)	72(8,3,16)	77(8,5,16)	82(8,7,16)
	68(12,1,16)	73(12,3,16)	78(12,5,16)	83(12,7,16)
	69(16,1,16)	74(16,3,16)	79(16,5,16)	84(16,7,16)

	N(x,y,z)	N(x,y,z)	N(x,y,z)	N(x,y,z)
E	85(1,1,12)	90(1,3,12)	95(1,5,12)	100(1,7,12)
	86(4,1,12)	91(4,3,12)	96(4,5,12)	101(4,7,12)
	87(8,1,12)	92(8,3,12)	97(8,5,12)	102(8,7,12)
	88(12,1,12)	93(12,3,12)	98(12,5,12)	103(12,7,12)
	89(16,1,12)	94(16,3,12)	99(16,5,12)	104(16,7,12)
F	105(1,1,8)	110(1,3,8)	115(1,5,8)	120(1,7,8)
	106(4,1,8)	111(4,3,8)	116(4,5,8)	121(4,7,8)
	107(8,1,8)	112(8,3,8)	117(8,5,8)	122(8,7,8)
	108(12,1,8)	113(12,3,8)	118(12,5,8)	123(12,7,8)
	109(16,1,8)	114(16,3,8)	119(16,5,8)	124(16,7,8)
G	125(1,1,4)	130(1,3,4)	135(1,5,4)	140(1,7,4)
	126(4,1,4)	131(4,3,4)	136(4,5,4)	141(4,7,4)
	127(8,1,4)	132(8,3,4)	137(8,5,4)	142(8,7,4)
	128(12,1,4)	133(12,3,4)	138(12,5,4)	143(12,7,4)
	129(16,1,4)	134(16,3,4)	139(16,5,4)	144(16,7,4)

Fig. 6-3-1 Virtual monitor points in cargo compressor room

Fig. 6-3-2 and 6-3-3 show the CH_4 volume fraction at after 10 seconds from gas detection alarm and 508 seconds of Case 3. As shown on the Fig. 6-1-23, 24, 25, Gas behavior for Case 1, 2 and 3 are similar, so Case 3 with the highest leak rate is analyzed. The highest CH_4 volume fraction exceeding 80,000 ppm is virtual monitor points 84, 103 and point 124 is between 70,000 and 80,000 ppm. All these points are located the highest position, it is verified leaked gas at 305 bar with 45℃ is distributed to the ceiling around due to lighter than the air. The points 7, 8 and 12, 13 are located the farthest and lowest position from the ventilators and they are right hand side of the cargo compressor room because leak point is located at the right hand side. The points 32 and 53 are around of high pressure fuel gas compressor, it is verified remaining gas is not easily ventilated due to the big obstacle with size 3,000 x 8,150 x 5,000 mm (WxDxH).

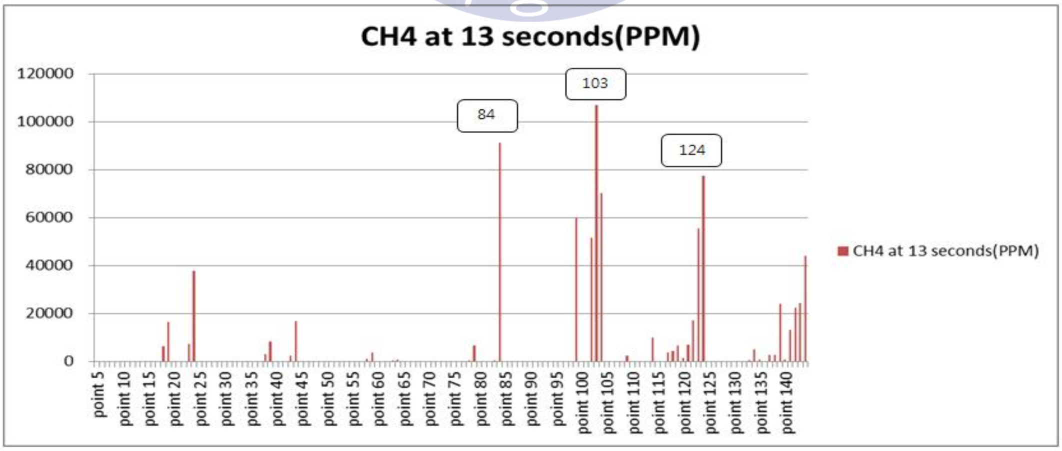

Fig. 6-3-2 Case 3, CH_4 volume fraction at after 10 seconds from gas detection alarm (High pressure leak)

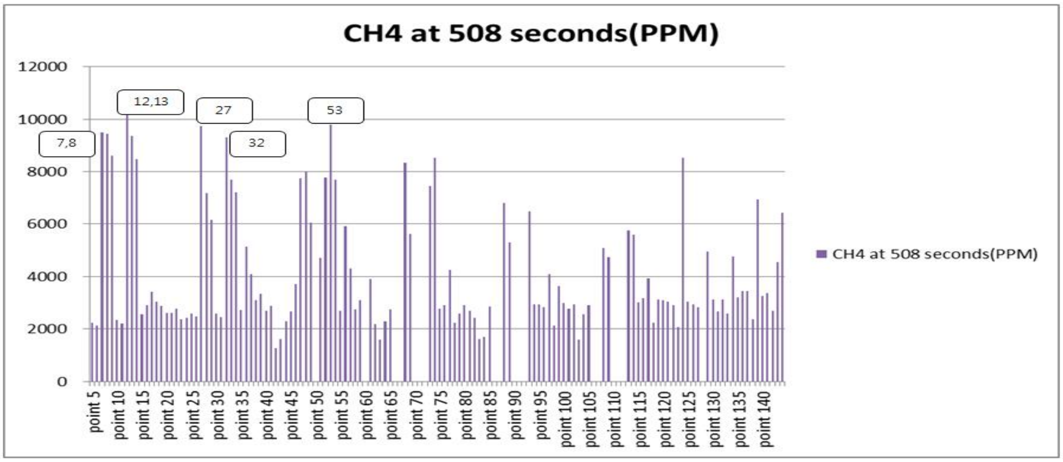

Fig. 6-3-3 Case 3, CH_4 volume fraction at 508 seconds (High pressure leak)

Fig. 6-3-4 shows the CH_4 volume fraction at gas alarm point(80 seconds) and 10 seconds after gas detection alarm and 900 seconds of Case 1. The highest CH_4 concentration at 80 seconds and 90 seconds is between 250,000 and 450,000 ppm, virtual monitor points 8, 13, 29, and 34. All these points are located around of the leaked position and farthest and lowest position from the ventilators under the first deck. It is verified leaked gas 1 bar with -110℃ is distributed to the lowest position due to heavier than the air. The points 46, 51, 65, and 85 with the highest CH_4 concentration exceeding 25,000 ppm at 900 seconds are located the farthest and lowest position from the ventilators. The points 101, 116 and 121 is the highest CH_4 concentration at 2,312 seconds on Fig. 6-3-5, the values are between 12,000 and 14,000 ppm. They are located around of high pressure fuel gas compressor, it is also verified remaining gas is not easily ventilated the same as high pressure leak.

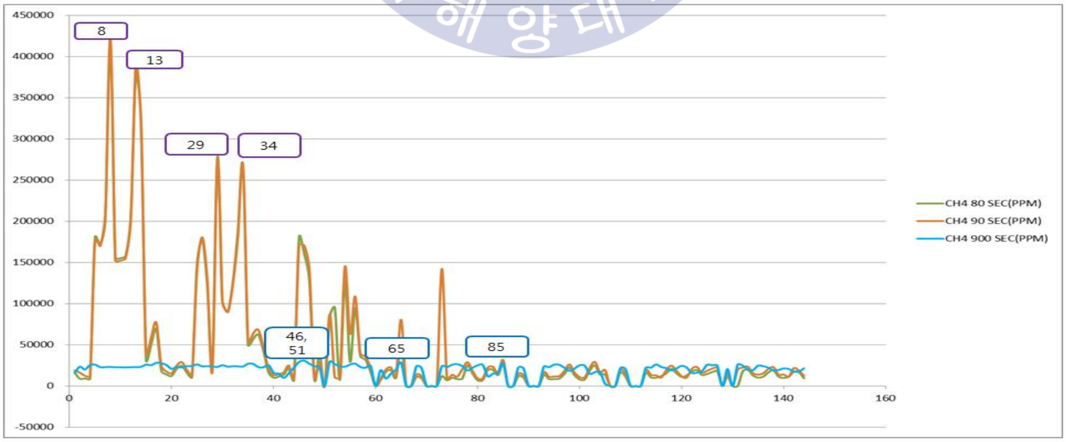

Fig. 6-3-4 Case 1, CH_4 volume fraction variation (Low pressure leak)

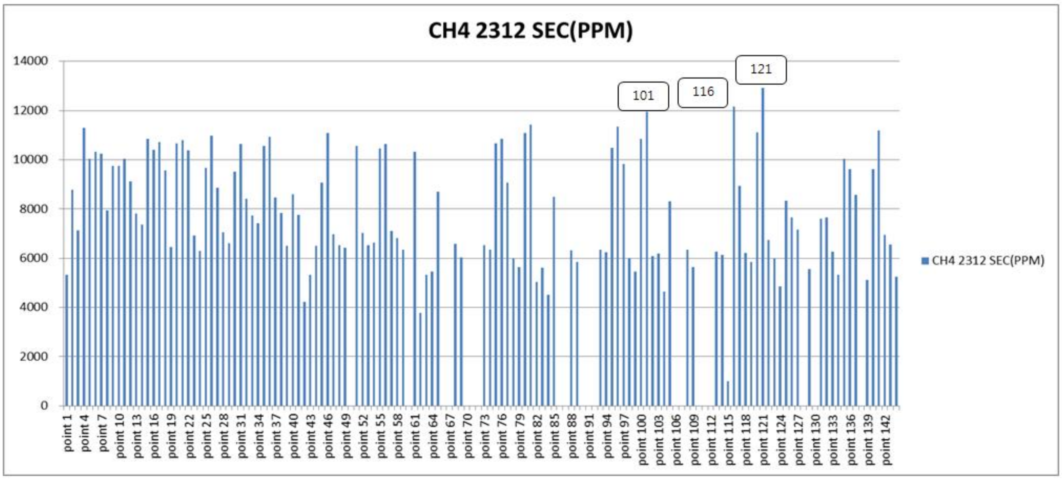

Fig. 6-3-5 Case 1, CH_4 volume fraction variation at 2,312 seconds

(Low pressure leak)

Fig. 6-3-6 shows the CH_4 volume fraction at gas alarm point(65 seconds) and 10 seconds after gas detection alarm and 1320 seconds of Case 2. The highest CH_4 concentration at 65 seconds and 75 seconds is between 350,000 and 450,000 ppm, virtual monitor points 9, 14, 29 and 34. All these points are located around of the leaked position and farthest and lowest positions from the ventilators under the first deck same as Case 1. The points 45, 46, 51, 65 and 85 with the highest CH_4 concentration at 1320 seconds are exceeding 35,000 ppm and located the farthest and lowest position from the ventilators. The points 101, 116 and 121 on Fig. 6-3-7 is the highest CH_4 concentration at 4,697 seconds, the values are between 8,000 and 10,000 ppm. They are around of high pressure fuel gas compressor, remaining gas is mainly accumulated the same as high pressure leak and Case 1 of low pressure leak.

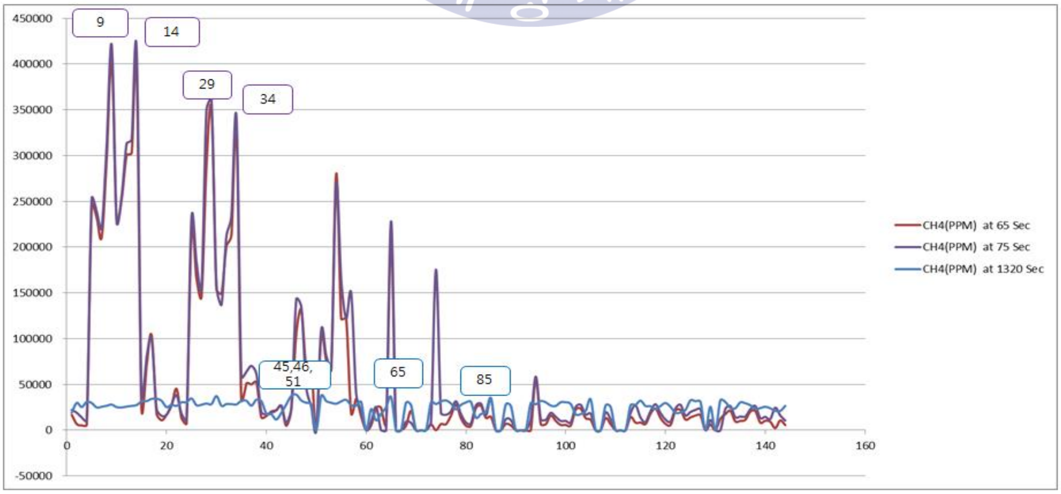

Fig. 6-3-6 Case 2, CH_4 volume fraction variation (Low pressure leak)

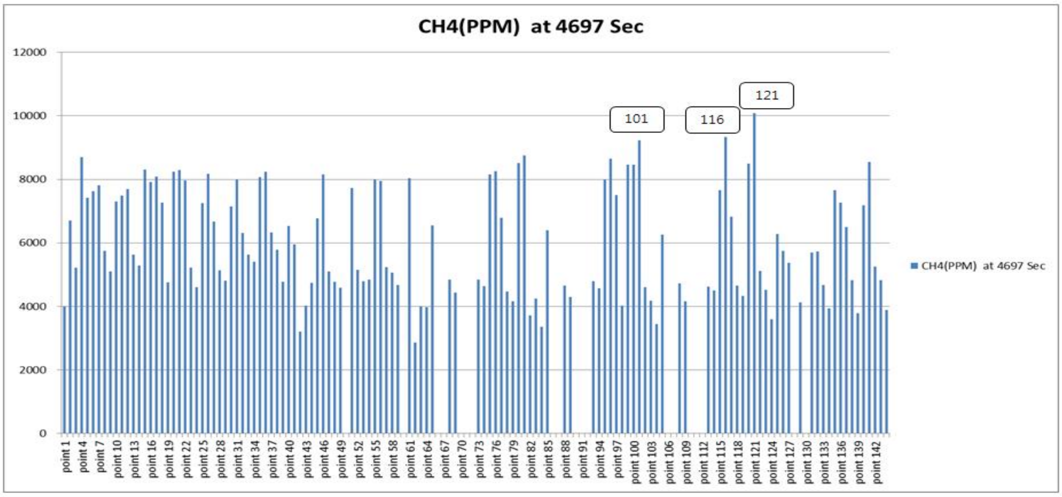

Fig. 6-3-7 Case 2, CH_4 volume fraction variation at 4,697 second

7. Conclusions

7.1 Conclusions

This study presents a method to identify the risk of explosion and to quantify the risk of a hazard. To do this, LNG gas dispersion simulation in the cargo compressor room of the 174K ME-GI LNG vessel was carried out according to the leak mass flow rate. The geometry of the cargo compressor room and the arrangement of equipment and piping are designed with the same 3-dimensional size as the actual structure in the vessel. LNG gas leak and dispersion were analyzed with high pressure and low pressure according to the pinhole size. Scenarios for a gas leak were examined for high pressure of 305 bar and low pressure of 1 bar. High pressure gas leak scenarios were examined for 4.5, 5.0 and 5.6mm pinholes size and Low pressure leak scenarios were examined for 100 and 140mm. Transient gas simulations were adopted to get the values of various time steps. The boundary condition of leaked gas pressure, temperature, leaked mass flow rates and the pressure of ventilators were selected the same as the actual condition.

Through this study we could identified the same as followings.

1. Quantitative data for leaked gas dispersion in a newly built ship were obtained.
2. Under certain scenarios, a flammable region could be visualized and identified.

3. The ventilation capability according to the new IGC code was identified under various scenarios.
4. The optimum gas detection sensor locations could be identified through a comparison with the actual gas sensors and virtual monitor sensor locations.

The high pressure gas leak was performed to pinhole size 4.5, 5.0, and 5.6 mm. Pinhole size 5.6 mm is rupture condition, 4.5 and 5.0 mm are the assumed sizes to be compared to the amount of rupture. The gas movement was observed up to 10 seconds after detection by the gas detector, and then the concentration was reduced by ventilation. The gas detectors were all triggered by alarm at the location of 1, and flammable gas clouds were identified in case 2 and 3.

Case 2 was alarmed at 3.5 seconds and the values of flammable limit were identified at 4 and 5 seconds, methane concentration was reducing since then. The methane concentration was increased again from 14 seconds the maximum value was reached in 28 seconds with flammable region.

In case 3, the alarm occurred in 3 seconds, and the values of flammable limit were identified around 3.5, and 4.0 seconds and then the methane concentration was reducing. The methane concentration was increased again from the 12 second, the maximum value occurred at 18 seconds without flammable region. In all cases, the methane concentration was reduced to between 5,000 and 6,000 ppm and was found to be significantly lower than the flammable region 50,000~150,000 ppm at 508 seconds.

After analyzing the concentration of gas at 508 seconds after ventilation, it was confirmed that additional gas detectors were necessary near the high pressure fuel gas compressor in the direction of leak point.

The low pressure gas leak was performed to pinhole size 100 and 140 mm. Pinhole size was assumed for simple gas simulation for optimum gas detector position. The gas movement was observed up to 10 seconds after gas detection alarm, and then the concentration was reduced by ventilation. Unlike the high-pressure gas leak, it was assumed that the leak occurred at a considerable distance from where the gas detector was located. The movement of the gas was observed at 30 seconds and 50 seconds before the alarm was triggered, and the gas alarm was triggered at position 1, which allowed both of them to identify a similar gas behavior. The gas leak was occurred far from the gas detectors and no flammable gas was made on any sensors.

In case 1, the methane concentration was observed at gas detection point No.1, 2 and 3 at below 9,000 ppm and the location of No.4 was detected at 11,216 ppm at 2,312 second ventilation time. This was found to be significantly lower than the flammable limits of 50,000 to 150,000 ppm.

In case 2, the value of methane concentration measured on the gas detectors in 3,975 seconds is similar to that measured in 2,312 seconds in case 1. In the final 4,697 seconds, methane concentration was less than 9,000 ppm. When comparing the ventilation times in case 1 and 2, case 2 took more than 1,663 seconds to observe a similar values on the gas detectors.

After analyzing the gas concentration after final ventilation of low pressure leak, it was confirmed that additional gas detectors were necessary at No. 101, 116 and 121 near the left hand side high pressure fuel gas compressor. It was found that the size of the fuel gas compressor is larger than the other equipment and that prevents the ventilation of the gas. When we observed the flammable gas cloud at 500 seconds and 900 seconds for case 1 and 2, observed it in the room in the rearmost direction of the ventilator and it was confirmed that additional gas detector is needed.

In this paper, we were able to check the behavior of high pressure gas and low pressure gas in the cargo compressor room, and also check their ventilation capability. Visualized and quantitative data obtained through the CFD simulation help the expectation of flow characteristics not only ME-GI LNG ship but also similar ships.

High pressure gas leak scenarios shows that the cargo compressor room of 174K ME-GI LNG vessels would not be a serious risk problem regarding the flammable gas concentration because ventilation assessment for 5.6 mm pinhole size as gas rupture condition was verified.

Low pressure gas leak scenarios show that leak flow rate of case 2 was nearly two times more than case 1. Case 2 takes nearly twice than Case 1 to ventilate CH_4 gas for all gas detection points comparing at the final measuring time. Ventilation time of case 2 is much more 1,663 seconds than case 1. The more leakage gas, the more time is taken to ventilate the gas.

High and low pressure gas leak and dispersion were implemented to allow visibility into the gas flammable region. Not only has the optimal gas detectors been positioned compare to the actual gas detection point using the virtual gas detectors, but also the types, features and equipment of the fuel supply system are easily described with the equipment pictures and cargo piping diagram including principal dimension and specification.

This paper is meaningful as the first quantitative analysis of gas leak and dispersion in the cargo compressor room of 174K ME-GI LNG vessel. The ship's fuel supply system has evolved into a dual fuel system from the steam engine and diesel engine system. Current typical competitive fuel supply systems are low pressure DFDE, middle pressure X-DF and hi pressure ME-GI. Fuel supply system for ME-GI has a good fuel efficiency compare to other systems and has the advantage of saving energy by re-liquefaction BOG. So more high pressure fuel supply vessels will be built to satisfy the requirement of the international community, analysis of the risk from the gas leak in the cargo compressor room will become more important day by day. The information on the high and low pressure gas behavior, the visibility of gas cloud and ventilation information in this paper will be considered to be a valuable source of reference at the shipbuilding industry.

Through this study, the CFD results will be useful for risk based design and analysis and optimum gas detection points can be applied.

References

AnayLuketa-Hanlin., Ronald P. Koopman. and Donald L. Ermak., 2007. On the application of computational dynamics codes for liquefied natural gas dispersion, Journal of Hazardous Material, 40, pp.504-517

ANSYS "FLUENT-14 solver theory manual"

Baek J.H., Lee H.J. & Jang C.B., 2016. Comparison of H2, LNG and LPG explosion characteristics in a limited space, Journal of the Korean Institute of Gas, 20(3), pp.12-21.

Båfjord J. Andre., 2011. Positioning of gas detector at offshore installations. M.D. University of Stavanger.

Benjamin R et al., 2009. Application of computational fluid dynamics for LNG vapor dispersion modeling : A study of key parameters, Journal of Prevention in the Process Industries, 22, pp.332-352.

Chan S. T., 1992. Numerical simulations of LNG vapor dispersion fenced storage area, Journal of hazardous Materials, 30, pp.195-224

Cho, H.C., 2005. A CFD Study on Thermo-Acoustic Instability of Methane/Air in Gas Turbine Combustor, Journal of Mechanical Science Technology, 19(9), pp.1811-1820.

Cho, H.W. et al., 2012. Study on Dispersion Characteristic for Fire Scenarios in an Urban Area Using a CFD-WRF Coupled Model, Journal of the Meteorological Society, 22(1), pp.47-55.

Cho, K.C., Kim, H.J. & Jang, S.B., 2011. Application of CFD in The Analysis of Aerodynamic Characteristics for Aircraft Propellers, Journal of the Korean Society for Aeronautical & space Sciences, 40(11), pp.917-926.

Choi, D.H. & Kang, D.H., 2013. Experimental and Computational Fluid Dynamics(CFD) Methods to Analyze Particle Resuspension and Dispersion Buildings, Journal of the Architectural Institute of Korea, 29(10), pp.275-282.

Choi. J.W. et al., 2015. Analysis of Risk Assessment Factors for Gas leakage and Dispersion in Underground Power Plant, Journal of ILASS-KOREA, 20(2), 101

Choi, N.J, et al., 2011. CFD Study on Aerodynamic Power Output of 6 MW Offshore Wind Farm According to the Wind Turbine Separation Distance, Journal of the Korean Society pf Marine Engineering, 35(8), pp.1063-1069.

Cormier, B.R., 2008. Computational Fluid Dynamics for LNG Vapor Dispersion Modeling: A Key Parameters study, Ph.D. Texas A&M University.

Dan, S.K., et al., 2011. Explosion Simulation for the Quantitative Risk Analysis of New Energy Filling Stations, Journal of the Korean Institute of Gas, 15(1), pp.61-67.

Eidsvik Karl J., 1980. A model for Heavy Gas Dispersion in the atmosphere, Journal of Atmospheric Environment, 14, pp. 769-777.

Gavelli Flippo, Bullister Edward & KytommaaHarri, 2008. Application of CFD to LNG spills into geometrically complex environments, Journal of Hazardous Materials, 159, pp.158-168.

Hanna Steven R. Hansen Olav R., Ichard Mathieu., 2009. CFD model simulation of dispersion railcar releases industrial and urban areas, Journal of Atmospheric Environment, 43, pp.262-270.

Ha, J.S. & Sim, S.H., 2014. Characteristics of Entertainment Flow Rate in a Coanda Nozzle with or without Coaxial Contractor, Journal of the Korean Institute of Gas, 18(2), pp.21-27.

Hannaa R. Steven, Hansen R. Olav and Dharmavaram Seshu., 2004. FLACS CFD air quality model performance evaluation with Kit Fox, MUST, Prairie Grass, and EMU observations, Journal of Atmospheric, 38, pp.4675-4687.

Heo, S.J., Kim, M.S., Han, H.S. & Jeong, W.B., 2011. Prediction of Two-phase Flow Pattern and Noise Evaluation for Evaporator Pipe in a Refrigerator, Journal of the Korean Society for Noise and Vibration Engineering, 21(10), pp.916-923.

Heo, Y. A., 2013. Structural Response of Offshore Plants to Risk-Based Blast Load, Journal of ARCHITECTURAL RESEARCH, 15, pp.151-158.

Hooff.T. van & Blocken.B., 2013. CFD evaluation of natural ventilation of indoor environments by the concentration decay method: CO_2 gas dispersion from a semi-enclosed stadium, Journal of the Building and Environment 61, pp.1-17.

IGC CODE, 2014. Resolution MSC 370(93) (adopted on 22 May 2014) Amendments to the international code for the construction and equipment of ships carrying liquefied gases in bulk

Jang, et al., 2012. CFD simulation study to analyze the Dispersion and Explosion of Combustible Gas, Journal of the Korean Institute of Gas, 16(15), pp.58-65

Jang, Y.R., Jung, S.H. & Park, K.S., 2015.Consequence Analysis for Accidental Gas Release in Labs, Journal of the Korean Institute of Gas, 19(4), pp.29-34.

Jin S.W. et al., 2009. Development of Gas Turbine Engine, Simulation Program Based on CFD, Journal of the Korean Society of Propulsion Engineer, 13(2), pp.42-53

Joo, H.J., Jung, I.Y., Yun, S.K. &Kwak, H.Y., 2015. CFD analysis on the flow Characteristics of Ejector According to the Position Changes of Driving Nozzles for F.W.G, Journal of the Korean Solar Energy Society, 31(3), pp.23-28.

Kang.H.K., 2013. An Examination on the Dispersion Characteristics of Boil-Off Gas in Vent Mast Exit of Membrane type LNG Carriers, Journal of the Korean Society of Marine Environment & Safety, 19(2), pp.225-231.

Kang S.K., Bang H.J. & Jo Y.D., 2013. Consequence Analysis of Hydrogen Blended natural Gas(HCNG) using 3D Simulation, Analysis of Hydrogen Blended Natural gas, Journal of the Korean Institute of Gas, Vo17(5), pp.15-21.

Kim, E.S. & Jeong, H.T., 2014, Aerodynamic Design and Performance Prediction of Rotor Blades in a Single-Stage Axial Fan Using CFD Method, Journal of the Korean Society for Computational Fluids Engineering, 29(3), pp.93-98.

Kim, J.H et al., 2011. Thermal Fluid Flow Analysis for Temperature Characterization of Mold Transformer in Distribution Power System, Journal of the Transactions of the Korean Institute of Electrical Engineer, 62(1), pp.6-11.

Kim, J.W., Han, Y.S., Choi, K. & Lee, J.H., 2013. Application of CFD Simulation In SIC-CVD Process, Journal of the Korean Society for Computational Fluids Engineering, 18(3), pp.67-71.

Kim, H.Y., Cho, L.S. & Cho, J.S., 2011. CFD analysis of the Dick Friction Loss on the Centrifugal Compressor Impeller, Journal of the Korean Society for Aeronautics & Space Science, 39(17), pp.596-604.

Kim J.W., Park J.K., Kang Y.S. & Jo J.S., 2015. Conjugate Heat transfer Analysis fir High Pressure Cooled Turbine vane in Aircraft Gas Turbine, Journal of the Korean Society for the Fluid Machinery, 18(2), pp.60-66.

Kim K. P., 2016. CFD study on the quantitative risk analysis for the fuel gas supply system of the gas fuelled ship. Ph.D. University of Korea Maritime and Ocean University.

Kim, K.P., Kang, H.K., Choung, C.H. & Park, J.H., 2011. On the Application of CFD Codes for Natural Gas Dispersion and Explosion in Gas Fueled Ship. Journal of the Korean Society of marine Engineering, 35(7), pp. 946-956, 2011.

Kim, K.P., Kim, Y.T. & Kang, H.K., 2015. CFD Approach on Gas Explosion for SIL in GAS Fuelled Ship, Journal of Marine Engineering, 39(2), pp.195-200.

Kim, S.E., 2011. CFD as a seakeeping tool for ship design, Journal of Naval Architecture and Ocean Engineering, 3(1), pp.65-71.

Kim, S.Y., Oh, Y.J., Park, S.W. & Lee, C.S., 2012. Reduction of a Numerical Grid Dependency in High-pressure Diesel Injector Simulation Using the Lagrangian-Eulerian CFD Method, Journal of the Korean Society for Computational Fluids Engineering, 20(1), pp.39-45.

Kim, Y.M., Shin, D.H. & Hwang, S.S., 2011. Experimental and Numerical Study on the Gas Mixing and Reaction in the Freeboard of a Fluidized Bed Incinerator for Sludge

Ko, M.W, Oh, C.B., Han, Y.S. & Do, J.H., 2015. Investigation of Turbulent Analysis Methods for CFD of Gas Dispersion around a Building, Journal of the Fire Science Engineering 29(5), pp.42-50.

Koopmana P. Ronald and Ermak L Donald., 2007. Lesson learned from LNG Safety

Research, Journal of Hazardous Materials, 140, PP. 412-428.

Kumar Satish et al., 2011. LNG: An eco-friendly cryogenic fuel for sustainable development, Journal of Applied Energy, 88, pp.4264-4273.

Lee, C et al., 2013. Coupled flow-structure Analyses on the Rotors Type Vacuum Pumps in Semiconductor Fabrication Facility, Journal of the Korean Society for the Fluid Machinery, Vo16(2), pp.10-14.

Lee, H.R., Ahn, J,H., Kim, D.K., Ahn, B.H. & Kim, H.Y., 2016. CFD Analysis and Explosion Test of a Crankcase Relief Valve Flame Arrester for LNG-Fuelled Ships, Journal of Korean Society of Manufacturing Technology Engineers, 25(3), pp.171-176.

Lee, H.R., Gong, H.J., Kim, B.S. & Lee, S.S., 2012. Prediction of Pitch and Roll Dynamic Derivatives for Flight Vehicle using CFD, Journal of the Korean Society for Aeronautical & space Science, 40(5), pp.395-404.

Lee, K.W., Heo, S.U., Kwon, S.J. & Lee, J.K., 2015. Study on Flow Analysis of Hot Gas valve with Pintle, Journal of the Korean Society of Propulsion Engineer, 19(6), pp.19-25.

Lee, S.K., Lee, D.E., Kim, S.C. & Yoon, K.B., 2015. Dependence of Explosion Overpressure of Flammable Gas on the Changes of Volume Blockage Ratio of Facilities, Journal of the Korean Institute of Gas, 19(6), pp.54-61.

Lee, W.J., Lee, J H., Hur, N. & Yoon, I.S., 2015. Cavitation Analysis in a centrifugal pump using VOF method, Journal of the Korean Society for the Computational Fluid Engineering, 20(4), pp.1-6.

Lim S.B., Kim M.K., Kang Y.H. & Park W.G., 2015. Honeycomb Labyrinth seal leakage Characteristic analysis with actual operating conditions on the compressor of Gas Turbine, Journal of the Korean Society for the Computational Fluid Engineering, 20(4), pp.102-108.

Mazzoldi Alberto, Hill, Tim and Colls J. Jeremy, 2008. CFD and Gaussian atmospheric dispersion models: A comparison for leak from carbon dioxide transportation and storage facilities, Journal of Atmospheric Environment, 42, pp.8046-8054.

Middha Prankul et al., 2010. CFD calculations of gas leak dispersion and subsequent gas explosions: Validation against ignited impinging hydrogen jet experiments, Journal of Hazardous Materials, 179, pp.84-94.

Min, D.C., Back, J.B., Ko, J.W. & Kown, H.M., 2012. CFD Simulation Study to analyze the dispersion and explosion of combustible gas. Journal of the Korean Institute of Gas, 16(5), pp.58-65.

Nam Y.J., Sung M.K. & Song D.S., 2011. Study on Non-uniform Thermal Comfort in Hubrid Air-Conditioning System with CFD Analysis, Journal of the Society of the Air conditioning and Refrigerating Engineers of Korea, 23(3), pp.216-222.

Park et al., 2015. Characteristics of flow and reactive pollutant dispersion in urban street canyons, Journal of Atmospheric Environment, 108, pp.20-31.

Park, S.H., Ryu, M.H., Cho, L.S. & Cho, J.S., 2014. Design optimization of the staking line for an electric fan blade using CFD, Journal of the Korean Society for Aeronautical and Space Sciences, 42(11), pp.903-910.

Pontiggiaa M. et al. 2010. Hazardous gas releases in urban areas: Assessment of consequences, Journal of Hazardous Material, 176, pp. 589-596.

Pontiggia M., M. Derudi, V. Busini and R. Rota 2009. Hazardous gas dispersion: A CFD model accounting for atmospheric stability classes, Journal of Hazardous Materials, 171, pp.739-747

Qi Ruifeng et al., 2010. Numerical simulations of LNG vapor dispersion in Brayton Fire Training Field tests with ANSYS CFX, Journal of Hazardous Material, 183, pp.51-61.

Rakibuzzaman, et al. 2015. Cavitating Flow Analysis of Multistage Centrifugal Pump, Journal of the Korean Society of Fluid Machinery, 1(2), pp.65-71.

Seo, HK., Song, S.W., Hwang, Y.I. & Ha, H.C., 2014. Numerical Study on the HCFC-123 Leak in Turbo Chiller by using CFD, Journal of Korean Institute of Gas, 18(5), pp.85-90.

Seok. J., Jeong. S.M., Park. J. C. & Paik. J.K., 2013. CFD Simulation of Methane Combustion for Estimation of Fire and Explosion in Offshore Plant, Journal of the Ocean Engineering and Technology 27(2) pp. 59-68.

Siddiqui, M., Jayanti,S. and Swaminathan, T., 2012. CFD analysis of dense gas dispersion in indoor environment for risk assessment and risk mitigation, Journal of Hazardous materials, 209-210, pp177-185.

Sinha, R.P. and Nik W.M.N., 2011. Investigation of Propulsion System for large LNG ships, International Conference on Mechanical Engineering Research, pp. 1-16.

Son, B.S. and Jang, C.H., 2012. A Study on Measures to Improve Smoke Control Performance in Case of Fire in a Clean Room as an LCD Manufacturing Process, Journal of the Korean Institute of Fire Science and Engineering, 26(5), pp.41-47.

Sun. Biao et al., 2015. Dynamic simulation of hazard analysis of radiations from LNG pool fire, Journal of Loss Prevention in the Process Industries,35, pp. 200-210.

Tauseef S.M, Rashtchian D. & Abbasi S.A., 2011. CFD-based simulation of dense gas dispersion in presence of obstacles, Journal of Prevention in the Process Industries, 24, pp. 371-376.

The International Group of Liquefied Natural Gas Importers (GIIGNL), 2017. LNG information Paper No.1-Basic properties of LNG

Wie, D.E., Kim, D.J., 2012. The Design Optimization of a Flow Control Fin Using CFD, Journal of the Society of Naval Architects of Korea, 49(2), pp.174-181.

Yi.J.S., Jeong I.K., Yun J.H. & Suh J.S., 2011. A Study on Flow Characteristic in Muffler for 125cc, Grade Motorcycle, Journal of the Korean Society of Manufacturing Technology Engineer, 21(2), pp.196-201.

Yoo S.J., Kang J.W. & Yang J.H., 2013. A Study on Evaluation of Ventilation Efficiency from Ventilation System and Volume in the Small Facilities Using CFD, Journal of the Architectural Institute of Korea, 29(6), pp.263-270.

Zhang, Bo and Chen, Guoming., 2010. Quantitative risk analysis of toxic gas release caused poisoning—A CFD and dose–response model combined approach, Journal of Process Safety and Environmental Protection, 88, pp253-262.

Zinn, C.D., 2005. LNG codes and process safety, Process Safety Progress, 24(3), pp.158-167.

Appendix

Computational setting of ANSYS FLUENT 14.0 version

1. Geometry work 1 to 1 scale

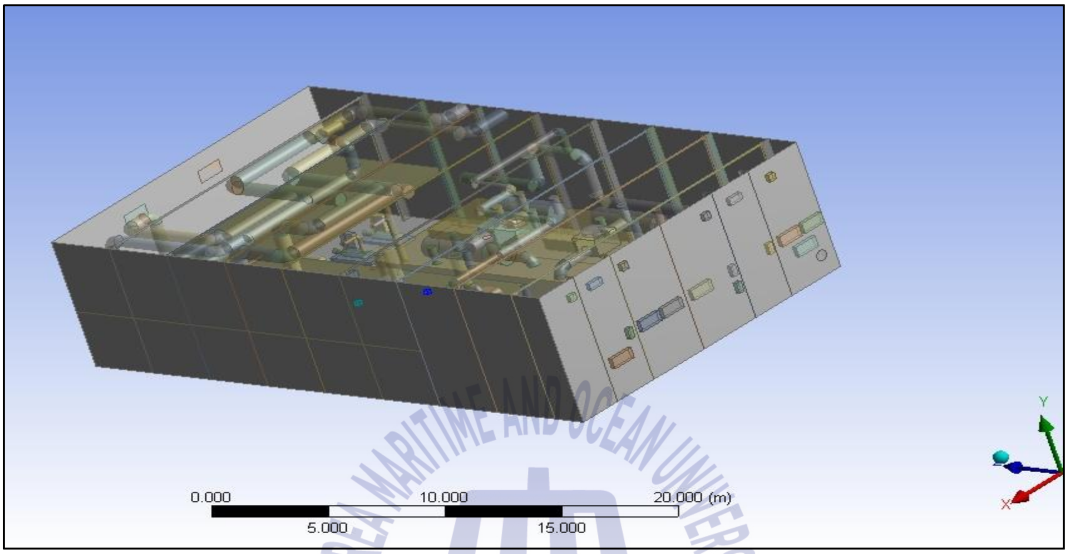

2. Meshing work(Name selection to the boundary condition : mass flow inlet – 1 point, pressure inlets – 2 points, pressure outlets-17 points)

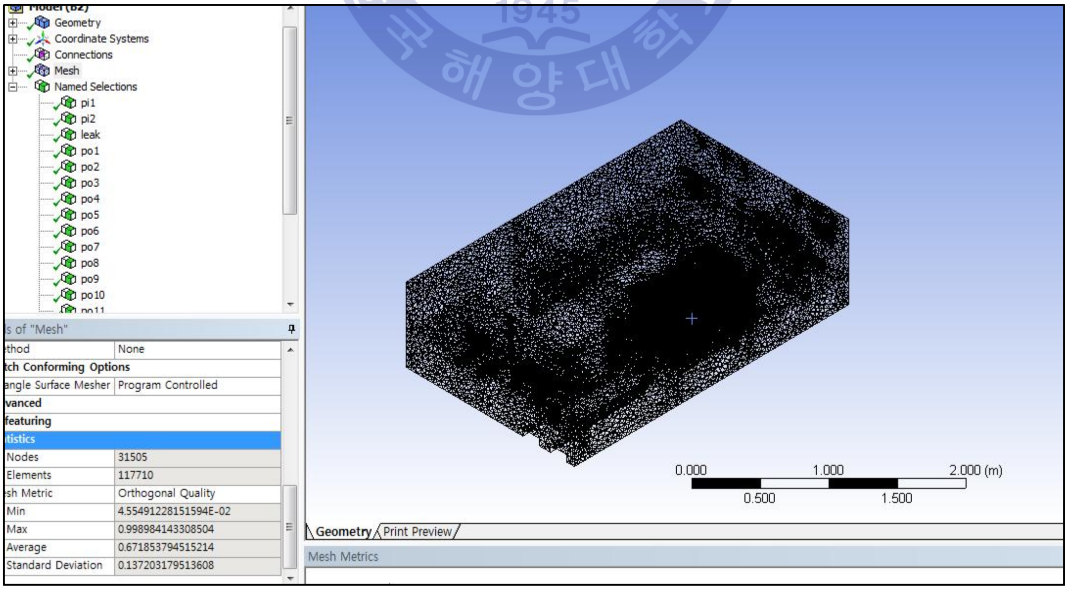

3. Solver setting (Density Based, Select Steady or Transient time selection)

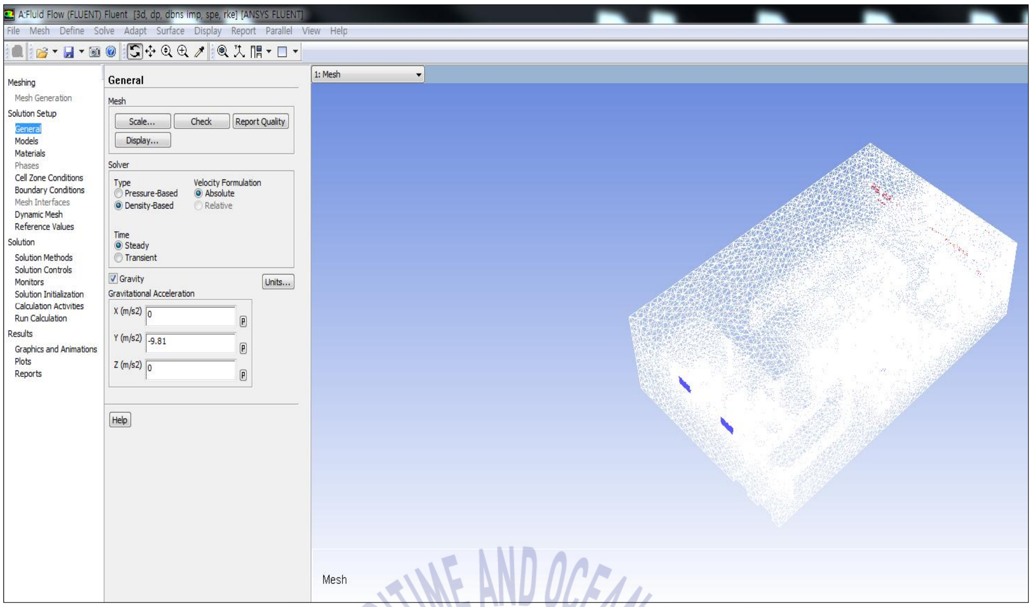

4. Species Model, Energy equation and K-epsilon model.

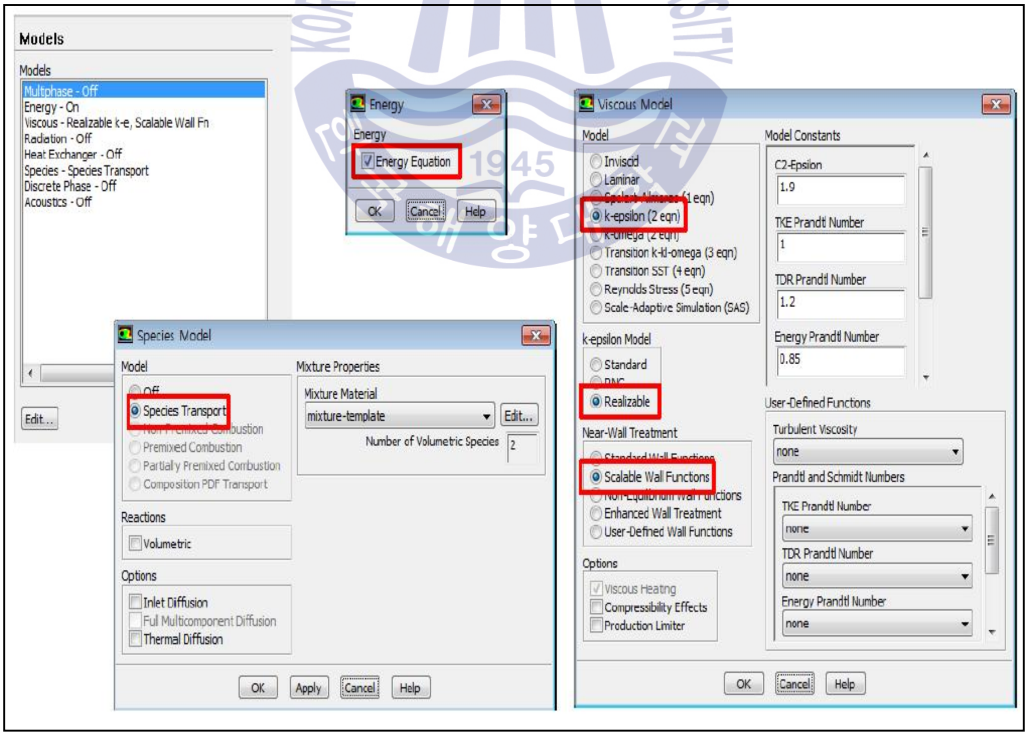

5. Select mixture template(Density, Specific heat, Thermal conductivity)

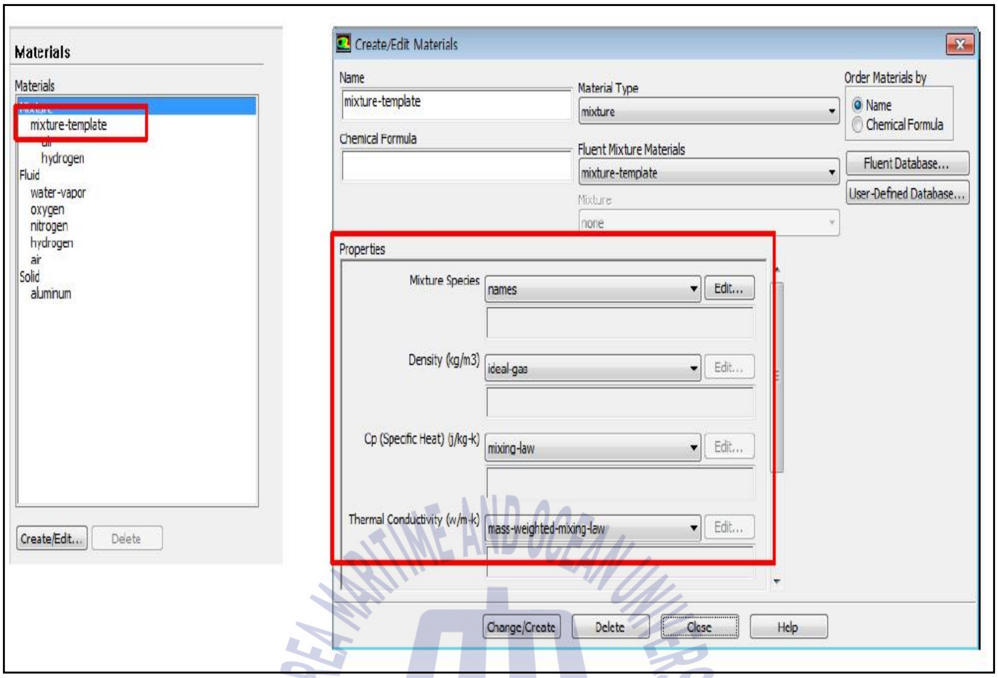

6. Select Species. (Choose CH_4 and air)

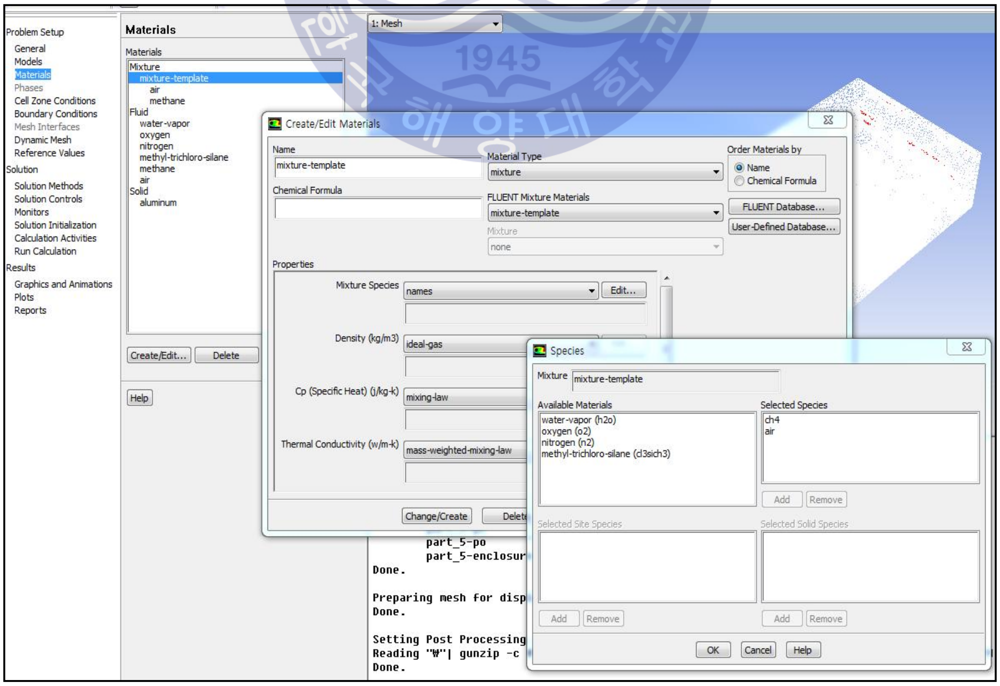

7. Operating pressure (input zero), Input absolute pressure at outside boundary. and check Gravity

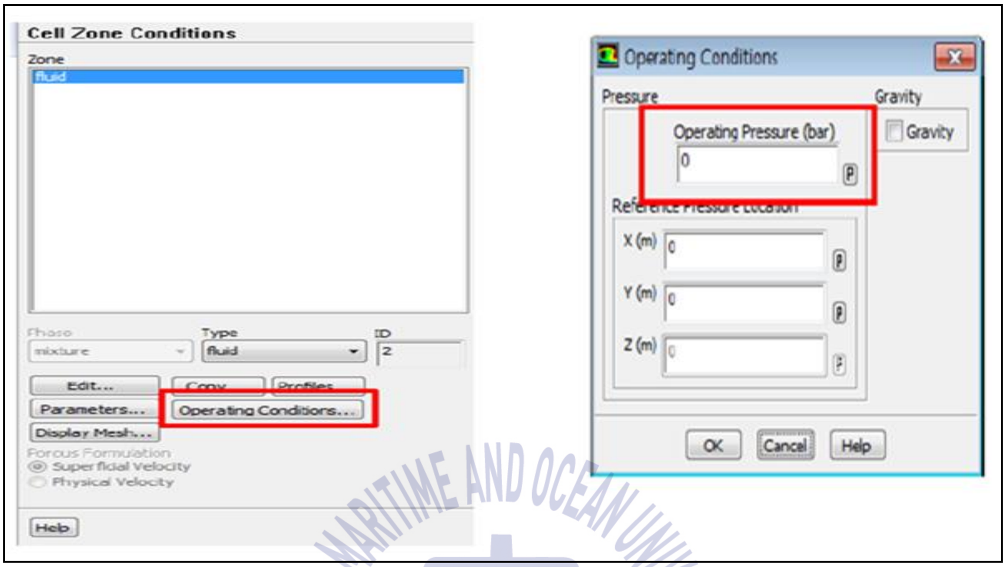

8. Input boundary condition(leak in : mass-flow-inlet)

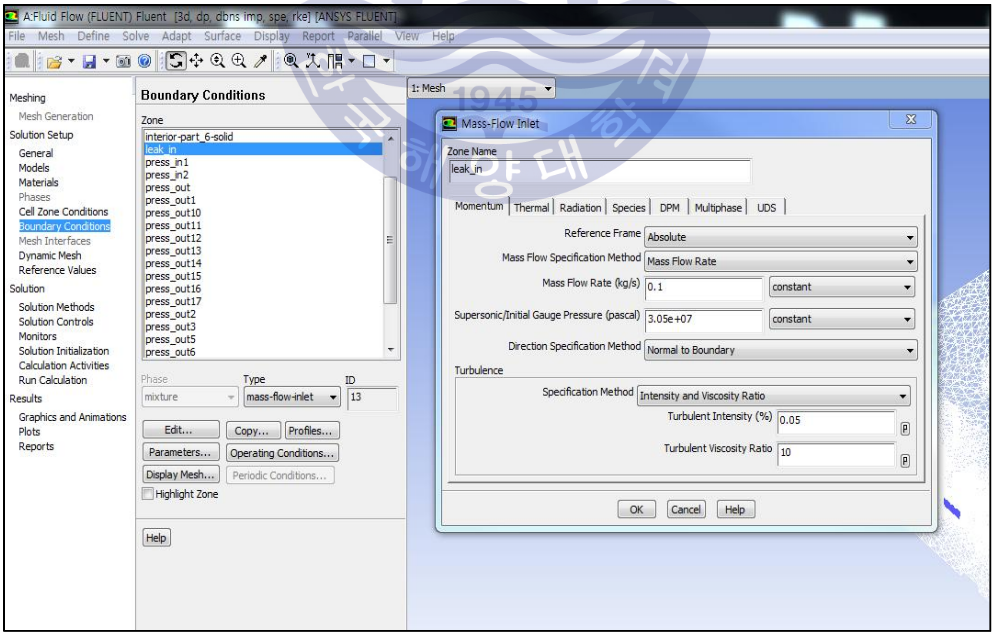

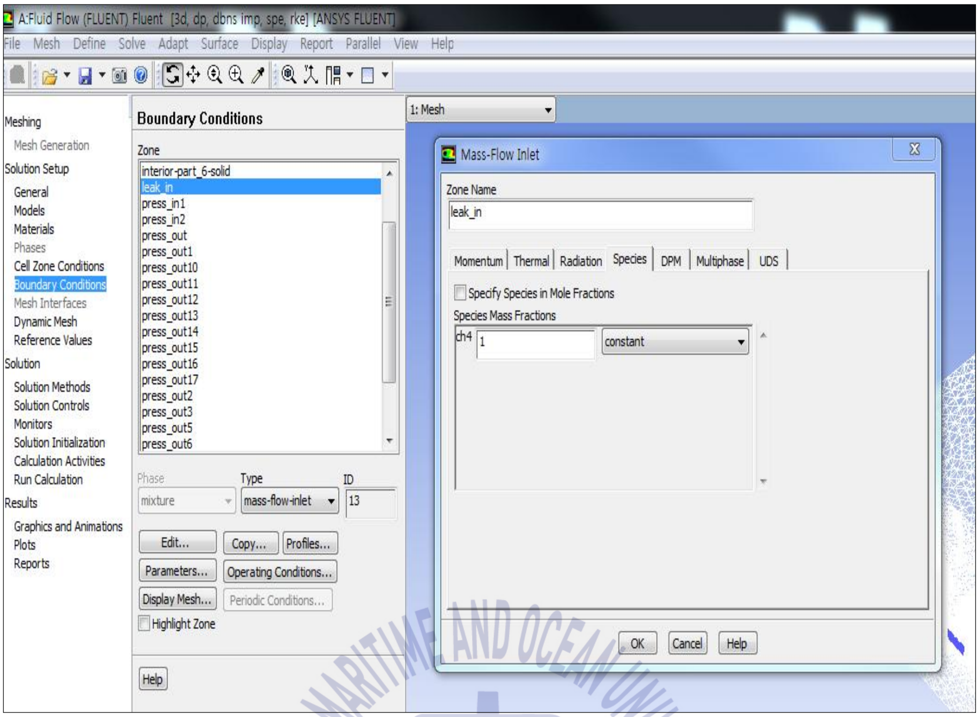

9. Input boundary condition(press in : pressure-inlet)

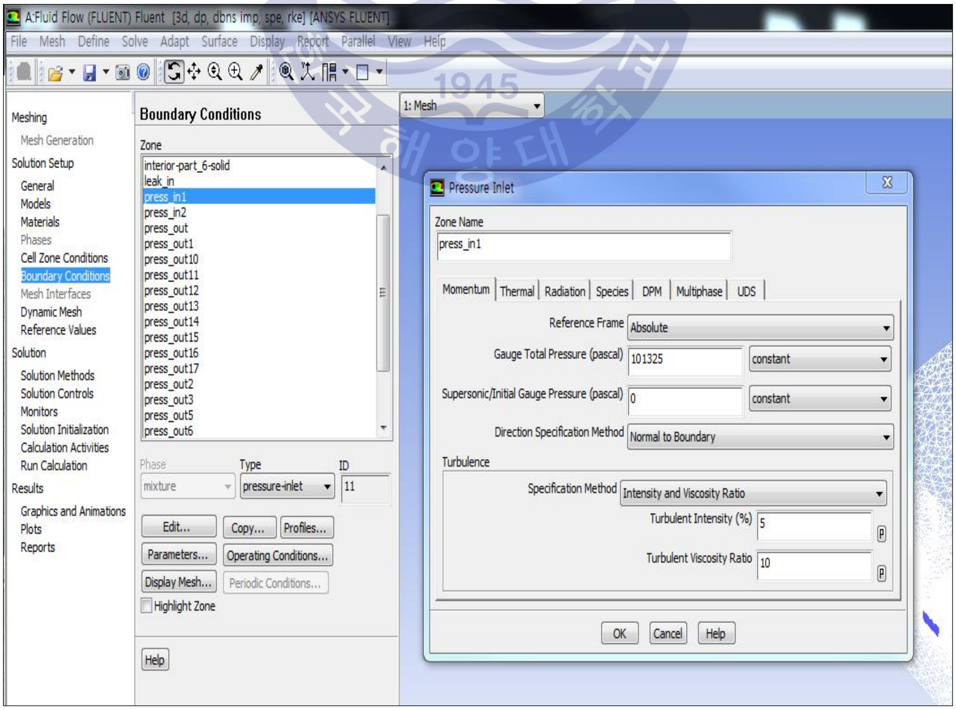

10. Input boundary condition(press out : pressure-outlet)

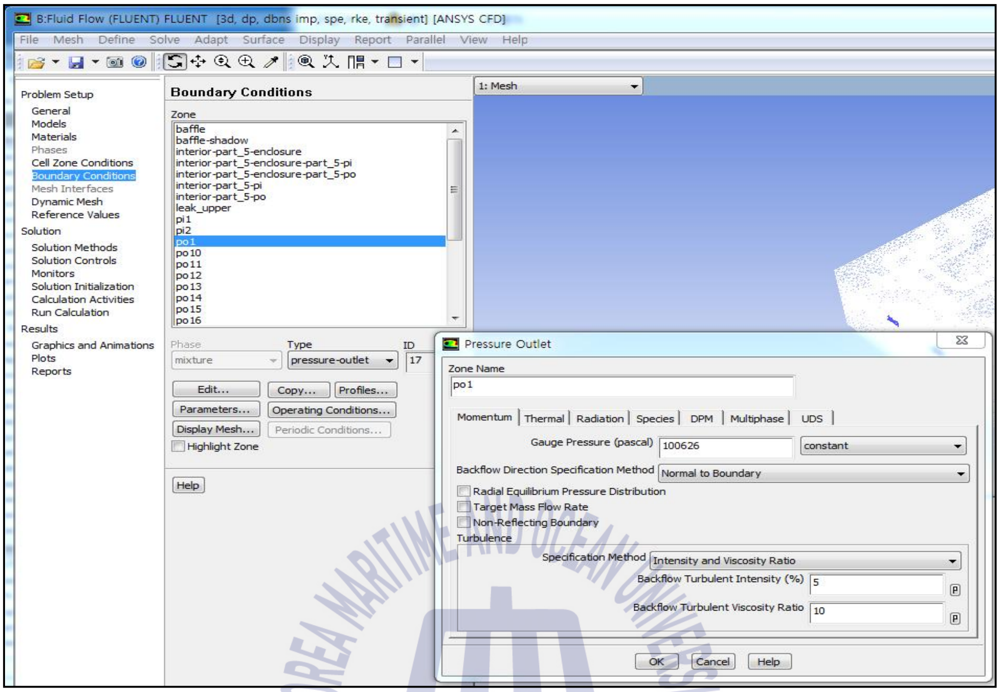

11. Solution Methods and Solution control.

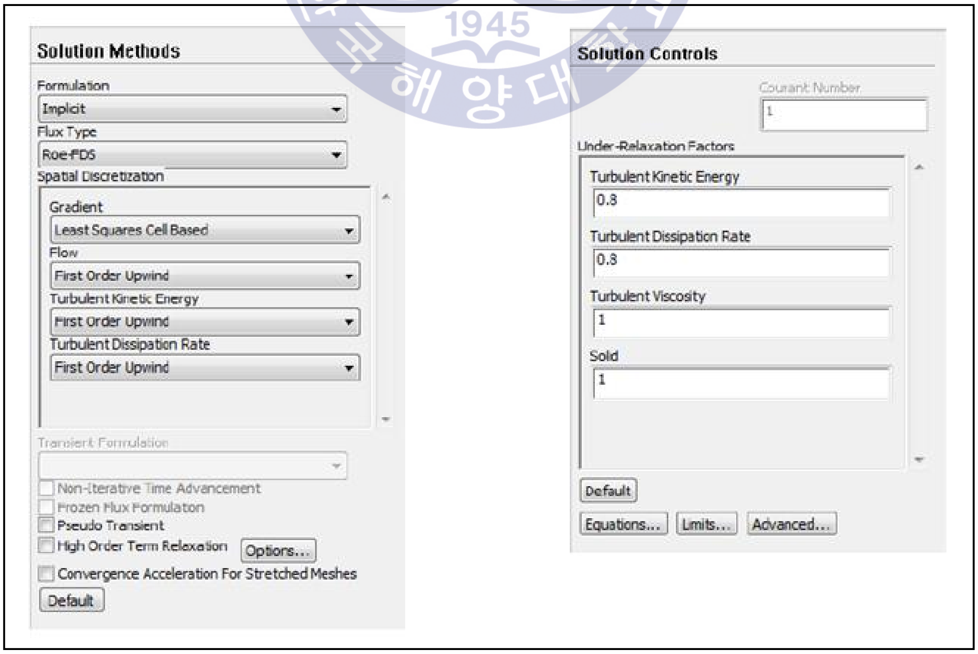

12. Solution Initialization and Run Calculation (Courant number setting is 0.0001 ~ 5) for stable convergence in case of steady state.

In case of transient time selection, time step size and number of time steps to be selected appropriately for convergence.

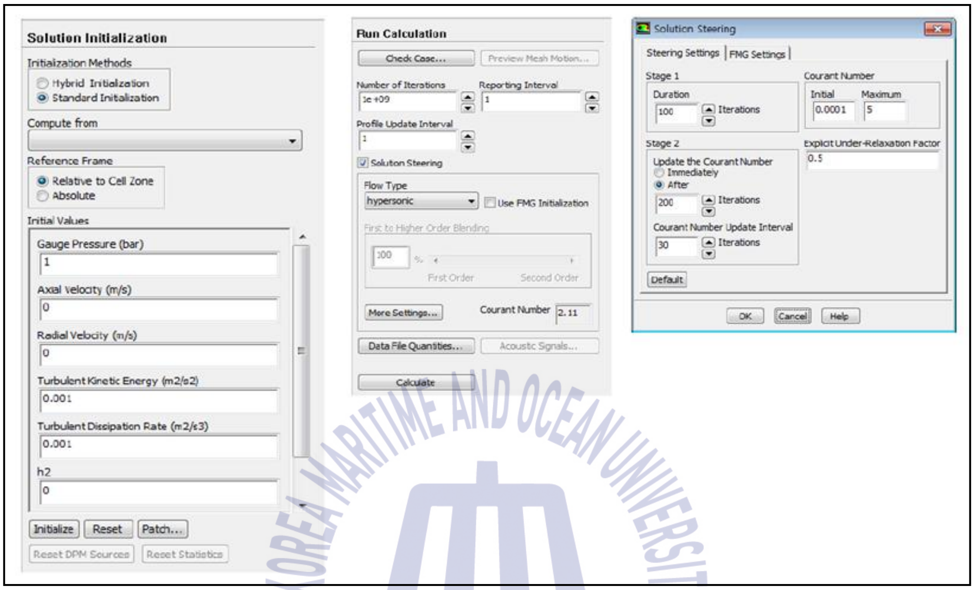

감사의 글

대학을 졸업하고, 1996년에 대우조선에 입사하여 선장배관설계 업무를 시작하였습니다. 입사 이래로 일을 하면서, 대학원에 진학하여 공학 관련한 공부를 하고 싶었지만 거제도에는 대학이 없어서 단념하고 마흔 살이 넘어 독학으로 조선기술사 공부를 시작하였습니다. 여러 차례 실패를 맛보고서야 기술사 자격증을 취득 할 수 있었습니다. 거제도와 부산간에 거가 대교가 놓이면서 2012년도에는 부경 대학교에서 기술경영학이란 학문을 공부 할 수 있는 기회가 왔고 석사도 마치고 박사 학위도 취득 할 수 있었습니다.

하지만 고교시절부터 물리학 공부에 관심이 있었지만, 그 당시 경제적 여건으로 대학원에 진학을 하지 못하고 취직을 하게 되었고, 직장생활 20년만에 해양대학교에 입학을 하여 일하면서 공부를 또다시 하게 되었고, 회사 업무를 통해 배운 것을 이론적으로 학문과 연계하여 CFD를 이용하여 논문을 쓰게 되었습니다. 자연현상을 컴퓨터로 구현하는 것이 저에겐 너무 흥미가 있었고, CFD 상용툴인 Fluent는 논문을 쓰기 위해서 처음 배웠기 때문에 수십 번 실패하고 다시 mesh를 짜야 했습니다. 하지만 그러한 과정에서 원하는 시뮬레이션에 성공하게 되면 희열을 맛보았습니다. 논문을 쓰면서 다양한 자연현상을 구현해 보지는 못했지만, 해양대학교에서 공부를 하여 회사 내에 배관설계에서 유체성능연구부서로 이동을 하게 되었고, CFD 툴로 다양한 자연현상을 마음껏 구현해볼 수 있게 되었습니다.

하루에도 여러 차례 전화로 논문관련 문의를 드려도 항상 친근하게 논문지도를 해주신 지도교수님이신 강호근 교수님과 부경 대학교에서 저의 지도교수님이시고 본 논문에도 심사위원으로 참석해 주신 김동준 교수님께 감사의 말씀을 드리고자 합니다. 회사에서 부서를 이동하여 연구업무를 할 수 있도록 배려해 주신 연구원장님이신 엄항섭 전무님과 부서이동뿐만 아니라 서울에서 논문심사를 위해 세 차례나 해양대학교까지 방문해 주시고, 여러 조언과 박사 공부하는 동안에 경험담을 말씀해 주신 이영범 박사님께 감사의 말씀을 드립니다. 본 논문이 통과 될 수 있도록 하여주신 심사위원장님이신 임태우 교수님과 논문의 잘못 된 점을 바로 잡아 주신 김도엽 교수님께 진심으로 감사의 말씀을 드립니다. 올바른 논평이 있었기에 박사학위를 받을 수 있게 되었습니다.

학위를 취득할 수 있었던 것은 무엇보다 사랑하는 아내와 아들이 인내해 주고 도와 주었기 때문입니다. 아버지께서 살아계셔서 축하해 주시고 기쁨을 같이 나누고 싶은 아쉬운 마음이 한량이 없으며, 수십 년을 매일 새벽에 저의 앞날을 위해 고향 평택에서 기도해 주시는 헌신적이고 자애로우신 어머니께 본 논문을 바칩니다.

2018년 6월 22일

이 상 원 올림